

Technische Universität München  
Fakultät für Informatik

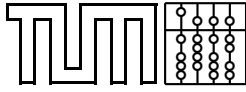


# Diplomarbeit in Informatik

Fast and efficient error correction of electromagnetic tracking and its application in prostate cancer treatment

Claudia Thormann





Technische Universität München  
Fakultät für Informatik



## Diplomarbeit in Informatik

Fast and efficient error correction of electromagnetic tracking and its application in prostate cancer treatment

Claudia Thormann

Advisor: Prof. Nassir Navab

Supervisor: Jörg Traub

Date: March 15, 2007

Ich versichere, dass ich diese Diplomarbeit selbständig verfasst und nur die angegebenen Quellen und Hilfsmittel verwendet habe.

München, den 15.3.2007

Claudia Thormann

## Abstract

Electromagnetic tracking systems are very popular for medical applications because they are able to track flexible instruments inside the human body. Unfortunately electromagnetic tracking systems are very sensitive to distortion caused by ferromagnetic metal and electromagnetic fields in their range. When the sources of distortion cannot be removed from the setting because they are needed to perform a task, error correction algorithms can be used to compensate the distortions.

In this diploma thesis an improved method for error correction algorithm was implemented and tested. The error correction method is based on a lookup-table containing correct positions of a magnetic sensor in an distorted setting and the corresponding distorted positions. The correct position of the sensor is acquired with the help of an optical tracking system and benefits from its high precision. The algorithm uses the lookup-table for online error correction of the position of the magnetic sensor in an distorted setting. An important requirement for this is the synchronization of the used magnetic and the optical tracking system.

The application was motivated by the medical domain of prostate cancer treatment. The current treatment is confronted with the problem of a prostate gland that moves slightly during radiotherapy. A magnetic sensor shall be used to track the position of the prostate gland and the cancer within. This diploma thesis provides an application that can be used for this purpose.

The results of my experiments are very promising. In every experimental setting the error correction method could improve the distortion of the tracking data. In the setting that was the most distorted by metal, the distortion could be reduced from 40.55 mm to 0.60 mm by the implemented method that is based on Hardy's multiquadric method.

## Zusammenfassung

Elektromagnetische Trackingsysteme werden sehr gerne in medizinischen Anwendungen eingesetzt, weil man damit flexible Instrumente innerhalb des menschlichen Körpers verfolgen kann. Unglücklicherweise sind elektromagnetische Trackingsysteme sehr anfällig gegenüber Störungen durch ferromagnetisches Metall und elektromagnetische Felder. Wenn die Störquellen nicht aus dem Versuchsaufbau entfernt werden können, weil sie für eine Aufgabe benötigt werden, können Fehlerkorrekturalgorithmen verwendet werden um die Störungen auszugleichen.

In dieser Diplomarbeit wurde eine verbesserte Methode zur Fehlerkorrektur implementiert und getestet. Die Methode zur Fehlerkorrektur basiert auf einer Nachschlagetabelle (englisch: *lookup-table*), die korrekte Positionen eines magnetischen Sensors in einem gestörten Umfeld enthält und die dazugehörigen verzerrten Positionen. Die korrekte Position des Sensors wird mit Hilfe eines optischen Trackingsystems ermittelt und profitiert von dessen hoher Genauigkeit. Der Algorithmus benutzt die Nachschlagetabelle zur Fehlerkorrektur der Position des magnetischen Sensors in einem gestörten Versuchsaufbau. Eine wichtige Anforderung dafür ist die Synchronisierung beider Trackingsysteme.

Die Anwendung wurde motiviert von dem medizinischen Gebiet „Behandlung von Prostatakrebs“. Die gegenwärtige Behandlung sieht sich konfrontiert mit dem Problem der Bewegung der Prostata während der Bestrahlung. Ein magnetischer Sensor soll benutzt werden, um die Position der Prostata und des Krebses darin zu verfolgen. Diese Diplomarbeit stellt eine Anwendung zur Verfügung, die zu diesem Zweck eingesetzt werden kann.

Die Ergebnisse meiner Experimente sind sehr vielversprechend. In jedem experimentellen Versuchsaufbau konnte die Methode zur Fehlerkorrektur die Verzerrung der Trackingdaten verbessern. In dem am meisten durch Metall gestörten Versuchsaufbau konnte die Verzerrung von 40.55 mm auf 0.60 mm verbessert werden durch die implementierte Methode, die auf einer multiquadrik-Methode von Hardy basiert.

## Acknowledgements

First of all I want to thank Prof. Dr. Navab for giving me the opportunity to work at his chair. I also want to thank him for the interesting lecture “Computer Aided Medical Procedures” that arose my interest for a field that combines computer science with medical applications.

I want to thank Prof. Dr. Kneschaurek from the Radiation Therapy Department of the hospital Rechts der Isar in Munich for providing me with medical background knowledge about prostate cancer and the intended application and for letting me watch radiations for a day.

I want to thank Dr. Zimmermann from the Radiation Therapy Department of the hospital Rechts der Isar for sharing his knowledge about prostate cancer treatment with me.

A big “thanks” goes to my advisor Jörg Traub for accompanying me during the course of my thesis, answering my questions so patiently and for his great job in proof-reading the first version of my thesis. Thanks a lot!

I also want to thank all the people who worked in the NaNuLab in the hospital Rechts der Isar with me:

Thomas Wendler Vidal always lend a helping hand regardless how much work was waiting for him. He always know what to do when the CAMPAR framework did not compile after a fresh checkout and his presence made the NaNuLab irradiate. Marco Feuerstein had useful tips for me on numerous topics. Claudio Alcérreca Alcocer and me always had much fun during our lunches and explored the delicacies of Mexico and Germany. He also helped me with some OpenGL problems. Tobias Reichelt and Jakob Vogel had useful hints for me regarding the camera calibration. Julian Much gave me good advice how to start with the magnetic tracking system and the framework. And thanks to Alexander Hartl and Tobias Lasser for nice chats during work.

Next I want to thank some of the assistant medical technicians (MTAs) from the nuclear medicine department of the Klinikum Rechts der Isar, Munich. This are Constanze Büst, Jutta Grahneis and Gabriele Michalke for nice conversations during my lunch breaks. A special thanks goes to Martin Finke for his warm welcome and our perirical talks.

I want to thank Dr. Silvia Reitz from the Radiation Therapy Department and the assistant medical technicians Franka Schramm and Susan Alavi for answering all my questions about radiation.

Thanks to Thomas Hoffmann for proof-reading some chapters.

And last but not least thanks to Christian Wlczek for proof-reading the whole thesis.

This diploma thesis would not have been possible without all of you. Thank you!



# Contents

<b>Abstract</b>	<b>i</b>
<b>Acknowledgements</b>	<b>iii</b>
<b>I Introduction and background Information</b>	<b>1</b>
<b>1 Introduction, Motivation and Overview</b>	<b>3</b>
1.1 Introduction and Motivation . . . . .	3
1.2 Overview over the thesis . . . . .	4
<b>2 Medical application: prostate cancer treatment</b>	<b>5</b>
2.1 About the staging of cancer in general . . . . .	5
2.2 Background information about prostate cancer . . . . .	6
2.2.1 Structure and function of the prostate . . . . .	6
2.2.2 The detection of prostate cancer . . . . .	6
2.2.3 Symptoms of prostate cancer . . . . .	8
2.2.4 Overview over the approaches of prostate cancer treatment . . . . .	8
2.3 External beam radiation therapy . . . . .	13
2.3.1 The effect of radiation to cancer cells . . . . .	13
2.3.2 Side effects of radiation . . . . .	14
2.3.3 Different ways of external beam radiation . . . . .	15
2.4 Status Quo of the medical workflow . . . . .	19
2.5 Current limitations of the treatment . . . . .	20
2.6 Approaches to localize the radiation target more precisely . . . . .	21
2.6.1 Stereotactic frames . . . . .	21

2.6.2	Roentgen-based methods . . . . .	22
2.6.3	Electromagnetic tracking . . . . .	22
2.6.4	Ultrasound navigation . . . . .	22
2.6.5	Implanted markers . . . . .	23
2.7	The proposed method . . . . .	24
2.8	The visionary medical workflow . . . . .	24
<b>3</b>	<b>Technical and theoretical background</b>	<b>25</b>
3.1	Tracking systems . . . . .	25
3.1.1	Electromagnetic tracking systems . . . . .	26
3.1.2	Optical tracking systems . . . . .	27
3.1.3	Coregistration of magnetic and optical tracking systems . . . . .	28
3.2	Mathematical background . . . . .	29
3.2.1	Homogeneous coordinates . . . . .	29
3.2.2	Hand-eye calibration . . . . .	31
3.2.3	Point-based registration . . . . .	33
3.2.4	Hardy's multiquadric method . . . . .	34
3.2.5	Statistics . . . . .	36
3.3	Preliminary work . . . . .	38
3.3.1	Motivation for Kaur's work . . . . .	38
3.3.2	Distortion correction with the polymer block . . . . .	38
3.3.3	Distortion correction with an optical tracking sytem . . . . .	39
3.3.4	Applied algorithms . . . . .	41
3.3.5	Comparison of different interpolation algorithms in 2D and 3D . . . . .	44
3.3.6	Discussion . . . . .	48
<b>II</b>	<b>The Implemented Application</b>	<b>51</b>
<b>4</b>	<b>The three-step algorithm</b>	<b>53</b>
4.1	Device calibration . . . . .	54
4.1.1	Performing hand-eye calibration to get the transformation $Y$ . . . . .	55
4.1.2	Reorganizing the equation to get the transformation $X$ . . . . .	56
4.2	Creating the lookup-table . . . . .	57
4.2.1	Ground truth values . . . . .	57
4.2.2	The lookup-table . . . . .	58

4.2.3	The Pacman Game . . . . .	59
4.3	Online error correction . . . . .	61
<b>III</b>	<b>Experiments and Results</b>	<b>63</b>
<b>5</b>	<b>System setup</b>	<b>65</b>
5.1	The electromagnetic tracking system . . . . .	65
5.1.1	3D Guidance by Ascension . . . . .	65
5.1.2	MicroBird by Ascension . . . . .	67
5.1.3	The specified magnetic working volume . . . . .	68
5.2	The optical tracking system . . . . .	68
5.2.1	The cameras . . . . .	68
5.2.2	The software for the cameras . . . . .	69
5.3	Custom-build hardware . . . . .	70
5.3.1	The combined target . . . . .	70
5.3.2	The field-generator-target . . . . .	71
5.4	The working volume for the experiments . . . . .	71
5.5	The used software . . . . .	71
<b>6</b>	<b>Experiment 1: Evaluation of the device calibration</b>	<b>73</b>
6.1	General course of experiment 1 . . . . .	73
6.2	Experiments 1.1 to 1.3 . . . . .	74
6.3	Suggested changes for the next experiment . . . . .	75
6.4	Experiment 1.4 . . . . .	76
6.4.1	The course of experiment 1.4 . . . . .	76
6.4.2	Results of Experiment 1.4 . . . . .	76
6.5	General conclusion of experiment 1 . . . . .	77
<b>7</b>	<b>Experiment 2: Evaluation of the applied error correction algorithm</b>	<b>79</b>
7.1	General course of experiment 2 . . . . .	79
7.2	Experiments 2.1 to 2.4 . . . . .	80
7.3	Suggested changes for the next experiment . . . . .	83
7.4	Experiment 2.5 . . . . .	83
7.4.1	The changed course for experiment 2.5 . . . . .	83
7.4.2	Results of Experiment 2.5 . . . . .	84
7.5	General discussion of experiment 2 . . . . .	86

<b>IV Conclusion and Future Work</b>	<b>87</b>
<b>8 Conclusion</b>	<b>89</b>
<b>9 Future Work</b>	<b>91</b>
9.1 Ensure the synchronization of the magnetic and the optical tracking system .	91
9.2 Expand the implemented application with a radiation therapy application . .	91
9.3 New medical approaches . . . . .	93
9.3.1 Attaching the sensor to the balloon catheter . . . . .	93
9.3.2 Permanently inserted intraprostatic markers . . . . .	93
<b>V Appendix</b>	<b>95</b>
<b>List of Figures</b>	<b>97</b>
<b>List of Tables</b>	<b>101</b>
<b>Bibliography</b>	<b>103</b>

## **Part I**

# **Introduction and background Information**



# Introduction, Motivation and Overview

## 1.1 Introduction and Motivation

The topic of this diploma thesis was motivated by the preliminary work at the chair for Computer Aided Medical Procedures & Augmented Reality at the technical university in Munich. The idea is to bring an electromagnetic tracking system into the therapy room and to use it to track a sensor of the tracking system inside the human body to improve the accuracy of locating the prostate gland for the radiation of prostate cancer.

The idea to use magnetic tracking in the medical application of prostate cancer radiation came from the collaboration of the chair with physicians from Klinikum Rechts der Isar in Munich. The prostate gland deforms naturally. This deformation makes a precise irradiation difficult. The prostate cancer radiation could benefit from magnetic tracking of the prostate gland inside the human body to localize the position of the gland and therefore the cancer more precisely. This would result in a reduced radiation area and in a more effective radiation of the cancer.

The disadvantage of a magnetic tracking system is that it is susceptible to metal. The metal present in the tracking volume results in distortions of the reported position of the sensor. This disadvantage can be compensated with an error correction algorithm.

Preliminary work was done at the chair and different error correction methods for magnetic tracking were implemented and compared. The algorithms worked well in the experimental setting, but the whole process of collecting distorted measurements and the corresponding noise-free data was too inconvenient and too time-consuming to integrate it into the medical workflow.

The motivation for this diploma thesis was to develop a more feasible process to perform the error correction. This thesis is one out of many steps on the way to clinically introduce magnetic tracking for prostate cancer treatment into the hospitals. More steps have to follow before this system can be used with patients.

The error correction algorithm is extended with functions that are needed to adapt it to the medical application of prostate cancer treatment. The approach is to collect distorted values of the sensor of the magnetic tracking system and corresponding correct positions of the

sensor at the same time and to use this displacement information in form of a lookup-table to correct distorted values of the sensor online. Tracking information from an optical tracking system is used to acquire the correct position for the sensor. The implemented application provides methods to calibrate the system, to collect a lookup-table using a combined target and to perform the error correction in a setting distorted by metal.

## **1.2 Overview over the thesis**

This diploma thesis consists of four main parts.

Part I provides the reader with an introduction to the topic and medical and mathematical background information. Information about cancer in general, prostate cancer in particular and prostate cancer treatment can be found here. Mathematical definitions are also given in this part as well as details about the used methods. Different kinds of tracking systems are discussed and preliminary work is presented.

Part II describes the application that was implemented in the course of this diploma thesis. The implemented application consists of a so called three-step algorithm for device calibration, the creation of a lookup-table and the online error correction. All three steps are described in detail.

Part III presents the experiments made to prove the benefit of the implemented application and the results of the experiments. Different experiments were performed to analyze the quality of the two main components of the implemented application.

Part IV recapitulates the done work and identifies starting points for future work. The thesis is reviewed afterwards from my point of view and I list topics that could not be treated. Issues that might be the basis for future developments are reported.

# Medical application: prostate cancer treatment

This diploma thesis is motivated by the medical problem of precise localization of prostate cancer for radiotherapy and, associated with this, a patient positioning system that brings the prostate cancer location in the isocenter of the gantry of the linear accelerator.

This chapter provides the background information to understand the medical side of this patient positioning problem. Additional information about cancer and prostate cancer treatment is included to show the classification of the medical treatment. The status quo of the medical workflow is explained as well as its current limitations. The proposed modified workflow using an electromagnetic tracking system for a more precise localization of the prostate cancer is introduced and defines the technical details of this thesis.

## 2.1 About the staging of cancer in general

Cancer is a major disease of men in the western world nowadays. This section introduces cancer in general and gives background information about the staging of prostate cancer.

Cancer generally means that cells in the body grow uncontrollable and displace and perhaps destroy healthy tissue. The different reasons for cancer all lead to an imbalance between growing and splitting of cells and the death of cells.

Scientists differ benign (“good”) tumors from malignant (“bad”) ones. Benign tumors like nevi and lipoma are usually not meant by the word “cancer” as cancer denotes malignant tumors.

Three attributes distinguish cancer from benign tumors. Cancer infiltrates neighboring tissue, destroys surrounding tissue and develops metastases.

Some genes observe the mechanism of copying cells during progeny. If a damage is detected, they start a repairing process, stop the progeny during repair and commence the cell death if the damage cannot be repaired.

Scientists believe that a malfunction in this observing genes is the reason for cancerogenesis. During progeny, the observing genes may also underlie copying errors. Errors in the

observing genes may also be congenital. The observing gene with dysfunction is not able to do its work properly. If one of the genes is affected that usually causes the death of a cell that cannot be repaired, the damaged cell becomes deathless. If more than one of the observing genes is affected, the negative effects increase.

The damaged cells with mutations in their genes develop new features: They can survive without oxygen, arrange their own blood supply and can settle in different tissue like bones or brain. The last property is called metastasis.

The immune system tries to stop the uncontrolled growth of the tumor cells, but the cells are still too similar to other cells of the body so that the attack of the immune system is too weak to stop the cancer.

Causes for the development of cancer may be influences that change the genotype of cells as well as things that stop the immune system from recognizing and deleting degenerated cells. Today chemicals as well as viruses are known to cause cancer, including nitrosamines, X-rays, hepatitis type B and human papilloma virus, just to mention a few.

## **2.2 Background information about prostate cancer**

Prostate cancer is the most common malign tumor in men. It develops most frequently in men older than fifty years. Prostate cancer is one of the leading causes of death of male due to cancer.

### **2.2.1 Structure and function of the prostate**

The prostate is an exocrine gland of male mammals. Female mammals do not have a prostate, but the Skene's glands is regarded to be the female pendant of the prostate.

The prostate is a small organ in the abdomen (see figure 2.1 on page 7). It is located under the bladder, in front of the rectum and encloses the urethra. Its shape and size is comparable to a chestnut.

The prostate gland produces and stores a secretion. It is called seminal fluid. The prostate produces 1/10th to 1/3rd of the seminal fluid, the rest is produced by the seminal vesicle. Semen is composed of sperm and seminal fluid from the prostate and the seminal vesicle.

The male hormone testosterone regulates growth and function of the prostate. This androgen is mainly produced by the testicles.

### **2.2.2 The detection of prostate cancer**

The prostate can be seen with ultrasound (US), in computer tomography images (CT) and on images taken with nuclear magnetic resonance devices (NMR).

An enlargement of the prostate gland can be the symptom of a tumor. The growth may be caused by benign tumors as well as by prostate cancer. The enlargement can be seen on medical images and it can also be detected during rectal examination. But these non-invasive methods do in general not enable the oncolist to know if the tumor is benign or malign. The

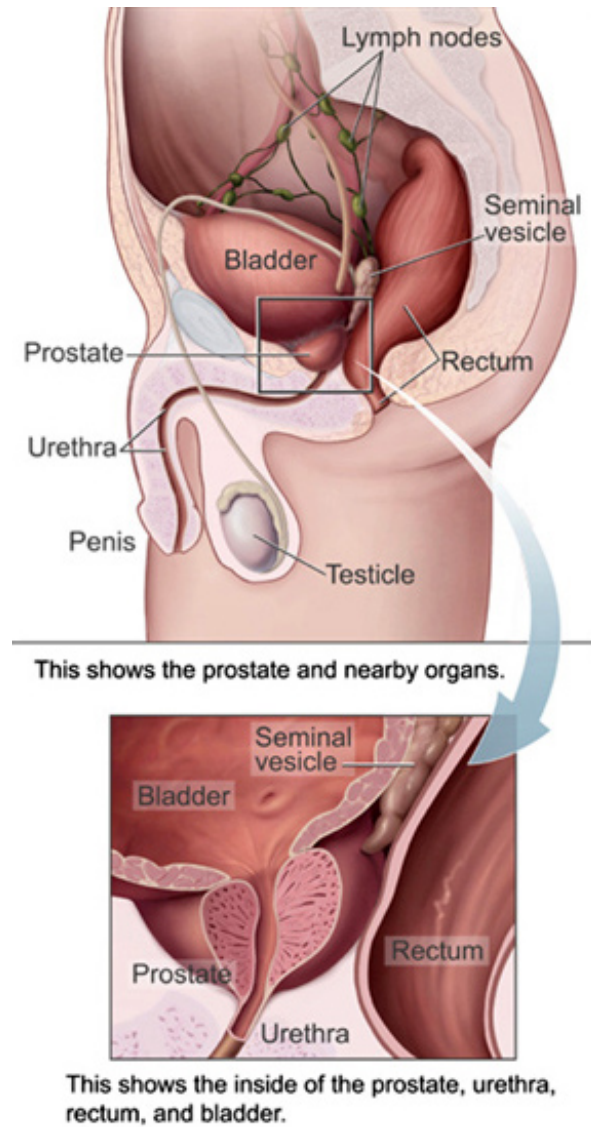


Figure 2.1: The picture shows the position of the prostate in the abdomen. Picture taken from <http://en.wikipedia.org/Prostate>

detection of prostate cancer is additionally made difficult due to the fact that older men often have an enlarged prostate and that they tend to the creation of lumps inside the prostate.

If the prostate has enlarged to a certain extend, it may constrict the urethra and cause problems during urinating. This may cause the man to take medical advice.

On the suspicion of prostate cancer the only proof of cancer is a biopsy of the prostate gland and a histological examination of cancer cells that were found in the tissue sample. Laboratory values like prostate specific antigen (PSA) or the number of leukozytes also help to detect prostate cancer.

### **2.2.3 Symptoms of prostate cancer**

In an early stage, prostate cancer usually has no symptoms.

Later, the tumor can block the flow of urine. This causes ailments like frequent urination of small quantities of urine, increased urination at night, difficulties starting and maintaining a steady stream of urine, and painful urination.

To much pressure of the cancer on special nerves can cause difficulties achieving an erection or painful ejaculations.

Blood in the urine or the semen occur rarely.

As the cancer spreads to other parts of the body, it can cause additional symptoms like bone pain of spine and pelvis, leg weakness, urinary and fecal incontinence, loss of weight and anemia.

As the cancer is usually without symptoms in its early stages, German doctors offer a preventive medical checkup for men older than fifty years. Part of the checkup is a rectal palpation and the test for prostate-specific antigen (PSA) in the blood.

### **2.2.4 Overview over the approaches of prostate cancer treatment**

Nowadays there are different ways how to treat prostate cancer treatment. The choice of treatment depends on several criterions like the size of the cancer, the condition of the patient, the degree of the symptoms and so on.

This section describes different approaches of treatments that are applied in hospitals nowadays. It uses information from [MHP<sup>+</sup>05].

Palliative and curative treatment are two very different ways of treatment. Most patients get curative treatment. This means, that the aim of treatment is to completely heal the cancer. This is usually done when the patient is rather young.

There are some older patients with additional diseases like diabetes or cardiac insufficiency. Their health is in a bad stage and they are likely to die within some years, but not because of prostate cancer, but because of one of their other diseases. This patients are not healthy enough to undergo most of the treatments. The aim of their treatment is to give them a better life quality and to slow down the growth of the cancer. The benefit of this palliative treatment is to enlarge the life span for one or two years.

The challenge for the doctors is to find a therapy that offers the best therapeutic effect and at the same time has as few side effects as possible. Doctors can choose between surgical removal of the prostate, radiation therapy, hormonal therapy, chemotherapy, watchful waiting and combined approaches. The different approaches are described in the following sections.

#### **2.2.4.1 Surgical intervention**

If the cancer is locally restricted in the prostate and the patient is in good health condition, one possible treatment is to remove the prostate gland, seminal vesicle and regional lymph nodes. This treatment is called radical perineal prostatectomy. The lymph nodes have to be

removed, too, because cancer cells can spread over the lymph channels. Malign tumors use the lymph channels to establish metastases in other organs.

There are three approaches for the removal of the prostate. They differ in the location where the surgeon cuts to enter the abdomen. The surgeon can enter the operation field either by a cut at the belly or a cut at the perineum (this is the skin between scrotum and anus). The third possibility is a minimally invasive laparoscopic approach.

Surgical removal of the prostate is either done for an early state prostate cancer or after the cancer did not respond to radiation therapy.

Perineal prostatectomy is very effective if the cancer has not spread beyond the prostate yet.

As a side effect of the surgical intervention, important nerves can be damaged. This can lead to a permanent loss of urinary control (incontinence) and impotence where usually erection and ejaculation are impaired. Both are common problems after this treatment. Very seldom rectal incontinence can occur when the relevant nerves are damaged.

More nerve-sparing techniques are applied by some specialized cancer centers.

#### **2.2.4.2 Radiation therapy**

Radiation therapy is a good complement to surgical removal for locally restricted forms of prostate cancer. It can be done after surgical removal or instead of surgical removal.

Radiotherapy uses ionizing radiation to kill prostate cancer cells. It can damage or destroy the DNA<sup>1</sup> crucial to cancer cell growth.

The radiation can either be delivered from outside through the skin, called external beam radiation therapy, or from inside the prostate, known as brachytherapy.

Radiation therapy is used when a surgical intervention is too risky for the patient due to health or age. If the cancer has already spread outside the prostate, radiation therapy can be used to slow down the course of the cancer.

Advantages of radiation are the non-existent operation risks and the possibility of an ambulant treatment.

Disadvantages of radiation are problems with digestion like temporary diarrhea. Some patients suffer from permanent damages on bowel and bladder as well as erectile dysfunction and problems with the sphincter.

**External beam radiation (EBRT)** As well as surgery, it is also applied to small tumors that have not spread outside the prostate gland.

A linear accelerator as shown on figure 2.2 on page 10 is used for external beam radiation. It produces ionizing radiation, gamma-rays more precisely. The patient is arranged on a treatment table in such a way that the beam crosses the patient's prostate.

The patient is treated with external beam radiation every weekday for several weeks.

As result of the exposure to radiation, side effects like inflammation of rectum and bladder can occur. Some patients get erectile dysfunction and rectal and urinal incontinence.

This kind of treatment will be explained more detailed in section 2.3 on page 13.

---

<sup>1</sup>desoxyribonuclein acid



Figure 2.2: The picture shows a linear accelerator that is used during external beam radiation. Picture taken from <http://de.wikipedia.org/wiki/Strahlentherapie>

**Internal radiation** Internal radiation is also called brachytherapy. Brachy is greek meaning "short" or "near". This denotes the fact that in brachytherapy the source of radiation is inserted directly into the cancerous organ and hence the source of radiation is put on a short distance to the cancer.

Two ways of applying the source of radiation are used: Either a low-dose source of radiation is given over a long period of time in the form of so called seeds (the source of radiation) that are permanently implanted to the prostate or a source delivering high-dose of radiation is put into the prostate for some minutes.

Low-dose radiation is given in the form of about a hundred rods containing iodine-125 or palladium-103. The rods (compare figure 2.3) emit low-energy X-rays. The seeds are implanted with a needle through the perineum (that is the skin between anus and testicles).

Men with permanently implanted seeds do not expose other people to radiation because the implanted source of radiation is very low-dose.



Figure 2.3: These seeds are implanted into the prostate during low-dose brachytherapy. Picture taken from [http://en.wikipedia.org/wiki/Prostate\\_cancer](http://en.wikipedia.org/wiki/Prostate_cancer)

In high-dose brachytherapy, a source of radiation is inserted into the prostate using an afterloading mechanism. The high-dose radiation is removed after five to eight minutes of treatment. As in external beam radiation, the treatment is pursued for several days.

Disadvantages of both ways of brachytherapy are diarrhea, rectal bleeding due to inflammation, damage to lower parts of the colon by X-rays, urinary incontinence and impotence. The symptoms commence some weeks after starting the treatment, but usually improve over time.

#### **2.2.4.3 Hormonal therapy, also known as androgen deprivation**

As testosterone regulates function and growth of the prostate gland, a reduced production of testosterone may slow down or stop the growth of some kinds of prostate cancer. But not all prostate cancers respond to this treatment. Hormonal therapy is especially used when the tumor has already spread from the prostate.

A very permanent way of androgen deprivation is the removal of the testicles. But due to the psychological impacts of this treatment, it is nowadays done very seldom.

Usually, androgen deprivation is achieved with the help of drugs. The applied drugs artificially lower the level of testosterone in the blood. LHRH<sup>2</sup>- or GnRH<sup>3</sup>-analogons are given as injection every month or every three months.

But unfortunately, the cancer becomes resistant after one or two years of hormonal therapy. Therefore hormonal therapy is used for palliative treatment to improve the life quality of patients that will die very probably due to their prostate cancer or additional illnesses.

Disadvantages of the loss of testosterone are depression, hot flashes, gain in weight, loss of libido, impotence, erectile dysfunction, anemia, breast enlargement and osteoporosis.

#### **2.2.4.4 Chemotherapy**

In chemotherapy drugs are used to treat cancer. These drugs either impair the division of cells or cause cell death and work very specific. It has not been possible yet to find features that are unique for cancer cells. Therefore, the drugs apply to all cells that divide rapidly. These are cancer cells as well as cells that cause hair growth and cells called intestinal epithelium that are located inside the colon that reabsorb nutrients. That means, chemotherapy does not only kill cancer cells but also non-cancer-cells, but normal cells are not damaged as much as cancer cells. Chemotherapy is used if the cancer already metastasized.

The drugs only work for cancers that have a great fraction of fast-dividing cells. Therefore, not all cancers respond to chemotherapy.

The drug is administered intravenously in most cases, but can also be applied oral in the form of pills.

The drug cannot kill all cancer cells at once. It must be given over a longer period of time to ensure that all cancer cells will be killed. If the treatment is stopped too early, resistant

---

<sup>2</sup>luteinising hormone releasing hormone

<sup>3</sup>gonadotropine releasing hormone

cells can survive and propagate. Different drugs can be given at the same time to avoid the creation of resistant cancer cells because the drugs differ in their mechanism and side effects. Cancer cells can become resistant to chemotherapy drugs because of different factors: It can happen that the drug cannot be delivered to the tumor cells due to a reduced blood flow or due to a not correctly working transport of the drug into the cells.

Dosing schemes were developed by the hospitals that depend on the body surface area of the patient. The body surface area is a composite measure of weight and height that mathematically approximates the body volume.

As told before, the drugs damage all fast-growing cells. This causes the loss of hair, nausea and vomiting, diarrhea or constipation and anemia. Chemotherapy is also very exhausting for the patient. Older people often have a reduced function of liver and kidneys. This makes them more susceptible to side-effects on these organs like damages of kidney and liver, but also damages to the heart. The dosage of the drugs should be adjusted to this circumstance.

Scoring schemes are available that tell if the patient is capable of chemotherapy or if the dosage should be reduced. The scoring scheme orientates on features like if the patient can care for himself or if he needs medical care, if he shows symptoms of the disease and so on.

Chemotherapy is often combined with other approaches.

#### **2.2.4.5 Watchful waiting**

Watchful waiting, also called "active surveillance", is a treatment where the patient is not treated at all but is observed and monitored regularly.

This kind of treatment is applied to older men with a slowly growing prostate cancer in an early stage. Watchful waiting can also be reasonable if the benefit of any other treatment like surgery or radiation does not prevail its risks and side-effects.

Other treatments can be started if the cancer leaves the early stage. Men who choose watchful waiting have a higher risk for metastasis.

Men younger than sixty years cannot choose active surveillance because they have a higher level of testosterone than older men and therefore require a more aggressive and urgent treatment.

The disadvantage of active surveillance is that additional health problems like diabetes and cardiac insufficiency make it harder to start a treatment of the cancer like surgical intervention or radiotherapy if the cancer progresses.

Old patients with additional illnesses and a non-aggressive cancer usually have the same or even a better life quality with watchful waiting instead of an active treatment of their prostate cancer because of the absence of side-effects like incontinence or impotence, diarrhea and anemia that arise from active treatment.

#### **2.2.4.6 Combined approaches**

Often, two approaches are combined to achieve better results. Usually, one approach is used to enable the second approach to work properly.

**Surgery and radiation** When surgery and radiation are combined, usually surgery is done first. Although the prostate gland and the prostate cancer were removed, some cancer cells may be remaining at the borders of the cancer area. The surgeons try to avoid this by cutting out a slightly enlarged area around the cancer. To ensure the kill of all cancerous cells, the area of operation is radiated later. This radiation treatment does not last as long as radiation for patients that have had no surgical intervention before.

There is also the other way round, when radiation is done first and surgery afterwards. Radiation might be used to make the cancer shrink. It is then easier to cut it out.

**Surgery and chemotherapy** Chemotherapy can be used either before or after surgery. It is called “neoadjuvant chemotherapy” if it is given before the operation and “adjuvant chemotherapy” if it is given after surgery. Neoadjuvant chemotherapy shall make the cancer shrink so that a smaller part of tissue needs to be removed. Adjuvant chemotherapy shall ensure that the cancer will not return. It also works against cancer cells that have spread to other parts of the body.

**Surgery and hormonal therapy** When the prostate gland was surgically removed, the patient can be treated with hormones that lower his testosterone level to avoid the return of prostate cancer.

**Radiation and hormonal therapy** After radiation, the patient can get hormones to avoid the return of the cancer.

## 2.3 External beam radiation therapy

Radiation therapy is a common treatment for prostate cancer. This section gives background information about radiation therapy and its physical properties. It is considered to be important to know with regard to the design of a system for patient positioning in order to enable more precise and thus less invasive therapy. This section refers to [MHP<sup>+</sup>05].

### 2.3.1 The effect of radiation to cancer cells

Radiation uses high-energy ionizing rays like gamma-rays, X-rays, electrons, neutrons and protons to treat malign tumors.

The effect of radiation is that it damages the DNA of the cancer cells. The ionizing radiation beams enter the cells and ionize the water inside the cells. As a reaction, free radicals are generated. These free radicals damage the DNA.

Cancer cells are stem cells that are undifferentiated and divide very fast. Their ability to repair damages to the DNA is very low compared to differentiated cells. The damage is done to the DNA and therefore is permanent. The damage also persists during cell division. In addition with normal mutation during cell division, the damages in the DNA of cancer cells add up and cause the cells to divide slower or to die.

Non-cancerous cells are differentiated cells. They have a better mechanism to repair DNA damages and recover.

It is important that oxygen is available in the cancer cells. Only the presence of oxygen makes the DNA damages permanent. The problem is that some cancers have grown so big that their blood supply is not sufficient. This causes a lack of oxygen in the cancer cell and therefore makes the radiation less effective. At the moment, research is done how to bring oxygen to this kind of cancers to make the DNA damage permanent.

Radiation is given in fractions over some weeks. This is done to allow the healthy tissue to recover.

### **2.3.2 Side effects of radiation**

Radiation itself causes no pain to the patient, but can have several side effects.

Low-dose radiation used for palliative treatment causes few or even no side effects. But nowadays, patients are very often treated with high-dose radiation. This high-dose radiation always causes side effects. Efforts are made for every radiotherapy patient to minimize side effects and to help the patient to deal with inevitable side effects.

Side effects can occur during treatment, called acute side effects. Long-term side effects are side effects that emerge month or years after the treatment. The third kind of side effects is called cumulative side effects. They arise after retreatment.

#### **2.3.2.1 Acute side effects**

One acute side effect is inflammation or damage to skin and mucosa that were radiated. Depending on the organs that were radiated, the skin of head, neck, the skin behind the ears or underneath the breast and the mucosa inside mouth, throat, esophagus and bowel can be affected. Inflammation of parts of the mouth is called stomatitis. It can cause problems with swallowing and may need medical intervention like nutritional support. Skin and mucosa turn pink and get sore. The patients usually recover quickly from these skin damages.

Another acute side effect is the swelling of soft tissues. This is only a problem if the swelling occurs inside the brain. It can cause damages to the brain and needs to be treated. Steroids can be given before the radiation to prevent swelling of the brain during brain radiation.

Radiation of the abdomen can cause a feeling of fullness, nausea, diarrhea and disorders of the bladder. Radiation of the prostate can cause proctitis. This is inflammation of the rectum.

Ovaries and testicles (called gonads) are very sensitive to direct radiation, even to low doses of radiation. So infertility can be another acute side effect of radiation. But it can only occur if ovaries or testicles are radiated directly. Medical staff as well as patients can save their gonads with aprons made from lead.

Radiation can also make the patients tired in general.

### **2.3.2.2 Long-term side effects**

Irradiated tissue can inflame and cause an increased production of connective tissue. The connective tissue is composed of collagen. The uncontrolled growth leads to scars, a loss of elasticity and the hardening of the tissue at organs. This process is called fibrosis.

If the brain is irradiated, hair loss can occur. This hair loss is permanent, but very likely restricted to the area that was radiated. Radiation of head and neck also affects salivary and and tear glands. The patient's life quality can be diminished by permanent xerostomia (dryness of the mouth) and xerophthalmia (dry eyes).

Irradiated sweat glands can stop working.

The radiated skin can get discolored.

Pelvic irradiation of women can cause the mucosa of the vagina to become dry.

As radiation causes changes in cancer cells and healthy cells, it can in turn cause cancer. This happens only to a very low number of patients several years after they were treated. The risk of getting cancer because of radiation is said to be outweighed by the fact that the primary cancer could be treated successfully.

### **2.3.2.3 Cumulative side effects**

Cumulative side effects occur as a result of a anew treatment of cancer.

## **2.3.3 Different ways of external beam radiation**

Radiation can be given either external with beams of a linear accelerator from outside the body or internal by inserting a source of radiation into the body. Internal radiation is called brachytherapy. Informations about brachytherapy applied to prostate cancer were given in section 2.2.4.2 on page 10.

Computer tomography images are nowadays the basis for planning external beam radiation as the images can be used to define structures to be radiated as well as structures that should be spared out and structures that should get as less dose as possible.

In prostate cancer treatment, the cancer shall be radiated while bladder and bowel shall be spared out. The development of new technologies over the last decades allowed to give a higher dose to the cancer cells and at the same time enabled to spare healthy tissue.

According to [MHP<sup>+</sup>05], different forms of external radiation have been established. These are conventional radiotherapy, 3D conformal radiotherapy and intensity modulated radiotherapy. They are discussed in the following sections.

### **2.3.3.1 Conventional radiotherapy**

Conventional radiotherapy is an outdated method now because the dose is limited and the beam of the linear accelerator cannot be shaped to the contour of the cancer.

### 2.3.3.2 3D conformal radiotherapy (3D-CRT)

3D conformal radiotherapy is the standard method of treatment nowadays. In comparison to older methods, 3D conformal radiotherapy has two advantages: The tumor can be radiated with a higher dose and the beam can be shaped to the contour of the tumor. This shaping made it possible to give a higher dose of radiation to the tumor, because the healthy tissue could be spared out from the radiation. 3D conformal radiotherapy also gives the possibility to use a variable number of beams.

A multi-leaf collimator (see figure 2.5) is used to shape the beam of the linear accelerator. It is a device composed of tungsten leaves (see figure 2.4) that are driven by engines and whose shift is controlled by a computer. The collimator blocks the radiation beam according to the pre-operatively devised treatment plan and is attached to the head of the linear accelerator.

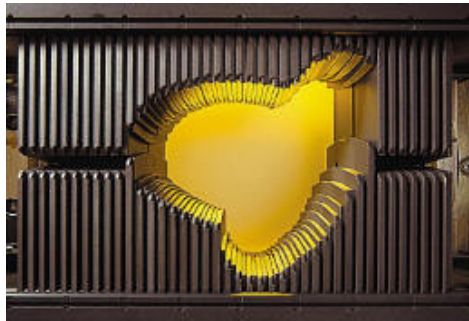


Figure 2.4: A multi-leaf collimator by Varian that is attached to the linear accelerator to shape the radiation beam during radiation. Picture taken from <http://welchcancercenter.org/Radiation%20Therapy%20Equip/multileaf%20collimator.htm>



Figure 2.5: The left picture shows a collimator by Brainlab. In the right picture you can see the same collimator attached to a linear accelerator. Pictures taken from [http://www.brainlab.com/scripts/website\\_english.asp?categoryID=19&pageTypeID=11&article\\_short\\_headline=Oncology%20Products](http://www.brainlab.com/scripts/website_english.asp?categoryID=19&pageTypeID=11&article_short_headline=Oncology%20Products).

For 3D conformal radiotherapy, an initial computer tomography scan of the patient is done, taking X-ray images in slices of two to five millimeters of the area of interest. These images are taken as input for the treatment planning software that generates the treatment plan. It allows a virtual simulation of the radiation and to plan the direction of the beams very precisely. The target volume (the prostate, in our case) and critical structures (bowel and bladder) are marked on every slice. Then the doctor arranges the radiation beams so that the dose adds up in the cancer while applying only a part of the dose to critical structures and healthy tissue.

3D conformal radiotherapy is now a standard method in radiation of cancer patients.

### **2.3.3.3 Intensity modulated radiotherapy (IMRT)**

Intensity modulated radiotherapy is an advanced method in cancer treatment. IMRT is the enhancement of 3D conformal radiotherapy. Multi-leaf collimators are still used in this approach. The beam is not only shaped to the tumor, but additionally the intensity of radiation across the beam is varied.

IMRT has two advantages over 3D-CRT: The delivered dose is not homogeneous and the dose for parts of the tumor can be “boosted”.

Intensity modulated fields are either achieved with dynamic multi-leaf collimators or with step and shoot multi-leaf collimators. Dynamic multi-leaf collimators move independently of each other during radiation while the beam is always on. Step and shoot multi-leaf collimators sequentially form fields with different shapes. This generates areas of high, low and intermediate dose in the target area. (Compare [MHP<sup>+</sup>05])

These new technological advances are in need of another way of treatment planning. Instead of going forward in planning like it was done for 3D-CRT, treatment planning for IMRT uses an inverse planning approach. The best solution for the great number of possible combinations of field intensities cannot be calculated with a forward approach. In the inverse approach, the wanted doses are defined for the target volume and critical structures. The software then calculates the corresponding beams to achieve this dose distribution. A screenshot of a treatment planning software can be seen in figure 2.6 on page 18.

According to [MHP<sup>+</sup>05], IMRT planning in comparison to 3D-CRT results in a larger part of cancerous tissue that receive the appointed dose, but IMRT is also expensive, time-consuming and complex and perhaps does not result in an advantage for all patients.

IMRT is used increasingly in hospitals nowadays.

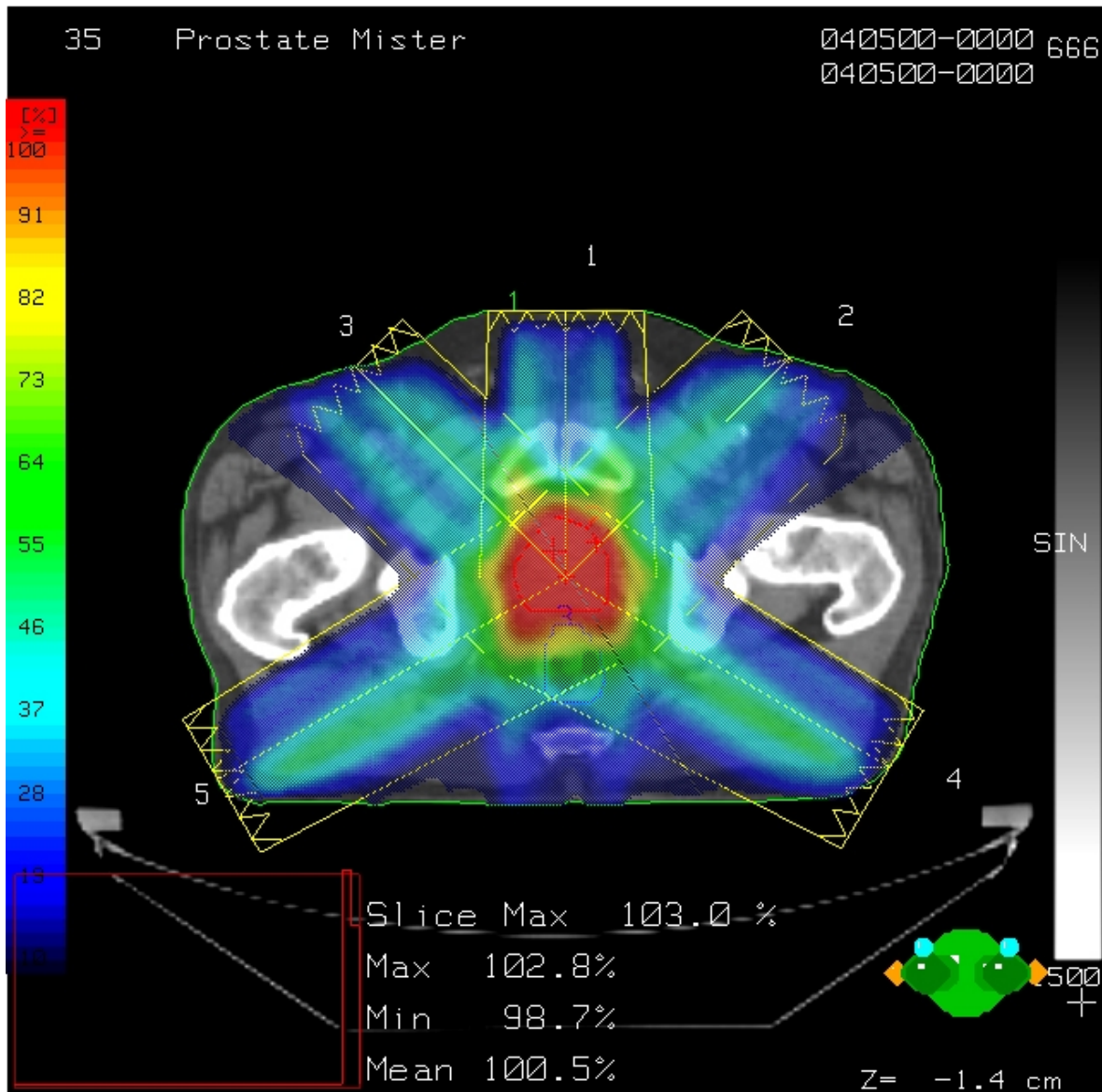


Figure 2.6: The picture shows the screen of the Varian Medical Systems Newsroom displaying an IMRT treatment plan for prostate cancer. The area of high dose is shown in red, low dose is shown in blue. Picture taken from [http://varian.mediaroom.com/index.php?s=media\\_library&cat=8](http://varian.mediaroom.com/index.php?s=media_library&cat=8)

## 2.4 Status Quo of the medical workflow

In the beginning, the patient has an initial talk with the physicist that will treat him. The doctor explains the workflow of the treatment and informs the patient about the number of treatments.

A first computer tomography scan of the patient's abdomen is done and the doctor assigns the position of the prostate cancer. These CT images are then used to calculate the area of radiation with the help of a treatment planning software. The calculated area includes the prostate and a small security area around it. That means that the radiation area is enlarged a little bit beyond the prostate to secure that the whole cancerous area gets radiated.

The treatment room has a laser pointer system that is calibrated with the linear accelerator. The patient is labelled on both thighs with a permanent marker during the first treatment to record his current position. The labels on the patient are adjusted to the laser pointer system. The labels later help to adjust the patient in a treatment position that corresponds to the patient's position during the first treatment.

The patient is treated every weekday. He enters the treatment room and has to lay down on the treatment table on the left side. The technical personnel prepares everything before the doctor comes in.

As soon as the patient is prepared, the physicist comes in to insert a balloon catheter (see figure 2.7) into the rectum. The balloon is inflated to adjust the prostate in its position. The prostate moves naturally due to rectal filling and the filling of the bladder. The patient is instructed to come in with the same filling of the bladder every weekday for the treatment. The balloon is used to compensate varying levels of rectal filling. It can also be seen on the computer tomography images. There is one catheter for every patient and a new balloon for every radiation. Lubricant is used to make the procedure more comfortable for the patient.

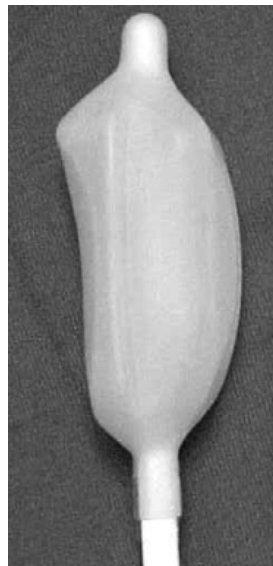


Figure 2.7: A rectal balloon catheter. Picture taken from [vLFH<sup>+</sup>06]

The patients come every weekday for several weeks. Most of the patients get radiated for seven weeks (33 to 37 radiations). Some patients had a surgery before, where the whole prostate gland was removed. These patients get radiated for five to six and a half weeks. There is a small number of patients with a malign cancer that has grown very fast recently and has emerged many metastases. These patients have a small chance of survival. They are radiated with the purpose to slow down the growth of the cancer.

Two X-ray shots are done regularly from above the patient and from the left side of the patient. This X-ray shots are done two weeks after the beginning of the radiation and then again four to six weeks after the beginning of radiation. The purpose of the X-ray shots is to check the patient positioning for correctness. If the prostate cancer is not in the isocenter of the images, the physicist instructs the assistant medical technicians to adjust the position of the table where the patient is laying for the following radiatons.

## **2.5 Current limitations of the treatment**

The current treatment works well, but due to the changing fillings of bladder and rectum, the prostate gland moves slightly. This results in an enlarged radiation area to ensure that the whole cancerous area gets radiated.

Different filling levels of the bladder cause a movement of the bladder of about 15 millimeters. To ensure that the bladder does not move too much, the patient is instructed to come with the same filling level of the bladder into the treatment room. Best for the treatment is a semi-filled bladder. Due to the radiation adverse effects, many patients get urethritis. This inflammation of the bladder makes the patients feel that the bladder is half filled, even if it is nearly empty. Unfortunately, that means it is not guaranteed that the filling of the bladder is the same for every treatment.

The different filling levels of the rectum leads to a movement of the rectum of 10 to 15 millimeters. The purpose of the rectal balloon is to control the natural movement of the rectum due to different filling levels. The balloon is inflated and expands the rectum to compensate natural changes in the filling level. The doctor inserting the ballon catheter always pulls it back until he feels resistance. This shall ensure that the balloon is inserted at the same position as it was when the initial CT scan was done.

The approach with the balloon can not eliminate differences that occur due to different doctors placing the balloon and due to slightly different positions of the balloon catheter despite the pull back of the balloon catheter. The result is that the position of the organs in the abdomen is not quite the same during the treatments in comparison to the initially done CT scan. To ensure that the whole prostate is radiated although the inner organs move slightly, the area of radiation is enlarged for some millimeters. It would be more useful to know the position of the prostate cancer more precisely instead of just enlarging the area of radiation.

One way would be to make a CT of the patient not only once in the beginning, but every day before the radiation is done. But this would mean that the patient is exposed to radiation, additional to the one he gets radiated with every day. This would result in a too high dose of radiation for the patients and is therefore omitted.

An other approach is to bring additional technical equipment into the radiation room with the purpose to find out the position of the prostate cancer more precisely.

## 2.6 Approaches to localize the radiation target more precisely

According to [KT07], four navigation methods allow a more precise localization of the tumor: stereotactical frames, Roentgen-based methods, electromagnetic tracking systems and ultrasound navigation.

Organ motions and deformations occur naturally in the body due to respiration, heartbeat and peristalsis. The purpose of all four approaches is to compensate organ motions and deformations, to localize the target point of the radiation more precisely and thus radiate the target within a smaller volume. This allows to radiate with an increased dose and therefore minimizes the possibility of the recurrence of the tumor.

### 2.6.1 Stereotactic frames

Stereotactic frames are attached to bony landmarks of the target area. They are used to establish a three-dimensional coordinate system and to localize targets inside the body in relation to the coordinate system of the frame. They can also be used to perform tasks like biopsies and ablation.

Medical images like computer tomography, magnetic resonance imaging or angiography are recorded for the target area. The stereotactic frame as well as the target area can be seen on the medical images. Therefore, the target area can be assigned relative to the center of the coordinate system of the device. Surgical instruments can be attached to the stereotactic frame that reside in the same coordinate system as the target area.

According to [Neu] there are two types of stereotactic devices: frame-based stereotactic devices and frameless ones. A frame-based stereotactic device for the head can be seen on figure 2.8. Frameless stereotactic devices consist of fiducial markers that are taped to the skin.

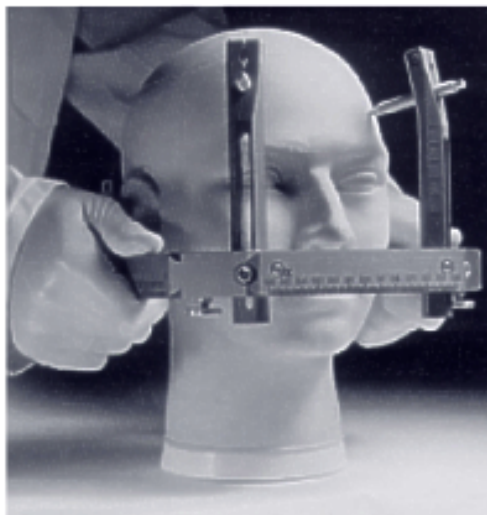


Figure 2.8: This images shows a frame-based stereotactic frame that is attached to the patient's head to establish a coordinate system. Picture taken from [Neu].

### 2.6.2 Roentgen-based methods

Roentgen-based methods like portal imaging, cone beam CT scans and mega-voltage CT scans are used to gain high quality images of the patient before the treatment. The status quo shown on the medical images are compared to the desired state during treatment planning. If necessary, the position of the patient is changed to correspond to the planned state.

### 2.6.3 Electromagnetic tracking

Electromagnetic tracking systems generate electromagnetic fields to track the pose of one or more sensor. There are systems where the sensors are connected to the tracking system with a wire as well as wireless systems. Both can be used to track inside the human body.

Wireless sensors (see figure 2.9) can be permanently implanted to the prostate gland. The sensor reports its position and can be used to bring the target volume into the isocenter of the linear accelerator during radiation therapy.

[WKP<sup>+</sup>06] evaluated the localization accuracy of the Calypso 4D Localization System. In comparison to X-ray localization, it showed a comparable localization accuracy.

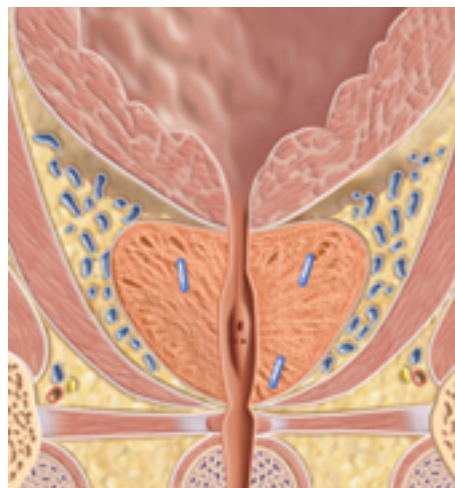


Figure 2.9: This image shows the prostate with permanently implanted wireless sensors, called “beacons” by the manufacturer Calypso Medical Solutions. Picture taken from [Cal].

### 2.6.4 Ultrasound navigation

Ultrasound imaging uses high-frequency sound with frequencies between 20 kHz and 1 GHz. 3D ultrasound is applied for ultrasound navigation. Ultrasound images of the treatment area are taken before the treatment. The patient’s position can be corrected then to fit the desired status of the treatment plan. Different ultrasound probes can be seen in figure 2.10 on page 23.

[FSC<sup>+</sup>04] describes the development and implementation of a strategy to use a stereotactic ultrasound-based image-guided targeting device to align intensity-modulated radiotherapy (IRMT) target volumes in the upper abdomen. Ultrasound targeting resulted in statistically significant improvements in patient setup.



Figure 2.10: Ultrasound probes for different purposes. Picture taken from [GE].

### 2.6.5 Implanted markers

Another possibility for a more precise localization of the tumor is to implant fiducial markers permanently and use the coordinate frame that they establish to track the tumor. Figure 2.11 shows gold markers in the form of rods that can be implanted into the prostate gland.



Figure 2.11: This pictures shows gold markers that are used to establish a permanent internal patient reference system. The special surface of the rods shall avoid movements after implantation. Picture taken from [MED]

[KWM<sup>+</sup>05] tested the assumption that implanted intraprostatic fiducials do not move within the prostate. The standard deviation of the inter marker distance variations were computed and found to range from 0.4 mm to 4.2 mm. 2 of 168 implanted markers changed their position in the course of the treatment. The authors consider that these changes were due to deformations of the prostate gland.

[SBI<sup>+</sup>06] compared different patient positioning techniques, imaging modalities and degrees of immobilization in patients with prostate cancer and implanted gold marker seeds regarding the accuracy of patient positioning.

[vLFH<sup>+</sup>06] did research on gold marker-based three-dimensional fusion of CT with dynamic contrast-enhanced and <sup>1</sup>H-spectroscopic MRI. According to the authors, a study with a larger patient population should follow to consolidate the preliminary results.

## 2.7 The proposed method

In this thesis, an electromagnetic tracking system is used to localize the position of the prostate cancer more precisely. A magnetic tracking system was chosen because it is the only possibility to track flexible instruments inside the patient's body.

The idea is to attach the magnetic sensor of the tracking system to the balloon catheter and to insert both into the rectum. The magnetic sensor and the balloon are seen on the images of the computer tomography scan that is done before the intervention. The distance between the magnetic sensor and the prostate cancer is calculated using the images from the CT scan. With the tracking data provided by the magnetic tracking system and the calculated distance between sensor and tumor, the treatment table can be moved in a way that the prostate cancer is then located in the isocenter of the linear accelerator.

The limitation of the described method is that the magnetic tracking system is distorted by metal in its range. Ideal would be to remove all interferences, but metal is present in the radiation room in the form of the linear accelerator, the treatment table and medical equipment that cannot be removed. An error correction algorithm has to be applied to the tracking data to compensate these distortions.

## 2.8 The visionary medical workflow

This section describes the visionary medical workflow for the proposed method.

An electromagnetic tracking system is put in the radiation room. A personal computer with the implemented application stands in the radiation room and is connected to the tracking system. The sensor of the magnetic tracking system is rigidly attached to the patient's balloon catheter.

The technical personnel is responsible for creating a lookup-table. It maps the distortion field in the radiation room and is used to correct measurements of the magnetic sensor that are distorted by metal in the room. A device called target with a second magnetic sensor inside is used to collect the lookup-table. The target is moved around and has to cover the entire volume at the place where the prostate of the patient will be located later. The creation of the lookup-table needs to be done whenever the setting has changed.

Before the first radiation of a patient, the balloon catheter with the attached magnetic sensor is inserted into the patients' rectum by a doctor and a CT scan of the patient is done. The balloon, the magnetic sensor and the prostate cancer are imaged on the CT. The distance between the prostate cancer and the magnetic sensor can be computed from this.

The patient comes into the radiation room every weekday to get irradiated. The balloon catheter with the attached magnetic sensor is again inserted to the rectum by a doctor. The data from the lookup-table is used to correct the tracking data coming from the magnetic sensor. Hence, the corrected position of the magnetic sensor is known. The distance between the magnetic sensor and the prostate cancer was computed before by the implemented application. It is used to calculate the needed shift of the treatment table for the x-, y- and z-axis. The table is then moved by an assistant medical technician according to the specifications of the software. Now the center of the prostate cancer is in the isocenter of the gantry. The radiation can be started.

## Technical and theoretical background

This chapter contains technical and mathematical background information about tracking systems and the used algorithms. It provides background information about electromagnetic and optical tracking systems, gives mathematical background information about homogeneous coordinates, hand-eye calibration, point-based registration and Hardy's multi-quadric method and presents related work and preliminary work done by Kaur.

### 3.1 Tracking systems

A tracking system is a device to determinate the position of an object in space with six degrees of freedom in real time. Rotation and translation of the object are given in the coordinate system of the tracking system. "Pose" describes rotation and translation of an object, that means position and orientation with six degrees of freedom.

In medicine, tracking is used for navigation systems. For example it can be used to localize surgical instruments.

There are different kinds of tracking system that use different approaches to track objects. Magnetic tracking systems use electromagnetic fields to track the object while optical tracking systems use infrared light and infrared light reflecting materials on the object. There are also ultrasound tracking system using ultrasound and mechanical tracking systems where the object is connected to the tracker via a linkage. (See [ABW01] for a classification of tracking systems.)

Every kind of tracking systems has advantages and disadvantages that are related to their functionality.

For my diploma thesis I used an electromagnetic and an optical tracking system. Both systems are explained in the following sections.

### 3.1.1 Electromagnetic tracking systems

Electromagnetic tracking systems assign the pose of an object with the help of electromagnetic fields. An electromagnetic transmitter, also called field-generator, uses three mutually orthogonal coils to generate an electromagnetic field. A sensor of the magnetic tracking system contains three mutually orthogonal coils, too. The current flows sequentially through each of the coils inside the field-generator. This causes the coil to become an electromagnet for a short moment. The coils in the sensor measure the strength of the magnetic field. The measurements are used to calculate the pose of the sensor relative to the transmitter. The tracking of both position and orientation is described more detailed in [RBSJ79].

A third component of a magnetic tracking systems is a so called control box that does the computations using data from the field-generator and the sensor for this purpose.

Electromagnetic tracking systems can use more than one sensor. The positions of the sensors can be calculated simultaneously.

Advantages of electromagnetic tracking systems are the tracking of flexible instruments, the low price and the good transportability. Its major advantage is that it can be used for tracking inside the human body what makes it very interesting for medical applications.

A disadvantage is that electromagnetic tracking systems are sensible to metal. The electromagnetic field that is generated by the magnetic tracking system makes it susceptible to metal, conductive material and equipment that produces an electromagnetic field near the transmitter or sensor. These sources of interference can be computer monitors, keyboards, power supplies and much more. Interferences cause erroneous computations of the sensor's pose in space.

Two kinds of errors can occur: static and dynamic errors. Dynamic errors occur over time by the earth's magnetic field and by moving metallic objects in its range, but because of its randomness they cannot be corrected. Static errors are caused by objects made from interfering materials that reside inside the tracking volume. These errors are composed of rotation and translation errors and can be corrected. Usually, the hardware already does some basically error corrections.

Static tracking errors can be corrected with several algorithms. [Kin00] gives the methods high-order polynomial fit, trilinear interpolation, Hardy's multiquadric method and neural network based methods as examples for correction algorithms. Hardy's multiquadric method was used for error correction in this thesis. It is explained in [Har71] and in section 3.2.4 on page 34. Trilinear interpolation as error correction algorithm was analyzed by Kaur in [Kau06] and is explained in 3.3.4.2 on page 43.

Nowadays several magnetic tracking devices are available. Their main difference is if they work with direct current (DC) or alternating current (AC).

Magnetic tracking systems on the market include "Aurora" by Northern Digital, "Flock of Birds" by Ascension Technology, "Isotrack" by Polhemus, "Fastrack" by Polhemus, "miniBird" by Ascension Technology and "microBird" by Ascension Technology, just to mention a few.

[IBHH01] and [Kin99] worked on the correction of orientation errors by applying a high order polynomial.

### 3.1.2 Optical tracking systems

An optical tracking system generates flashes of infrared light and uses special cameras that can detect reflections to track an object. For this purpose, the object is equipped with markers made from optically retroreflecting material. The infrared light is emitted by LEDs<sup>1</sup> that are placed around the lens of the camera. A tracking software uses the images of the cameras and additional information about the distance between the cameras and the configuration of the markers attached to the object to compute the position of the object in space with six degrees of freedom.

The object needs to be extended by material that reflects infrared light. Either retroreflecting stickers or spheres are attached to the object that reflect the light passively or LEDs are attached that actively emit light.

The object can be any kind of tool, e.g. a surgical instrument. It has to be extended with reflecting spheres or LEDs. The arrangement of the markers is announced to the software via a calibration procedure. For six degree-of-freedom tracking, at least three not-colinear markers need to be attached. The optimal arrangement of the markers is a complex problem. The configuration of the markers depends on the purpose of the tool and the required accuracy and the markers should not interfere with the medical workflow during surgery and should be detected easily by the tracking cameras.

If more than one tool shall be tracked, the marker configuration of the tools need to differ when passive markers are used. In case of active markers, the markers of the tools need to use different flash frequencies.

At least two cameras are needed for optical tracking. Additional cameras can increase the accuracy of the tracking system when the cameras are arranged to each other in a way such so that the possibility of the occlusion of markers is reduced. The distance and orientation of the cameras to each other needs to be announced to the tracking software.

The region where the cameras can track objects is known as working volume or tracking volume. This is the area where the visual fields of the cameras overlap.

The advantage of optical tracking systems is their high precision. The error is smaller than 1 mm. According to the manufacturers the accuracy is 0.3 mm in the defined working volume. This high accuracy makes optical tracking a good choice for surgical interventions and other applications that rely on a high accuracy. Optical tracking is wireless; there is no linkage between the tracked objects and the cameras.

One disadvantage of optical tracking systems is the high price. Another disadvantage is that optical tracking cannot be used to track flexible instruments inside the human body. The reason is that a free line-of-sight between the cameras and the markers on the object is needed. Additional, optical trackers need much space to be put up.

The software and cameras called "dtrack" by Advanced Realtime Tracking GmbH are one recent optical tracking system. The stereo camera system "smARTtrack" is also manufactured by A.R.T. Another optical tracking system is "Polaris" by NDI.

---

<sup>1</sup>light emitting diodes

### 3.1.3 Coregistration of magnetic and optical tracking systems

Whenever an electromagnetic and an optical tracking system are used together, a coregistration of both systems is needed. During coregistration the transformation between the coordinate systems of the two coordinate systems is determined.

Auer and Pinz in [AP99] combined a magnetic tracking system with an optical tracking system for robust and precise tracking of position and orientation. The user wore a helmet with a head-mounted display, a magnetic sensor and two cameras. Their tracking primitives were corners in the camera images. Pose information from the magnetic tracking system was used to predict search areas on the images. The optical tracking system computed position and orientation of the cameras and thus the user. The result of the optical tracking system was checked against the result of the magnetic tracking system to detect features that were misidentified.

Birkfellner in [Bir00] computed the rigid body transformation between the reference frames of an electromagnetic tracking system and an optical tracking system using a point-to-point registration. He created a magnetic-optical probe by putting two magnetic sensors into a stylus with active optical markers. His hybrid tracking system could be used in situations when tracking data from both tracking systems was available so that the optical tracking system could correct erroneous magnetic tracking data as well as in situations when only the magnetic tracking system was available. He attached two magnetic sensors to the stylus in a distance of 100 mm and monitored the distance between them. As the sensors were attached in a fixed distance, a deviation of the computed distance proved that the readings of the magnetic tracking system were distorted. In this case, the readings of the magnetic tracking system were discarded. The mean localization precision of an optimized hybrid tracking system was  $2.1 \text{ mm} \pm 0.9 \text{ mm}$  according to Birkfellner.

In this work, an optical tracking system is used to compute the undistorted pose of a potentially distorted pose of a magnetic sensor of an electromagnetic tracking system. Two unknown transformations within a loop of transformations of both tracking systems have to be computed during an initial device calibration step to be able to register the tracking systems to each other. This is done using hand-eye calibration. The readings of the optical tracking systems can then be transformed into the coordinate system of the magnetic tracking system. A lookup-table containing undistorted values and corresponding distorted values of poses of the magnetic sensor is used as basis for an error correction method. The algorithm corrects the current distorted sensor pose by using information about the actual distortion field stored in the lookup-table.

## 3.2 Mathematical background

This sections describes the mathematics that is used in this diploma thesis. The main topics are homogeneous coordinates, calibration, registration and Hardy's multiquadric method. Some statistical background regarding the analysis of errors is also treated.

### 3.2.1 Homogeneous coordinates

Cartesian coordinates represent a point  $\vec{q}$  in 3D space as a vector with three elements, usually written as

$$\vec{q} = \begin{pmatrix} x \\ y \\ z \end{pmatrix}$$

In homogeneous coordinates, a point  $\vec{p}$  in 3D space has an additional fourth element:

$$\vec{p} = \begin{pmatrix} x \\ y \\ z \\ w \end{pmatrix}$$

Mostly  $w = 1$ , but in general  $w$  is defined as  $w \neq 0$ . Points with  $w = 0$  are points at infinity. They are used seldom.

Two points where the elements of one point are a multiple of the elements of the other point represent the same point with  $w = 1$ . For example, the point  $p$  can be represented in two ways:

$$\vec{p} = \begin{pmatrix} x \\ y \\ z \\ w \end{pmatrix} = \begin{pmatrix} \frac{x}{w} \\ \frac{y}{w} \\ \frac{z}{w} \\ 1 \end{pmatrix} \quad p \in \mathbb{P}^3$$

More detailed information about homogeneous coordinates can be found in [ABW01].

#### 3.2.1.1 Coordinate transformations

Points are often transformed during computations. The transformations I used most are translation and rotation around an axis.

In cartesian coordinates, rotation  $R$  and translation  $\vec{t}$  of a point are written like

$$q' = R \cdot q + \vec{t}$$

There  $R$  is a  $3 \times 3$ -matrix and  $\vec{t}$  a vector with three elements.

In homogeneous coordinates, both rotation and translation are represented as  $4 \times 4$ -matrices that can be multiplied into one matrix  $M$ :

$$p' = M \cdot p$$

where  $M$  is a  $4 \times 4$ -matrix with a  $3 \times 3$ -rotation part  $R$  and a  $3 \times 1$ -translation part  $T$ .

$$M = \left( \begin{array}{ccc|c} & & & t \\ & R & & \\ \hline 0 & 0 & 0 & 1 \end{array} \right)$$

An advantage of homogeneous coordinates in comparison to cartesian coordinates is that in homogeneous coordinates rotation and translation can be written in one matrix. It is also possible to write several rotations and translations as a chain of matrix-multiplications instead of using addition for translations. This makes calculation with translations and rotations easier than it is in cartesian coordinates.

Scaling can also be written in matrix form.

Rotation, translation and scaling are represented by  $4 \times 4$ -matrices.

**Translation** A translation  $T$  is written as a  $4 \times 4$ -matrix that is composed of a  $3 \times 3$  identity matrix and a  $3 \times 1$ -translation part  $\vec{t}$ . A translation  $T$  is denoted as:

$$T = \begin{pmatrix} 1 & 0 & 0 & t_x \\ 0 & 1 & 0 & t_y \\ 0 & 0 & 1 & t_z \\ 0 & 0 & 0 & 1 \end{pmatrix}$$

**Rotation** The appearance of the rotation matrix  $R$  depends around which axis the rotation is performed. The angle of rotation is denoted by  $\theta$ .

$$R_x = \begin{pmatrix} 1 & 0 & 0 & 0 \\ 0 & \cos \theta & -\sin \theta & 0 \\ 0 & \sin \theta & \cos \theta & 0 \\ 0 & 0 & 0 & 1 \end{pmatrix}$$

$$R_y = \begin{pmatrix} \cos \theta & 0 & \sin \theta & 0 \\ 0 & 1 & 0 & 0 \\ -\sin \theta & 0 & \cos \theta & 0 \\ 0 & 0 & 0 & 1 \end{pmatrix}$$

$$R_z = \begin{pmatrix} \cos \theta & -\sin \theta & 0 & 0 \\ \sin \theta & \cos \theta & 0 & 0 \\ 0 & 0 & 1 & 0 \\ 0 & 0 & 0 & 1 \end{pmatrix}$$

**Scaling** Scaling  $S$  of a point can be written as

$$S = \begin{pmatrix} s_x & 0 & 0 & 0 \\ 0 & s_y & 0 & 0 \\ 0 & 0 & s_z & 0 \\ 0 & 0 & 0 & 1 \end{pmatrix}$$

where  $s_x$ ,  $s_y$  and  $s_z$  are the scaling factors in x-, y- and z-direction.

### 3.2.1.2 Euler angles

Euler angles specify the rotation of an object in regard to a coordinate system. The rotation is given in the form of three successive rotations around the x-, y- and z-axis.

Due to the non-commutative matrix multiplication, the order of the multiplication matters. This is a disadvantage of the representation by Euler angles. The multiplication order is also the reason that the axis interact. When the original point is rotated around the first axis, the second rotation has a different source in comparison if the second rotation would have been done first.

Another disadvantage is that the same rotations can be achieved by different combinations of Euler angles. Therefore there is no unique way to track back from the resulting rotation to the three used Euler angles.

I used Euler angles to measure the distance between two poses in the 3D space and to ensure that I only save a pose if its distance to all previously stored poses exceeds a certain threshold.

For more information about Euler angles, please refer to [ABW01].

### 3.2.2 Hand-eye calibration

Hand-eye calibration refers to an algorithm that derives from the field of robotics. The original setting is a robot with a gripper and a tool mounted to the robot's hand. This tool can be a camera, an infrared sensor, a motion sensor et cetera. With the help of the tool, a task is assigned to the robot. The aim of the task is given in the tool's coordinate system. Therefore, the displacement between the tool's coordinate system and the robot's coordinate system needs to be known.

The distance between the origin of the robot's coordinate system and the robot's gripper is known (denoted with  $A$ ) as well as the distance between the tool's coordinate origin and the coordinates of the aim of the desired task ( $B$ ). The displacement between the tool's center and the gripper ( $X$ ) is unknown as well as the distance between the robot's origin and the coordinates of the aim's position ( $Y$ ). (See figure 3.1.)

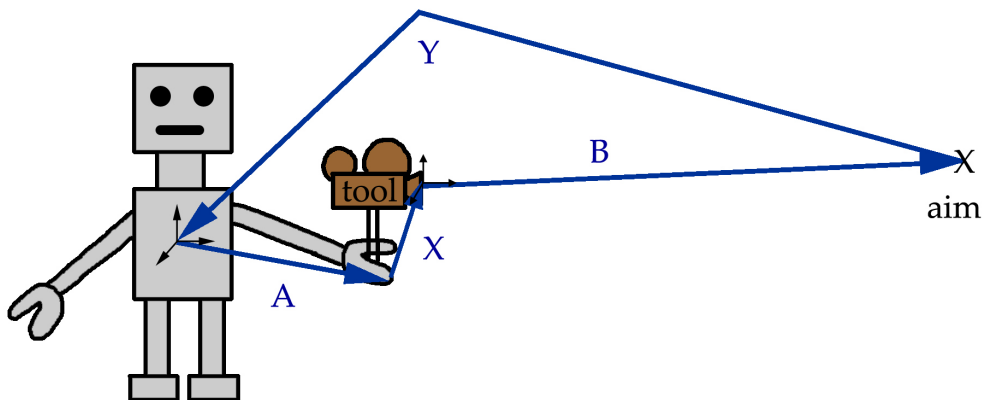


Figure 3.1: This image illustrates the original setting of hand-eye calibration.

The two unknown transformations  $X$  and  $Y$  need to be computed. Hand-eye calibration describes an algorithm that can compute  $X$  without the knowledge of  $Y$ . The unknown transformation  $X$  is calculated using different motions of the tool in the robot's hand. These motions form a loop so that the unknown transformation  $Y$  is not necessary to calculate  $X$ .

The hand-eye calibration algorithm can also be used to calculate  $Y$  afterwards in the same way by taking motions of the tool without using the transformation  $X$ .

The basic equation of the hand-eye calibration is

$$AX = XB \quad (3.1)$$

where (according to [Dan99])

$$A = A_2 \cdot A_1^{-1}$$

$$B = B_2^{-1} \cdot B_1$$

$A$  is the motion of the gripper,  $B$  is the corresponding motion of the tool.  $A_1$  and  $A_2$  are poses of the gripper and  $B_1$  and  $B_2$  are the corresponding poses of the aim of the robot's task in the coordinate system of the tool. (Compare figure 3.2.) A condition for proper poses for the hand-eye calibration is that the robot must be able to move the tool in six degrees of freedom.

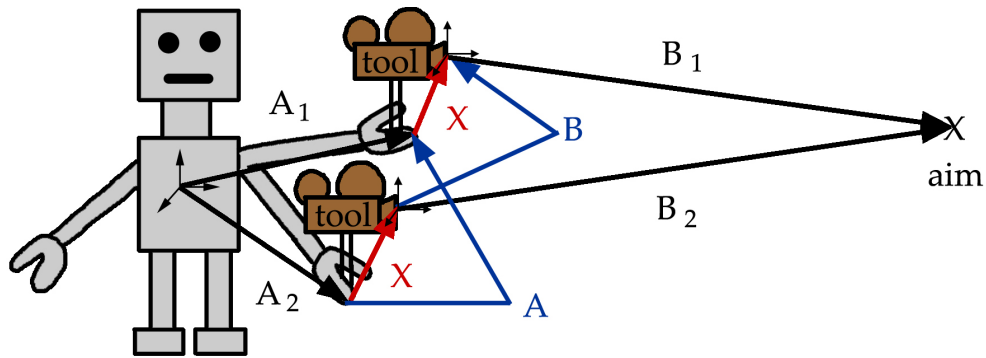


Figure 3.2: This images illustrates the situation according to equation 3.1 where one motion is given as input to the hand-eye calibration algorithm.

As  $A$  and  $B$  are known, the transformation  $X$  can be calculated with equation 3.1.

At least three motions of the tool are needed. For the given data sets of  $A_i$  and  $B_i$ , the algorithm calculates the motions between all poses of one data set and forms more equations than in equation 3.1. The hand-eye calibration then expands to a system of linear equations of the form

$$A_1 \cdot X = X \cdot B_1$$

$$A_2 \cdot X = X \cdot B_2$$

$$\vdots$$

$$A_n \cdot X = X \cdot B_n$$

where  $A_1, A_2, \dots, A_n$  are motions of the gripper and  $B_1, B_2, \dots, B_n$  are motions of the tool. This system of equations can be solved for  $X$  as the  $A_i$ 's and  $B_i$ 's are all known.

A closed-form solution for a system with two equations of the form

$$\begin{aligned}A_1 X &= X B_1 \\A_2 X &= X B_2\end{aligned}$$

was described 1995 in [SA89].

A precondition for the hand-eye algorithm is that the transformation  $X$  does not change during the collection of the thirteen poses. If  $X$  would change in between, the transformation would not be computed correctly. Therefore it has to be ensured that the tool is attached rigidly to the robot's hand and that it cannot move.

Tsai and Lenz formulated the hand-eye calibration problem in [TL88] and also described a solution. Daniilidis presented his approach for solving the hand-eye calibration problem using dual quaternions in [Dan99]. [HD95] developed an different formulation for equation 3.1 of the hand-eye calibration algorithm,  $MY = M'YB$ , where  $M$  is the projective transformation between the calibration frame and the camera frame and found a solution that solves the equation simultaneously for rotation and translation.

The authors of [SVN03] identified several factors that increase the robustness of the hand-eye calibration algorithm like taking motions with different rotation axes and eliminating outliers.

The hand-eye calibration algorithm cannot only be used in the setting with a roboter with a gripper and a tool mounted to the robot's hand. It can also be used in every setting where a sensor is rigidly mounted to a body with a similar configuration.

### 3.2.3 Point-based registration

Point-based registration finds a transformation matrix between two corresponding sets of points in space given in different coordinate systems that maps the two sets of points and the corresponding coordinate systems.

The algorithm is often used in medical applications to compute the transformation between two coordinate systems.

The two data sets can be acquired in different ways. It is possible that the coordinates of the points are directly given in both coordinate systems. Another possibility is to use markers for this purpose. The markers can be attached to the points in space and used to record the coordinates of this points by touching them with a sensor of a tracking system.

The points does not need to be stored in the same order in both data sets. An algorithm can detect corresponding points from both data sets.

Point-based registration can be used to register a patient (and his coordinate system) with his preoperatively acquired computer tomography images (and their corresponding coordinate system). The algorithm can also be used to register two tracking systems with each other.

[Ume91] presented a possibilty to solve this problem based on a closed-form solution for a least-squares problem and the solution in [WSV91] was based on dual quaternions.

### 3.2.4 Hardy's multiquadric method

Hardy's multiquadric method is a global interpolation method. Global method means that the interpolation function depends on all data points. Whenever a data point is changed, added or removed, the interpolation function needs to be solved again. This global method uses all points instead of only neighboring points.

Hardy's multiquadric interpolation method was developed by Hardy in 1971 to generate topographic maps using elevation informations of arbitrarily spread points in a plane. It is described in [Har71].

Hardy's multiquadric method solves the following equation:

$$q = f(p) = \sum_{i=1}^n A_i w_i(p) \quad p, A_i \in \mathbb{R}^3 \quad (3.2)$$

where  $f(p_i) = q_i \quad i = 1, \dots, n$   
and  $w_i(p) = \sqrt{(p - p_i)^2 + R^2} \quad R > 0$

$p$  is the point in the plane and  $q$  the elevation information for this point.

The vector  $A$  containing 3D values needs to be approximated first. Then,  $q$  can be calculated with the above formula.

**Approximating the vector  $A$**  The above formular for  $q$  gives:

$$f(p) = A_1 w_1(p) + A_2 w_2(p) + \dots + a_n w_n(p)$$

This equation can be written as system of linear equations:

$$\begin{aligned} A_1 w_1(p_1) + A_2 w_2(p_1) + \dots + a_n w_n(p_1) &= q_1 \\ A_1 w_1(p_2) + A_2 w_2(p_2) + \dots + a_n w_n(p_2) &= q_2 \\ A_1 w_1(p_3) + A_2 w_2(p_3) + \dots + a_n w_n(p_3) &= q_3 \\ &\vdots \\ A_1 w_1(p_n) + A_2 w_2(p_n) + \dots + a_n w_n(p_n) &= q_n \end{aligned}$$

It can also be written as a matrix equation:

$$\begin{pmatrix} w_1(p_1) & w_2(p_1) & w_3(p_1) & \dots & w_n(p_1) \\ w_1(p_2) & w_2(p_2) & w_3(p_2) & \dots & w_n(p_2) \\ w_1(p_3) & w_2(p_3) & w_3(p_3) & \dots & w_n(p_3) \\ \vdots & \vdots & \vdots & & \vdots \\ w_1(p_n) & w_2(p_n) & w_3(p_n) & \dots & w_n(p_n) \end{pmatrix} \cdot \begin{pmatrix} A_1 \\ A_2 \\ A_3 \\ \vdots \\ A_n \end{pmatrix} = \begin{pmatrix} q_1 \\ q_2 \\ q_3 \\ \vdots \\ q_n \end{pmatrix} \quad (3.3)$$

With the formular for  $w_i(p)$  from the beginning in equation 3.2,  $w_i(p_i)$  and  $w_i(p_j)$  can be simplified to

$$\begin{aligned} w_i(p_i) &= \sqrt{(p_i - p_i)^2 + R^2} && = R \\ w_i(p_j) &= \sqrt{(p_j - p_i)^2 + R^2} && = \sqrt{(p_i - p_j)^2 + R^2} = w_j(p_i) \end{aligned}$$

This reduces the matrix equation 3.3 to

$$\begin{pmatrix} R & w_2(p_1) & w_3(p_1) & \dots & w_n(p_1) \\ w_1(p_2) & R & w_3(p_2) & \dots & w_n(p_2) \\ w_1(p_3) & w_2(p_3) & R & \dots & w_n(p_3) \\ \vdots & \vdots & & \vdots & \\ w_1(p_n) & w_2(p_n) & w_3(p_n) & \dots & R \end{pmatrix} \cdot \begin{pmatrix} A_1 \\ A_2 \\ A_3 \\ \vdots \\ A_n \end{pmatrix} = \begin{pmatrix} q_1 \\ q_2 \\ q_3 \\ \vdots \\ q_n \end{pmatrix}$$

It gives the following system of matrix equations:

$$W \cdot A = Q \tag{3.4}$$

The 3D-vector A is computed using LU decomposition of the matrix W. As soon as A is known, the values q for points in space p can be calculated with equation 3.2 on page 34:

$$\begin{aligned} q &= f(p) = A_1 w_1(p) + A_2 w_2(p) + A_3 w_3(p) + \dots + A_n w_n(p) \\ \text{with } w_i(p) &= \sqrt{(p - p_i)^2 + R^2} \end{aligned}$$

**LU-decomposition** LU-decomposition is a method from linear algebra to compute a product of a lower and upper triangular matrix, called L and U, to a given matrix. It can be used to solve systems of linear equations.

L has the form of an identity matrix in the upper right part and on the diagonal and distinct values in the lower left part.

**Properties of the matrix W** The matrix W has the following properties:

- W has the order  $n \times n$ .
- The diagonal matrix is  $diag|W| = R$ .
- W is symmetric:  $w_i(p_j) = w_j(p_i)$ .
- W is not positive definite.
- W is conditionally positive and invertible for distinct points  $(x_i^p, y_i^p, z_i^p)$ . (Compare [Mic86] and [Pow92].)

**Parameters affecting the HMQ** The parameter  $R$  has an effect on the smoothness of the HMQ interpolant.  $R$  is also called “shape parameter”. The parameter  $R$  was analyzed in detail in [CF91]. Different formulas for  $R$  are given in the literature. Finding an optimal value for  $R$  is still an open problem. Hardy in [Har71] chose  $R$  to be:

$$R^2 = (0.815d)^2 \quad (3.5)$$

$$\text{with } d = \frac{1}{n} \sum_{i=1}^n d_i$$

$d_i$  denotes the distance from one data point to its nearest neighbour. Franke in [Fra79] used the following formula for  $R$ :

$$R^2 = \left( \frac{1.25D}{\sqrt{n}} \right)^2$$

where  $D$  is the diameter of the smallest circle containing all data points.

[CF91] found out that *the size of the matrix  $W$*  effects its condition number. The number increases as the size increases. [HL93] gave 200 as maximum size of the matrix  $W$ .

Another factor of influence is the *condition numbe of the matrix  $W$* . If the points  $p$  in the lookup-table are very near to each other, the matrix  $W$  is poorly conditioned. Precondition can be done before applying Hardy’s interpolation to avoid this problem.

**Related work about Hardy’s multi-quadric method** [Fra82] analyzed several scattered data interpolation algorithms and concluded that Hardy’s multiquadric method is one of the best algorithms.

Kaur in [Kau06] compared Hardy’s multiquadric method with trilinear interpolation for the distortion correction of an electromagnetic tracking systems. Her results are described in detail in section 3.3 about preliminary work on page 38.

[Zac97] implemented Hardy’s multiquadric method to correct the distortions that occurred during magnetic position tracking.

For large data sets, Franke and Nielson in [FN80] proposed to compute Hardy’s multi-quadric interpolant for previously defined subdomains.

### 3.2.5 Statistics

For analysis and comparison of the results of my experiments, the statistical measures mean error and standard deviation were used. They are described in this section as well as different kind of errors that can occur during measurements.

#### 3.2.5.1 Mean error

The mean error, also called mean squared error, is a quantity telling the average value of a sample.

For  $n$  values  $x_i$  collected in the trials, the mean squared error  $\bar{x}$  is defined as

$$\bar{x} = \frac{1}{n} \sum_{i=1}^n x_i$$

### 3.2.5.2 Standard deviation

The standard deviation  $\sigma$  measures the average variation of the  $n$  values in a data set around the mean error  $\bar{x}$ .

$$\sigma^2 = \frac{1}{n} \sum_{i=1}^N (x_i - \bar{x})^2$$
$$\sigma = \sqrt{\frac{1}{n} \sum_{i=1}^N (x_i - \bar{x})^2}$$

A small  $\sigma$  tells that the values in the data set are very close to the mean error  $\bar{x}$ , while a large standard deviation tells that the values vary very much around the mean error.

The standard deviation has the same unit as the  $n$  values.

Mean error and standard deviation are often given together as  $\bar{x} \pm \sigma$ , for example  $5.3 \pm 1.7$  mm.

### 3.2.5.3 Different kinds of errors

In my diploma thesis, the error is defined as distance between the true position and the measured distorted position of an object in space. There, two kinds of errors can occur. They are called random error and systematic error.

**Random error** Terms like bias, non-systematic error, static error, outlier or noise mean the same as random error. Random errors occur randomly in the data sets. They do not follow a mathematical function. Therefore, they can not be anticipated and they also cannot be removed from the data set.

An example for a random error is the electromagnetic field of the earth that can influence all kinds of electronic equipment randomly. Therefore, electromagnetic tracking systems can be distorted by the earth's field. Another example is a surgical tool that is moved in the range of an electromagnetic tracking system during an intervention.

**Systematic error** Systematic errors are errors that obey a mathematical function. If this function is known, the systematic error can be calculated and removed from the data set.

For example, a metallic object that lies still in the range of an electromagnetic tracking system can cause a systematic error. The hardware itself can also cause systematic errors.

### 3.3 Preliminary work

Preliminary work concerning error correction for electromagnetic tracking was done at the chair by Suhkbansbir Kaur. Her Master's Thesis is entitled "Error Correction for Electro-Magnetic Tracking", handed in April 2006. This section gives an overview over her work. For more details, please refer to her thesis in [Kau06].

#### 3.3.1 Motivation for Kaur's work

From the various kinds of tracking systems, optical and electromagnetic trackers are most commonly used in medical applications. Both can be used to track medical instruments.

Optical tracking systems are very precise, but they need a line-of-sight between the tracking cameras and the tracked objects. Therefore they cannot be used for tracking inside the human body. Electromagnetic tracking systems have very small sensors that can be used for tracking inside the human body. But they are susceptible for distortions by metal like technical instruments in the room. Tracking errors due to metal in the room could be avoided by removing all metal in the operational range tracking system. But in medicine, this is not very feasible because one would need to replace all metal equipment in the operating room like the medical instruments, monitors, the patient's table with equipment made from plastic or wood. This would be very expensive and besides not doable for all kinds of equipment.

Distortion correction is needed to be able to use electromagnetic tracking nevertheless. Kaur implemented two approaches for distortion correction. The idea behind both approaches is to know the true position and orientation of the electromagnetic sensor in space and create a lookup-table containing the true position in space, called ground truth data, and the measured position. This lookup-table is created in the distorted setting and can be used later to track the sensor inside the human body. The first approach used a polymer block with  $11 \times 11$  holes in it every 1 cm to create the lookup-table. The sensor was inserted in one hole after the other and the position of the sensor was recorded. Kaur's second approach used an optical tracking system to create the lookup-table.

#### 3.3.2 Distortion correction with the polymer block

In the first approach for correcting the distortion of the electromagnetic tracking system due to metal in the operational range of the electromagnetic tracking system, a polymer block was used to create the lookup-table.

The used polymer block measures  $12 \times 12 \times 8$  cm. On top, the polymer block has  $11 \times 11$  holes in it, with a displacement of 1 cm in each direction. The holes are approximately 1.7 cm deep. It is shown in figure 3.3 on page 39.

One corner point was appointed to be the origin of the block. Therefore, the position of every point on the block was known in the coordinate system of the block.

The corrected position of the sensor was needed in the coordinate system of the electromagnetic tracking system. Therefore, the wooden block was registered to the tracking system using point-based registration (compare section 3.2.3 for details). The positions of the four



Figure 3.3: The polymer block used by Kaur for one approach of distortion correction for electromagnetic tracking. Picture taken by Kaur.

corner points of the block were recorded, once in the coordinate system of the tracking system and second in the coordinate system of the block. This two data sets were used as input for the point-based registration and gave the transformation  ${}^tT_b$  from the coordinate system of the wooden block into the coordinate system of the tracking system as result.

The lookup-table needed to be in the coordinate system of the electromagnetic tracking system, too. The positions of the measurements of the sensor inside the 121 holes were already given in the coordinate system of the electromagnetic tracking system. But the true position of the sensor was given in block coordinates and therefore needed to be transformed into the electromagnetic coordinate system using the transformation  ${}^tT_b$  from the previous step.

The lookup-table then contained of 121 lines. Every line gave the position of one hole on the wooden block, first the true position of the sensor in the hole, called ground truth value, and then the -probably distorted- measured position of the sensor for the same hole.

The lookup-table was used to correct positions of the sensor on a 2D grid.

This lookup-table method can also be used for obtaining 3D lookup-tables. For this purpose, the polymer block needs to be moved additionally in the third direction.

Validation data was recorded by Kaur to analyze the quality of the error correction method.

### 3.3.3 Distortion correction with an optical tracking system

The method with the polymer block is very accurate, but inconvenient and rather time-consuming. Therefore Kaur decided to try an other approach for collecting the lookup-table. The second approach used an optical tracking system for creating the lookup-table. The optical tracking system was used to compute the true positions of the electromagnetic sensor.

### 3.3.3.1 The setting

The sensor of the electromagnetic tracking system was rigidly attached to an optical reference frame, consisting of optical markers. The pose of the sensor was given in the coordinate system of the electromagnetic tracking system and the pose of the optical target attached to the sensor was given in the coordinate system of the optical tracking system. The idea was to get two poses for the sensor, one reported directly by the electromagnetic sensor and the other pose obtained with the help of the optical tracking system. The pose reported with the help of the optical tracking system was regarded as the true position of the sensor (due to the high precision of optical tracking systems) and therefore saved as ground truth values in the lookup-table. The position of the sensor given by the electromagnetic tracking system was seen as probably distorted and in need of distortion correction. It was also saved in the lookup-table, in one line together with the corresponding ground truth value.

Some preparation was needed before the lookup-table could be created because the optical system did not give the ground truth values directly. A transformation was needed from the center of the optical target to the tip of the electromagnetic sensor. This transformation is denoted  ${}^{os}T_{ms}$  in figure 3.4.

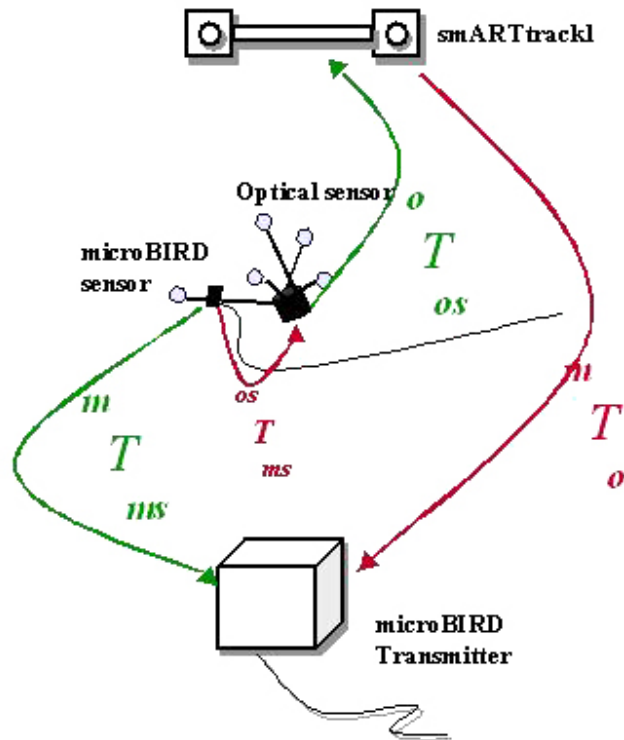


Figure 3.4: The optical setting with the involved transformations. Picture taken from [Kau06]

To be able to transform the optical values for the sensor into the electromagnetic coordinate system, another transformation was needed. This is the transformation between the origins of the optical and the electromagnetic tracking systems. It is denoted  ${}^mT_o$  in figure 3.4.

If both transformations  ${}^{os}T_{ms}$  and  ${}^mT_o$  are known, the transformation for the ground truth values from the optical origin to the origin of the electromagnetic tracking system can be calculated with this formula:

$${}^mT_{ms} = {}^mT_o \cdot {}^oT_{os} \cdot {}^{os}T_{ms} \quad (3.6)$$

Transformation  ${}^mT_{ms}$  from figure 3.4 denotes the position of the sensor reported by the electromagnetic tracking system while  ${}^oT_{os}$  is the position of the optical target given by the optical tracking system.

### 3.3.3.2 Calculating the unknown transformations

The two unknown transformations are  ${}^{os}T_{ms}$  and  ${}^mT_o$ .  ${}^{os}T_{ms}$  is the transformation inside the target, transforming from the magnetic sensor to the optical reference frame.  ${}^mT_o$  denotes the transformation from the origin of the optical tracking system to the origin of the electromagnetic tracking system.

Kaur solved this problem with the help of hand-eye calibration as described in section 3.2.2 on page 31.

As soon as all transformations were known, the lookup-table could be created. The lookup-table was created by moving the target through space and collecting the ground truth poses of the magnetic sensor given by the optical tracking system and the poses given by the magnetic tracking system at the same moments in time. The poses of the optical tracking system needed to be transformed into the real ground truth values by applying formula 3.6.

Moving the target around in space was faster and more convenient than collecting the lookup-table with the polymer block. This method is more useful than the first approach when the setting changes frequently because the lookup-table has to show the actual displacement vector.

### 3.3.4 Applied algorithms

A lookup-table was collected in the step before to be able to correct static position errors of the electromagnetic tracking system. In this step, different interpolation-algorithms for the online error correction were compared. After the lookup-table was collected, an algorithm was applied to the lookup-table to get the corrected value for the current position of the magnetic sensor in the distorted setting. The distorted setting may not change during the creation of the lookup-table and the online error correction or otherwise the algorithm will give a wrong result because it then uses an outdated distortion field.

Giving the lookup-table as input with its set of distorted points and corresponding ground truth values of the magnetic sensor as input, the aim of the compared interpolation algorithms was to find a function that mapped the two sets of points. Herbey, P denoted the set of points that was measured with the magnetic tracking system and therefore was distorted due to metal in the tracking volume, while Q was the set of corresponding ground truth values. The points were denoted with  $p_i \in P \subset \mathbb{R}^3$  and  $q_i \in Q \subset \mathbb{R}^3$  respectively.

The mapping function  $f$  is given as

$$f : P \rightarrow Q \quad \text{with } f(p_i) = q_i \quad \forall i = 1 \dots N$$

$$\text{where } p_i = (x_i^p, y_i^p, z_i^p) \text{ and } q_i = (x_i^q, y_i^q, z_i^q)$$

Kaur analyzed bilinear interpolation in 2D and compared trilinear interpolation in 3D with Hardy's multiquadric method. All mentioned interpolation methods are introduced in the following.

### 3.3.4.1 Bilinear interpolation

The bilinear interpolation error correction algorithm is applied to 2D data. That means the bilinear interpolation can only be applied if the lookup-table was created in 2D without moving the polymer block or the combined target along the third axis. In this 2D case,  $p_i \in P \subset \mathbb{R}^2$  and  $q_i \in Q \subset \mathbb{R}^2$ . Bilinear interpolation is a local method.

The formula for the bilinear interpolation is

$$q(x, y) = (1 - t)(1 - u)q_1 + t(1 - u)q_2 + (1 - t)uq_4 + tuq_3$$

$$\text{where } t = \frac{x^p - x_1^p}{x_2^p - x_1^p}$$

$$\text{and } u = \frac{y^p - y_1^p}{y_4^p - y_1^p}$$

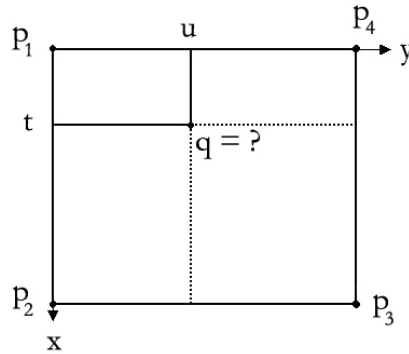


Figure 3.5: This picture illustrates the formula for the bilinear interpolation. Picture taken from [Kau06]

The points from the lookup-table are divided into non-intersecting squares for the algorithm as bilinear interpolation uses the vertices of a square to interpolate locally inside it. The corrected value  $q$  is calculated for a measured point  $p$  with the help of the above formula. The four points  $p_i$  that surround  $p$  in a square are found using the lookup-table.

Bilinear interpolation restricted the topology of the lookup-table. It should be composed of non-intersecting squares. The bilinear interpolation algorithm only worked properly when the distortion was linear in the setting. Bilinear interpolation is discontinuous at boundaries of grid squares, but  $C^1$ -continuous inside the squares.

### 3.3.4.2 Trilinear interpolation

The trilinear interpolation algorithm works on a 3D grid. Like bilinear interpolation, it is a local method.

$Q$  with  $q_i \in \mathbb{R}^3$  denotes the set of ground truth values, while  $P$  with  $p_i \in \mathbb{R}^3$  is the set of tracking data coming from the magnetic tracking system and therefore assumed to be distorted by metal.

The formula for trilinear interpolation is as follows:

$$q = (1-t)(1-u)(1-w)q_1 + t(1-u)(1-w)q_2 + tu(1-w)q_3 + (1-t)u(1-w)q_4 + (1-t)(1-u)wq_5 + t(1-u)wq_6 + tuwq_7 + (1-t)uwq_8$$

where  $t = \frac{x^p - x_1^p}{x_2^p - x_1^p}$ ,

$$u = \frac{y^p - y_1^p}{y_4^p - y_1^p}$$

and  $w = \frac{z^p - z_1^p}{z_5^p - z_1^p}$

Trilinear interpolation works similar to bilinear interpolation, but in 3D instead of 2D. For correcting a point  $p$ , it uses the information of eight surrounding vertices  $p_i$  that form a cube. The corresponding ground truth value  $q$  to the distorted value  $p$  is calculated with the above formula.

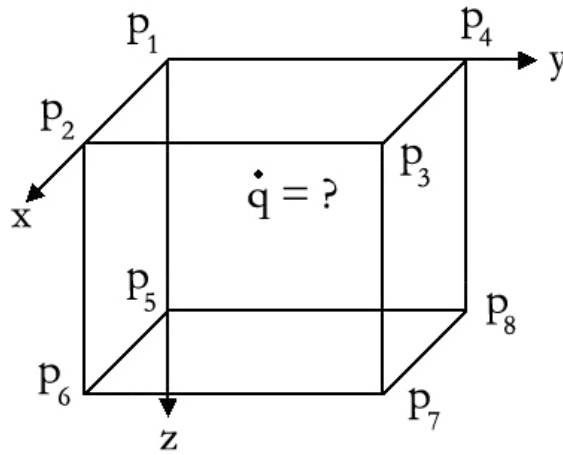


Figure 3.6: This picture illustrates the formula for the trilinear interpolation. Picture taken from [Kau06]

Trilinear interpolation could only be applied to a lookup-table containing non-intersecting cubes. If the lookup-table did not fit this restriction, it had to be resampled or recreated. Trilinear interpolation assumed that the distortion is linear. Therefore, the algorithm could only be applied in cases where the distortion was linear. Trilinear interpolation is  $C^1$ -continuous inside the cube but  $C^0$ -continuous on the borders of the cubes.

### 3.3.4.3 Hardy's multiquadric interpolation

Hardy's multiquadric interpolation algorithm is a global interpolation method that comes from the field of cartography. It was developed by Hardy 1971. The algorithm is explained in detail in [Har71] and is summarized in section 3.2.4 on page 34.

Kaur used Hardy's multiquadric method to interpolate distorted magnetic tracking values  $p$  using corresponding ground truth values  $q$  from a lookup-table using the formula

$$q = f(p) = \sum_{i=1}^n A_i w_i(p) \quad p, A_i \in \mathbb{R}^3 \quad (\text{compare equation 3.2 on page 34})$$

where  $f(p_i) = q_i \quad i = 1, \dots, n$   
and  $w_i(p) = \frac{1}{\sqrt{(p - p_i)^2 + R^2}} \quad R > 0$

Hardy's multiquadric method used a point  $p$  from the magnetic tracking system, assumed to be distorted, as input and gave the corresponding interpolated ground truth values  $q$  as result.

**Calculating the vector A** The vector  $A$  needed to be approximated first before calculating  $q$  with the above formula.

In order to calculate  $A$ ,  $A$  and  $Q$  were considered being  $n \times 3$  vectors containing  $x$ -,  $y$ - and  $z$ -values in  $n$  lines each called  $X_a, Y_a, Z_a$  and  $X_q, Y_q$  and  $Z_q$  respectively. Therefore, equation 3.4 from page 35 could be rewritten as system of three linear equations:

$$\begin{aligned} W \cdot X_a &= X_q \\ W \cdot Y_a &= Y_q \\ W \cdot Z_a &= Z_q \end{aligned}$$

where  $X_a, Y_a, Z_a, X_q, Y_q$  and  $Z_q$  are of order  $n \times 1$ .

**A suitable value for R** Kaur chose  $\sqrt{0.815d}$  as value for  $R$ . with  $d = \frac{1}{n} \sum_{i=1}^n d_i$  where  $d_i$  denotes the distance from one data point to its nearest neighbour after testing several values for  $R$ . This is the value proposed by Hardy himself.

### 3.3.5 Comparison of different interpolation algorithms in 2D and 3D

Kaur compared the results from the three algorithms on the basis of position errors, mean errors and standard deviation. For the definition of mean error and standard deviation, see section 3.2.5 on page 36. The experimental courses for each algorithm are explained in the following as well as the results.

### 3.3.5.1 2D error correction with bilinear interpolation

Suhkbansbir Kaur recorded a 2D data set with the help of the polymer block in a distorted setting. The error correction was done using bilinear interpolation.

The setting was distorted by a metallic light source of an endoskope that was put in the middle between the field-generator of the microBird magnetic tracking system and the block. The setting can be seen on figure 3.7.



Figure 3.7: The distorted setting for the bilinear interpolation. Picture taken by Kaur.

Data was collected by putting the magnetic sensor successively in the 121 holes on the block. Only 66 of the collected 121 points were used for the lookup-table, the other 55 points was used for validation. The collected data set can be seen in figure 3.8 on page 46.

### 3.3.5.2 Results for 2D error correction

Mean errors were calculated before and after the bilinear interpolation was applied to the data set in the setting distorted by the light source. The mean error in the uncorrected case was 6.711 millimeters, in the corrected case the mean error was 1.4374 mm. The maximum mean error for the uncorrected data was 15.173 mm, the minimum mean error for the uncorrected case was 3.4753 mm. For the corrected data set, the maximum mean error was 4.4575 mm and the minimum mean error was 0.10439 mm. The bilinear interpolation achieved an improvement of 78.5%.

The amount of the position errors depended on two factors: the distance of the sensor from the metallic light source and the distance of the sensor from the field-generator. When the sensor was close to the field-generator, it was also close to the source of distortion. The position error was then mainly because of the metal box. When the sensor was farther away from the field-generator, it was also farther away from the source of distortion. In this case, the position error was mainly because of the distance from the field-generator.

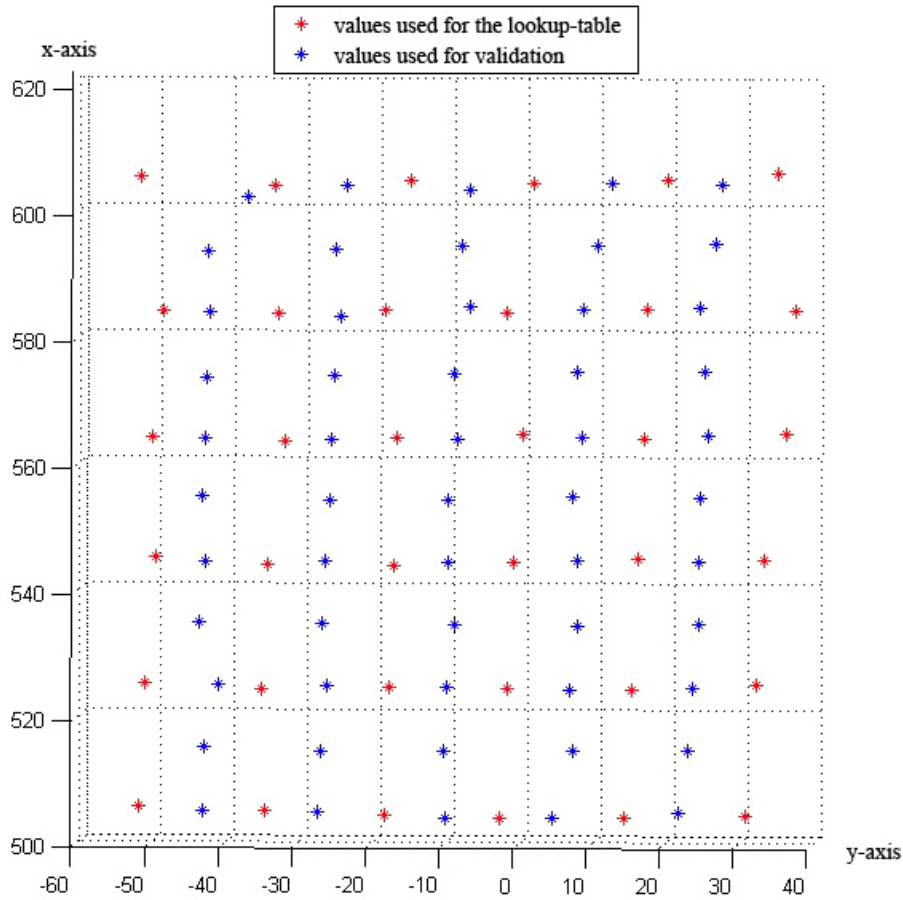


Figure 3.8: The points used for the lookup-table are marked with a red asterisk, blue asterisks mark the points used for validation. Picture taken from [Kau06]

### 3.3.5.3 3D error correction with trilinear interpolation and Hardy's multiquadric interpolation

A dataset was collected and used for trilinear error correction as well as for Hardy's multiquadric method.

The data set was recorded in the radiation room of the Klinikum Rechts der Isar, Munich, Germany. In this room, the main source of distortion is the gantry of a linear accelerator.

The lookup-table was recorded using the polymer block. To obtain 3D data, the process was changed slightly in comparison to the 2D case. The block was not put with the holes on top but was rotated so that the holes faced the field-generator of the electromagnetic tracking system. In order to obtain 3D data, the sensor was placed inside all the holes on the block and then the block was moved 1 cm away from the transmitter and the sensor was again put in the holes on the block. The block was then again moved away 1 cm from the field-generator and the sensor was put in the holes for the last time. The shifts of the block were done in the x-axis in the coordinate system of the electromagnetic tracking system.

The recorded data set was composed of three subdata sets, each subdata set taken with the block at another x-position in space. The data set was composed of 3\*121 points. For each of the 363 points, two values were stored. One value was the ground truth position of the corresponding hole on the block in the coordinate system of the magnetic tracking system, the other value was the distorted position of the magnetic sensor, also given in the coordinate system of the magnetic tracking system. So all in all, the complete recorded data set consisted of 726 points arranged in three subsets, each composed of two parts.

Both outer subdata sets were used for creating the lookup-table, while the inner data set was used to validate the trilinear interpolation and Hardy's multiquadric method.

For the trilinear interpolation algorithm, the lookup-table needs to form cubes in the tracked space. Therefore the lookup-table had to be adjusted to this requirement and differed from the lookup-table that was used for Hardy's multiquadric method. The displacement of the three data sets was changed to 2 cm in x-, y- and z-directions for the lookup-table that was used for trilinear interpolation. The lookup-table for Hardy's multiquadric algorithm was also changed slightly so that the displacement of 1 cm in y- and z-direction remained, but for the x-direction, it was changed to 2 cm.

#### **3.3.5.4 Results for 3D error correction**

The mean error for the uncorrected values (that is before applying any error correction algorithm) was 50.6488 mm. The minimum mean error was 18.4630 mm, the maximum mean error was 106.5555 mm.

The mean error after applying trilinear error correction was 5.0921 mm with a maximum mean error of 21.1484 mm and a minimum mean error of 0.53903 mm.

After applying Hardy's multiquadric method, the mean error was 1.4039 mm. The maximum mean error was 10.4276 mm, the minimum mean error was 0.17025 mm.

Comparison of the mean errors shows that trilinear interpolation as well as Hardy's multiquadric method could correct the uncorrected data set. That means that the intended improvement could be realized. Regarding the mean errors, Hardy's multiquadric method gave the best result because the maximum error and the standard deviation for this method were smaller than for the trilinear interpolation. Both methods could improve the distortions, but the trilinear interpolation was not so successful for larger distortions and jumps at grid borders occurred while Hardy's multiquadric method did not have these disadvantages.

The parameter R for Hardy's multiquadric method was chosen as given in equation 3.5 on page 36 and proved to be suitable.

Errors are dependant on the distance from the transmitter. Therefore, Kaur generated figure 3.9 on page 48 that shows the position error in mm as function of the distance of the sensor from the transmitter. Usually a higher distance between sensor and transmitter results in an increased error, but the opposite occurred for Kaur's setting. She said the reason for this was that metal near the transmitter had a greater effect on the error than the distance between transmitter and sensor. This meant that whenever the sensor was nearer to the transmitter (this resulted in a decreased error), it was also nearer to the metal (so that this error source dominated over the decreased error).

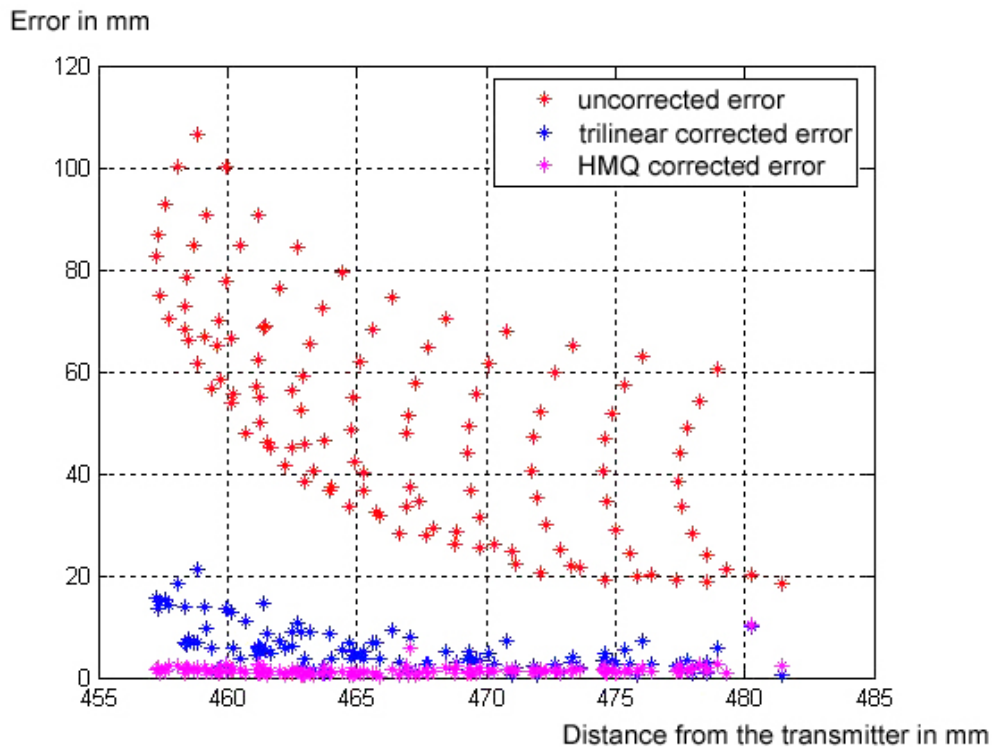


Figure 3.9: Position error as function of the distance from the sensor to the transmitter. Picture taken from [Kau06]

You can also see in figure 3.9 that Hardy’s multiquadric method could reduce the effect of metal better than the trilinear interpolation. The position error for Hardy’s multiquadric method is about 4 mm for all locations, while the position error for trilinear interpolation varies depending on the distance (5 mm to 21 mm for close points and 4 mm to 7 mm for distant points).

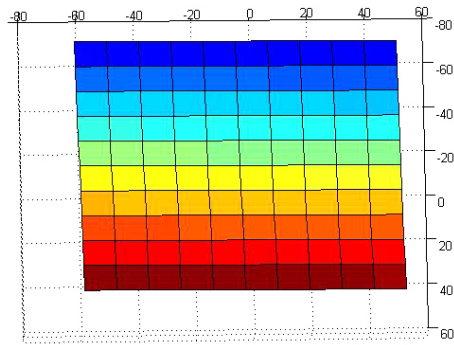
Kaur visualized the measured grid to see the distortion in figure 3.10 on page 49.

### 3.3.6 Discussion

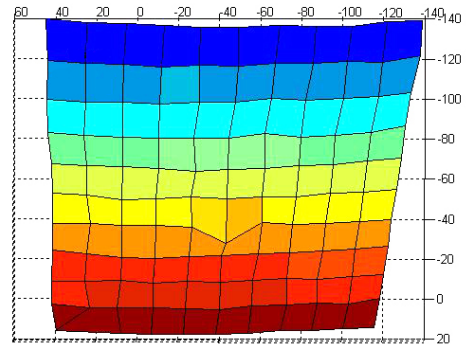
Kaur’s approach for error correction for magnetic tracking with the lookup-table was very promising. The motivation for my thesis were two issues that turned out to be not optimal during Kaur’s thesis.

The first issue is to develop a better procedure for the registration of the block because it is done with distorted data at the moment. The result is expected to improve if the registration is done with undistorted tracking data.

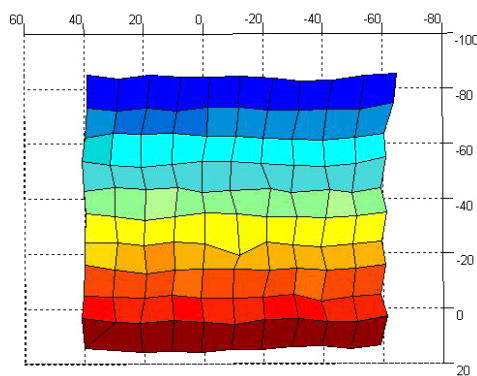
The second issue is to consider a method to create the lookup-table without using the polymer block. Collecting points with the block is sufficient for an experimental setting, but came up to be too inconvenient and time-consuming to integrate it into the workflow of a medical application.



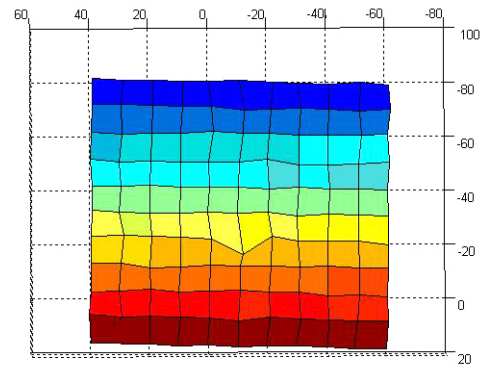
(a) Original grid



(b) Uncorrected grid



(c) Grid after applying trilinear interpolation



(d) Grid after applying HMQ method

Figure 3.10: These grids visualize the  $y$ - $z$ -plane in the coordinate system of the magnetic tracking system. All graphs are in the same orientation as the polymer block was during data collection. The horizontal axis is the  $y$ -axis. It ranges from -60 mm to 40 mm. The vertical axis is the  $z$ -axis, ranging from -80 mm to 20 mm. The original grid in subfigure (a) is based on the ground truth data. Grids taken from [Kau06]



## **Part II**

# **The Implemented Application**



## The three-step algorithm

This part explains the implementation of the visionary workflow from section 2.8 on page 24. The implemented application is called three-step algorithm. It is a tool that can also be used as basis for further applications.

The three-step algorithm provides methods to correct the distortions of an electromagnetic tracking system. The application can be used to track inside the human body in a room that is distorted by metal equipment. An electromagnetic and an optical tracking system are needed to perform this task.

The error correction algorithm uses information from a lookup-table that contains distorted and corresponding undistorted positions of the sensor of an electromagnetic tracking system. The undistorted values are collected with the help of an optical tracking system. The lookup-table is later used in the distorted setting to correct the distorted data of the magnetic sensor during tracking inside the human body. Hardy's multiquadric method is used for error correction.

The used hardware consists of an electromagnetic tracking system, an optical tracking system and a combined target that contains sensors of both tracking systems.

The implemented algorithm for error correction consists of these three steps:

1. Device calibration
2. Creating the lookup-table
3. Online error correction

The device calibration is the first step. In this step, the magnetic and the optical tracking system are coregistered with the help of the combined target with rigidly attached sensors of both tracking systems in a noise-free scenario. This step needs to be done only once in the beginning as long as the configuration of the markers does not change. The device calibration has to be done before the other steps.

A lookup-table is created in the distorted setting in the second step. It contains tracking data gained from both tracking systems for the same position in the distorted space. Tracking data

from the optical tracking system is used to remove distortions caused by metal in the room in the readings of the electromagnetic tracking system. Creating the lookup-table needs to be done whenever the settings changes. The reason for this is that the distortion field is different in a different setting. If the lookup-table is not collected again, the previous lookup-table contains the previous distortion field that differs from the current distortion field.

Device calibration and creating the lookup-table need to be prepared before the patient is treated so that the online error correction can be used during radiation.

The online error-correction is the last step. It is done in the distorted scenario. It uses the information from the lookup-table to correct the current position of the magnetic sensor. The optical tracking system is not needed for this step.

The three steps are explained in detail in the following sections.

## 4.1 Device calibration

The device calibration must be done in an undistorted setting to prevent errors that may come from distorted tracking data.

During the device calibration step, the spatial relationship between the optical and electromagnetic coordinate systems is computed to be able to transform both coordinate systems into the same coordinate system. The coordinate system of the magnetic tracker is used as reference coordinate system. A so called combined target is used to compute the coordinate transformation. Optical markers and the sensor of the electromagnetic tracking system are rigidly attached to it. The relationship between both tracking systems and the combined target is illustrated in figure 4.1 on page 55.

The transformations  $X$  and  $Y$  are unknown in the beginning of the device calibration.  $X$  is the transformation between the origin of the coordinate system of the optical markers on top of the magnetic field-generator and the origin of the coordinate system of the magnetic tracking system.  $Y$  is the transformation between the origin of the coordinate system of the magnetic sensor and the origin of the coordinate system of the optical markers attached to the combined target.

When  $X$  and  $Y$  are known, they are used together with tracking data from the optical tracking system to compute the position of the magnetic sensor inside the combined target without using tracking data from the magnetic tracking system. This position benefits from the high precision of the optical tracking system and is therefore regarded as true position of the sensor. This optically calculated position of the sensor is used as ground truth value for the likely distorted position reported by the magnetic tracking system.

The transformations from figure 4.1 are linked with each other by this formula:

$${}^{optical}T_{S3} \cdot X \cdot {}^{magnetic}T_{S1} = {}^{optical}T_{S2} \cdot Y \quad (4.1)$$

${}^{optical}T_{S3}$  denotes the position of the center of the optical markers on top of the field-generator, given by the optical tracking system.  ${}^{magnetic}T_{S1}$  is the position of the electromagnetic sensor given by the electromagnetic tracking system. It describes the position of the combined target in the coordinate system of the electromagnetic tracking system.  ${}^{optical}T_{S2}$

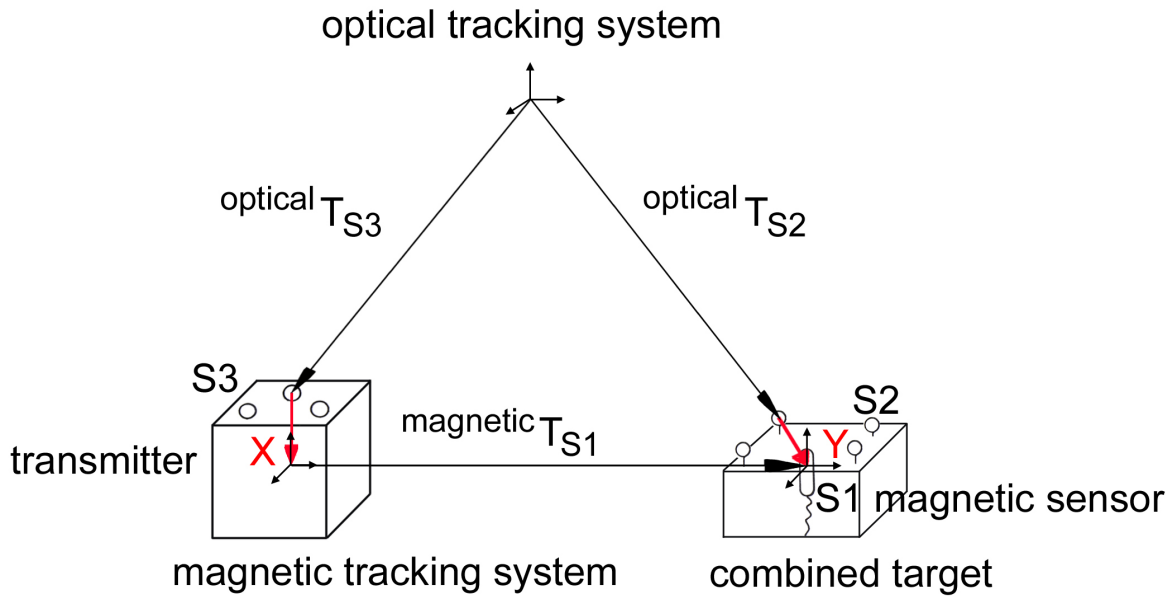


Figure 4.1: The involved transformations for the device calibration.  $S1$  denotes the magnetic sensor inside the combined target, while  $S2$  stands for the optical markers attached on top of the combined target.  $S3$  describes the optical markers on the transmitter of the electromagnetic tracking system that are used to track the field-generator by the optical tracking system.

is the position of the center of the optical markers attached to the combined target, reported by the optical tracking system. It gives the position of the combined target in the coordinate system of the optical tracking system.

The transformations  $Y$  and  $X$  are calculated in two steps. First, the transformation  $Y$  is computed using hand-eye calibration. Then equation 4.1 is rearranged and  $Y$  is substituted into the equation to get the transformation  $X$ .

#### 4.1.1 Performing hand-eye calibration to get the transformation $Y$

Hand-eye calibration is used to calculate  $Y$ . Background information about this algorithm is provided in section 3.2.2 on page 31.

This step needs to be done in a distortion-free environment. If it is done in a distorted setting, the poses from the magnetic tracking system may get distorted and hence the transformation  $Y$  is falsified.

For the hand-eye calibration algorithm the pose of the magnetic sensor inside the combined target and the corresponding pose of the optical markers attached to the target are saved while placing the target at several poses in the working volume of the electromagnetic tracking system. The poses for the magnetic sensors are given in the coordinate system of the electromagnetic tracking system while the poses for the optical markers are given in the coordinate system of the optical tracking system.

The hand-eye calibration algorithm does not use the poses as input, but the motion between this poses. The two sets of poses taken for the sensor and the optical markers form two sets of motions A and B. All distinct motions between the poses of one data set are computed, not only motions to the next and previous pose.

These motions for the sensor and the optical markers together with the missing transformation Y inside the target establish the principal equation for the hand-eye calibration:

$$A \cdot Y = Y \cdot B$$

Two sets of poses with  $n$  computed motions each set up a system of linear equations:

$$\begin{aligned} A_1 \cdot Y &= Y \cdot B_1 \\ A_2 \cdot Y &= Y \cdot B_2 \\ A_3 \cdot Y &= Y \cdot B_3 \\ &\vdots \\ A_n \cdot Y &= Y \cdot B_n \end{aligned} \tag{4.2}$$

The hand-eye calibration algorithm then computes the transformation Y solving the system of linear equations 4.2. A condition for the hand-eye calibration algorithm is that Y does not change during collecting the poses.

The quality of the hand-eye calibration depends on the number of poses taken and on the method used. Marco Feuerstein compared the two hand-eye calibration algorithms of Daniilidis (see [Dan99]) and of Tsai and Lenz (see [TL88]) in combination with different number of poses in [FWBN05]. Feuerstein confirmed that a certain number of poses is needed to obtain stable results and that the implementations of Daniilidis and Tsai and Lenz showed the same behavior regarding the reconstruction error. You can see his results in figure 4.2 on page 57. In regard to Feuerstein's paper I chose thirteen as number of poses to be taken for hand-eye calibration. I used the algorithm of Daniilidis.

#### 4.1.2 Reorganizing the equation to get the transformation X

As Y is known now due to hand-eye calibration, we can calculate the unknown transformation X between the center of the field-generator and the optical markers attached to it.

As we assume to work in an undistorted setting, equation 4.1 is rearranged to compute X. It turned out later during the experiments that it had been better if we would have computed X with a second hand-eye calibration instead to become independent of the error of the first hand-eye calibration for Y.

Equation 4.1 is rearranged as follows:

$$\begin{aligned} \textit{optical } T_{S3} \cdot X \cdot \textit{magnetic } T_{S1} &= \textit{optical } T_{S2} \cdot Y && = \text{equation 4.1} \\ X &= (\textit{optical } T_{S3})^{-1} \cdot \textit{optical } T_{S2} \cdot Y \cdot (\textit{magnetic } T_{S1})^{-1} && (4.3) \end{aligned}$$

Now X can be calculated very easily by just substituting all transformations and the previously computed transformation Y into equation 4.3 as all transformations on the right side of equation 4.3 are known.

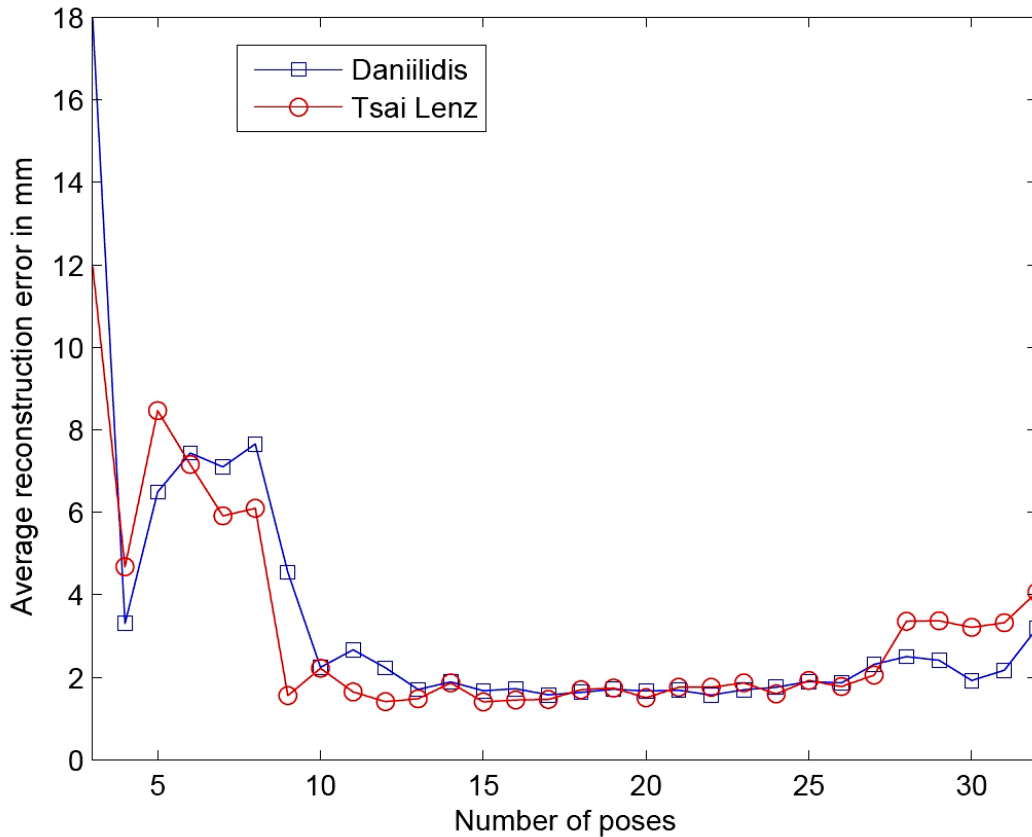


Figure 4.2: Average reconstruction error for retroreflective markers depending on the hand-eye calibration method and number of poses. Picture taken from [FWBN05].

To make the computation of  $X$  more stable against errors, several values for  $X$  are calculated using the previously saved poses of the field-generator, ( $^{optical}T_{S3}$ ). The thirteen values for  $X$  are then averaged to the final  $X$ .

The transformations  $X$  (inside the transmitter) and  $Y$  (inside the combined target) are known now. They are used for the following step, the creation of the lookup-table.

## 4.2 Creating the lookup-table

### 4.2.1 Ground truth values

The optical system is used to recognize distortions of the electromagnetic tracking system. For this purpose, the position of the magnetic sensor is additionally computed using only tracking information from the optical tracking system and the transformations  $X$  and  $Y$ . This position of the magnetic sensor computed the optical way is called “ground truth value”. It is regarded to be the true position of the magnetic sensor.

The formula for the ground truth values derives from equation 4.1 on page 54. Equation 4.1 only needs to be rearranged to give the ground truth values for the magnetic sensor:

$$\underbrace{\text{magnetically reported pose of the sensor}}_{\text{magnetic } T_{S1}} = \underbrace{X^{-1} \cdot (\text{optical } T_{S3})^{-1} \cdot \text{optical } T_{S2} \cdot Y}_{\text{ground truth values for the sensor, optically computed}} = \text{equation 4.1} \quad (4.4)$$

Since X and Y are already known, the ground truth values (the right side of equation 4.4) can be computed without problems. The left side of equation 4.4 is the position of the magnetic sensor as it is directly reported by the electromagnetic tracking system.

With this rearranging of the equation, both positions for the magnetic sensor are already in the same coordinate system, namely in the coordinate system of the electromagnetic tracking system.

### 4.2.2 The lookup-table

To combine the advantages of both tracking systems (the high precision of the optical tracking system and the ability of the magnetic system to track inside the human body), a lookup-table approach is used for error correction.

A lookup-table is a mapping function. It transforms the incorrect values coming from the distorted magnetic tracking system to corrected values computed with the help of the optical tracking system and the transformations X and Y. It reflects the distortion field inside the tracking volume at the moment when it is recorded. The distortion field of an exemplary lookup-table is illustrated in figure 4.3.

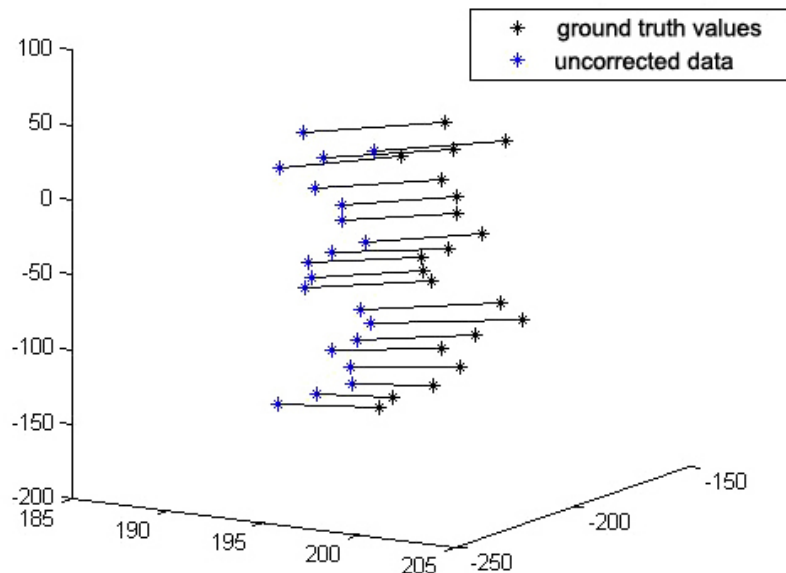


Figure 4.3: An exemplary distortion field stored in a lookup-table, illustrated by 20 displacement vectors

The lookup-table is recorded in a distorted setting and is then used as basis for the error correction of the magnetic sensor in the same distorted setting. If the setting changes in between in regard of metal in the tracking volume of the magnetic tracking system, the lookup-table will provide the error correction method with an outdated displacement field and therefore the error correction will output false results. The lookup-table implements formula 4.4 from page 58. Both sides of equation 4.4 are identical in an undistorted setting. We use it in a distorted setting, so the values for both sides may differ.

The lookup-table is implemented as text-file with two entries per line. The first entry is the computed ground truth value for the magnetic sensor inside the combined target, the second value is the position of the sensor reported directly by the magnetic tracking system. Each of the two entries consists of values for x, y and z. Rotation is not considered, only the translation is saved.

The lookup-table is created by moving the combined target within the tracking volume of the magnetic tracking system and saving the two sets of positions of the target.

The lookup-table has to cover the whole tracking volume where the magnetic sensor will be used later. As the lookup-table has to be recorded whenever the setting changes, the creation of a lookup-table should be easy to execute, not time-consuming and not error-prone. We thought about several approaches how to help the assistant medical technicians during the creation of the lookup-table. We decided to use a visual assistance and called it “the pacman game” because it uses a similar game philisohy as the popular arcade game.

### 4.2.3 The Pacman Game

The pacman game is designed to give a visual feedback while collecting the entries for the lookup-table with the combined target and to ensure that points from the whole magnetic tracking volume are recorded so that the complete distortion field is displayed in the lookup-table.

The pacman game uses a “Philips ToUCam Pro Camera” webcam in addition to the optical and the magnetic tracking system. The webcam is focused on the scene during collecting the lookup-table to see the pacman scenario and is used to augment the real world with virtual information. It is equipped with four optical markers for optical tracking. (See figure 4.4).



Figure 4.4: This is the ToUCam Pro Camera, a webcam manufactured by Philips that is used during the pacman game.

The position of the sensor inside the combined target is augmented with a pacman-like character. It is shown in figure 4.5.



Figure 4.5: The pacman character, used to visualize the pose of the combined target during the creation of the lookup-table

Green balls looking like peas are shown every 5 cm in x-, y- and z-direction inside the tracking volume of the magnetic tracker. Although the spheres are shown every 5 cm, the position of the sensor is saved every 1 cm. The distance of 1 cm was chosen to achieve an optimal sampling lattice for the lookup-table. The spheres are only drawn every 5 cm to avoid that the scenario looks to crowded and confusing. The pacman scenario is shown in figure 4.6.

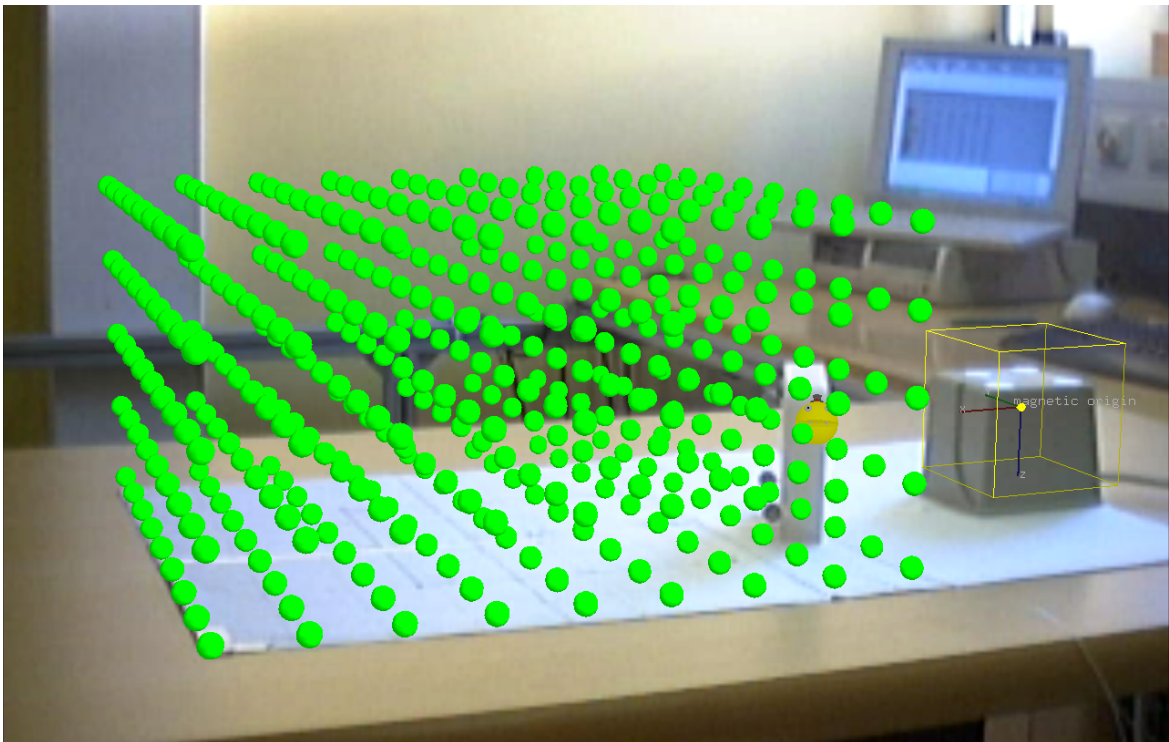


Figure 4.6: This screenshot of the pacman game reflects the view of the webcam. The yellow frame does not quite match the field-generator due to insufficient optical tracking data for the webcam that was hold outside the tracking volume to take the picture.

Before a set of values is stored in the lookup-table file, it is tested if the current distorted position of the sensor is at least 1 cm away from all other collected positions. When the target is moved around in the volume of the magnetic tracker, the application calculates if the pacman is near enough to one of the spheres to eat it. If a sphere is eaten, it disappears. A threshold is implemented as a value in centimeters, how near target and spheres have to be so that the spheres will be eaten.

The aim for the person collecting the lookup-table is to let the pacman eat all the spheres. The pacman and the spheres help to ensure that the whole volume is covered. The most convenient way is to collect the spheres along a 3D space-filling curve, but the application will also work if the spheres are collected in a “chaotic” way.

The lookup-table serves as input for the next step, the online error correction.

### 4.3 Online error correction

As the position of the magnetic sensor may be distorted due to metal, the position of the sensor is corrected using the lookup-table that was created in the step before. The online error correction needs to be performed in the same distorted setting where the lookup-table was created so that the recorded distortion field matches the current distortion. The optical tracking system is not used during this step.

The implementation of the interpolation algorithm is based on Hardy’s multiquadric method. For more information about Hardy’s multi-quadric method, see [Har71] and have a look at the work of Kaur in [Kau06]. Hardy’s multi-quadric method is also described briefly in section 3.2.4 on page 34.

The current position of the magnetic sensor is given as input to the algorithm as well as the lookup-table. The algorithm searches the current position of the sensor in the lookup-table in the columns with distorted values. If the same position is stored in the table as distorted value, the corresponding ground truth value is returned as corrected position for the sensor. If the current position cannot be found in the lookup-table, several values in the table that are near to the searched distorted position are used. Their corresponding ground truth values are interpolated to one corrected position for the current position of the sensor.



## **Part III**

# **Experiments and Results**



## System setup

This chapter describes the hardware and the software used during my thesis. The electromagnetic and the optical tracking system are introduced as well as custom-build hardware. The three-step algorithm was implemented using a software framework of the chair of computer aided medical procedures. The framework is also explained in this chapter.

### 5.1 The electromagnetic tracking system

Electromagnetic tracking systems were explained in general in section 3.1.1 on page 26. This section introduces the used tracking system.

I used two electromagnetic tracking systems with equivalent properties from Ascension during my diploma thesis, the 3D Guidance system and the MicroBird system. Both are DC<sup>1</sup> tracking systems. Both tracking systems were used at the default measurement rate of 68.3 measurements per second. The manufacturer claims this to be the measurement rate with the most accuracy.

The two tracking systems are explained in detail in the following sections according to the manual from the manufacturer Ascension, [Asca].

#### 5.1.1 3D Guidance by Ascension

The 3D Guidance system from Ascension consists of a field-generator, a control box and up to four sensors. The transmitter as well as the sensors are plugged into the control box. The 3D Guidance is connected to the computer via an USB<sup>2</sup> cord. The system is illustrated on figure 5.1 on page 66.

---

<sup>1</sup>direct current

<sup>2</sup>Universal Serial Bus



Figure 5.1: The 3D Guidance system by Ascension Technologies. The control box is shown in the center, the transmitter on the left side and the sensor is inside the combined target in the right. The target does not belong to the tracking system.

#### 5.1.1.1 The transmitter

The field-generator acts as source of current with a maximum output of 3.33A. The transmitter consists of three coil loops in the x-, y- and z-axis being orthogonal to each other. A pulsed DC current is applied to one coil a time. This generates a magnetic fields along the x-, y- and z-axis. 90 V are applied at the beginning of every axis-cycle.

The magnetic field is strongest near the transmitter. It decreases with the distance from the transmitter according to the formula

$$\text{field strength} = \frac{1}{(\text{distance from transmitter})^2}$$

The transmitter can be seen on figure 5.1.

#### 5.1.1.2 The magnetic sensor

The position of the magnetic sensor is computed by comparing the measured field strength for the three axis in the sensor with the theoretical knowledge about the generated magnetic field. The sensor can be seen in figure 5.2 on page 67.

At the sensor, a magnetic field strength that is about the magnetic field of the earth ( $\approx 0.6$  gauss) is sustained. The amount of the current flowing through the coils is therefore adjusted. An upper border for the distance between field-generator and sensor are twelve inches. When the sensor exceeds this distance from the transmitter, the current can not be increased any more.

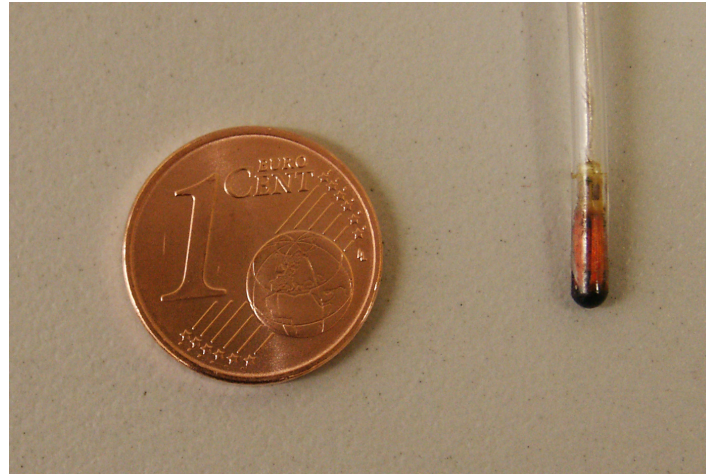


Figure 5.2: One Model 130 sensor of the 3D Guidance tracking system

### 5.1.1.3 The control box

The control box of the 3D Guidance system fulfills several functions at once. It computes the adequate field strength, generates the field with DC current flowing consecutively through each of the three coils of the transmitter, collects data from the connected sensors and computes the position of the sensors. It is protected against ground shorts.

The control box can be seen on figure 5.1 on page 66.

### 5.1.2 MicroBird by Ascension

The manufacturer Ascension Technologies says that the MicroBird tracking system is similar to the 3D Guidance system. The MicroBird only consists of different components than the 3D Guidance and is connected to the computer in a different way than the 3D Guidance.

The MicroBird system consists of a transmitter, up to two sensors and a PCI<sup>3</sup> card that is plugged into the mainboard of the computer. The MicroBird tracking system can be seen on figure 5.3 on page 68.

During the use of the MicroBird device instead of the 3D Guidance system, one sensor of the MicroBird tracking system was put into the hole inside the combined target. The device calibration was repeated after this to get to know the new values for X and Y.

---

<sup>3</sup>Peripheral Component Interconnect

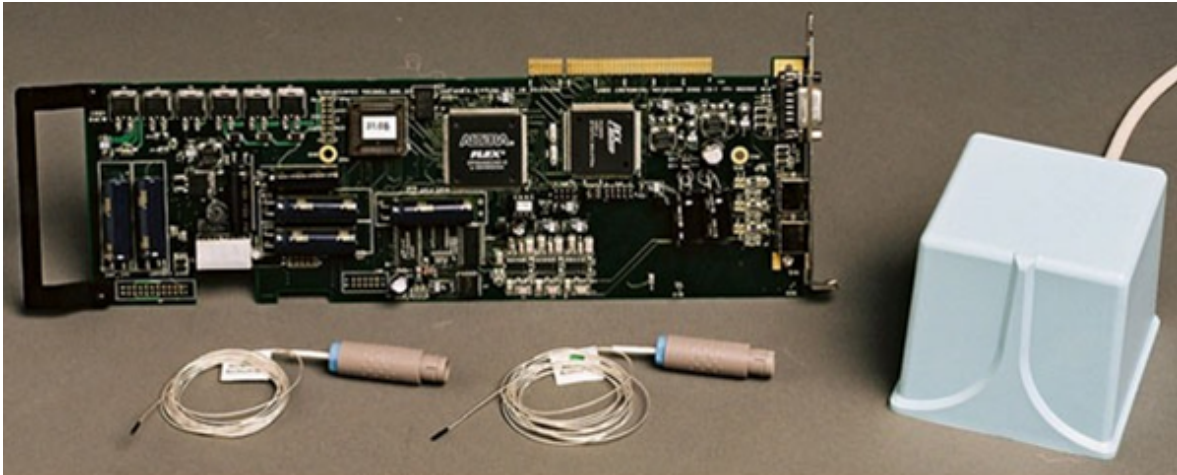


Figure 5.3: MicroBird manufactured by Ascension Technologies. Picture taken from [Ascb]

### 5.1.3 The specified magnetic working volume

According to the manufacturer there is a region that gives the best results for measurement. This region applies for the 3D Guidance as well as for the MicroBird.

The center of the coordinate system of the 3D Guidance system is located in the center of the coil set of the field-generator. This is about in the center of the transmitter. The arrangement of the three axis is as follows: Being inside the origin and looking out of the transmitter with the transmitter's wire in the back, the positive x-axis goes straight forward, the y-axis goes to the right and the z-axis goes up. Measured from the origin, the magnetic volume that achieves the best results goes from +20 cm to +36 cm in x-direction, from +20 cm to -20 cm in the y-direction and from +20 cm to -20 cm in the z-axis.

The working volume applied during the experiments differs slightly from the specified working volume and is described later in section 5.4 on page 71.

## 5.2 The optical tracking system

Optical tracking systems were explained in general in section 3.1.2 on page 27. This section describes special features of the used optical tracking system.

The used optical tracking system is dtrack by Advanced Realtime Tracking GmbH (A.R.T.). This section is explained according to [Adv].

The dtrack system I used consists of four cameras, model ARTtrack2, a computer software called "dtrack" and a computer running the software.

### 5.2.1 The cameras

The four cameras are mounted in the four corners of a rectangular frame made from aluminium. The frame measures  $3 \times 3 \times 2.75$  m. The cameras hang  $\approx 2.60$  m over the ground.

In the cameras, a ring of LEDs emit infrared flashes with a frequency up to 60 Hz. A flash lasts 380  $\mu$ s. An ARTtrack2 camera can be seen on figure 5.4.



Figure 5.4: The picture shows one camera, model ARTtrack2, manufactured by Advanced Realtime Tracking GmbH.

## 5.2.2 The software for the cameras

The dtrack system comes with a software and a computer to run it. Some initial calibration settings are done by A.R.T. before delivering the system to the customer.

The dtrack-software runs on a computer of its own. The software communicates with the cameras using ethernet and synchronizes the cameras. The dtrack computer has a fixed IP adress. The application shows the positions of the tracked objects and provides, among other things, methods for room calibration and body calibration. It is also possible to display the view of each camera.

The optical tracking system comes with two tools for room calibration. The tools are used to measure the fundamental matrix between the cameras. Room calibration has to be done once in the beginning and then afterwards every time the relativposition or orientation of the cameras to each other has changed.

One of the tools for room calibration defines the origin. It can be put on an arbitrary place within the optical tracking volume where the origin shall be located. The software offers different possibilites for the orientation of the axes.

Targets that shall be tracked optically need to be defined in the dtrack-software. This process is called body calibration.

The origin of a target is defined after certain rules. The two markers with the biggest distance are searched. They are marker number 1 and 2. A third marker is searched that has the smallest distance to marker 1 or 2. The numbers are assigned in such a way that the marker of marker 1 and 2 with the smallest distance to marker 3 becomes marker number 1. The target's origin is marker 1. From the origin to marker 2 is the positive x-axis. Markers 1, 2 and 3 span up the x-y-plane in such a way that marker 3 has a positive y-coordinate. As the systems puts a right-handed coordinate system into the target, the z-axis is already defined with this.

## 5.3 Custom-build hardware

### 5.3.1 The combined target

The combined target is custom-build. It is called "combined" because it has optical markers and a magnetic sensor attached to it. (See figure 5.5). It can be tracked by both tracking systems simultaneously.

The combined target consists of a polymer block measuring  $10 \times 10 \times 2.7$  cm. A hole ranges from the bottom of the block to the top. The magnetic sensor was inserted into the hole with its tip facing the bottom of the block.

Four optical markers were rigidly attached to the top of the block. The distance from the corresponding edge to the marker varies for every marker and one marker is attached lower than the others. This non-symmetric configuration of the optical markers was chosen in order for the optical system to identify the target unambiguously in space.

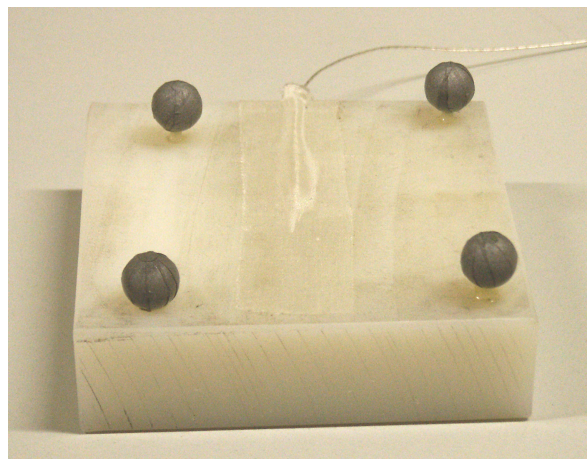


Figure 5.5: The combined target with four optical markers attached on top. The electromagnetic sensor is located in a hole inside the target.

### 5.3.2 The field-generator-target

Four optical reflecting markers were attached to the field-generators of the 3D Guidance and the MicroBird tracking systems as they need to be tracked by the optical tracking system during device calibration. The transmitter of the 3D Guidance system can be seen on figure 5.6. The field-generator of the MicroBird looks the same.

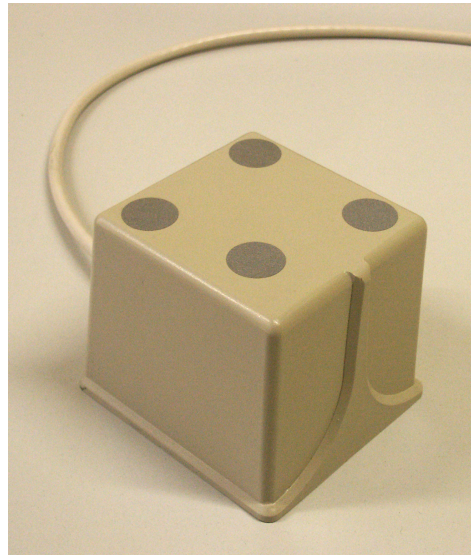


Figure 5.6: The transmitter of the 3D Guidance system with attached optical markers on top.

## 5.4 The working volume for the experiments

During my experiments, I worked in a volume that slightly differed from the specified magnetic volume described in section 5.1.3 on page 68. I put the transmitter on a table and took no poses underneath the table as the optical system would not see the optical markers of the target then. The center of the transmitter was approximately 3 cm over the surface of the table. The z-values therefore ranged from -3 cm up to 10 cm or 15 cm, depending on the course of the experiment. The y-values ranged from -20 cm to +20 cm. I tracked x-values from +20 cm up to +60 cm. (Compare figure 5.7 on page 72.)

## 5.5 The used software

The experiments were realized using the CAMPAR-framework developed at the chair for computer aided medical procedures of the technical university in Munich. The framework is written in C++ and implements methods for the synchronization of the involved hardware like optical and magnetic tracking systems, Ultrasound probes and the computer of the user and it provides several algorithms needed for augmented reality. See [SFT<sup>+</sup>06] for more information about the CAMPAR-framework.

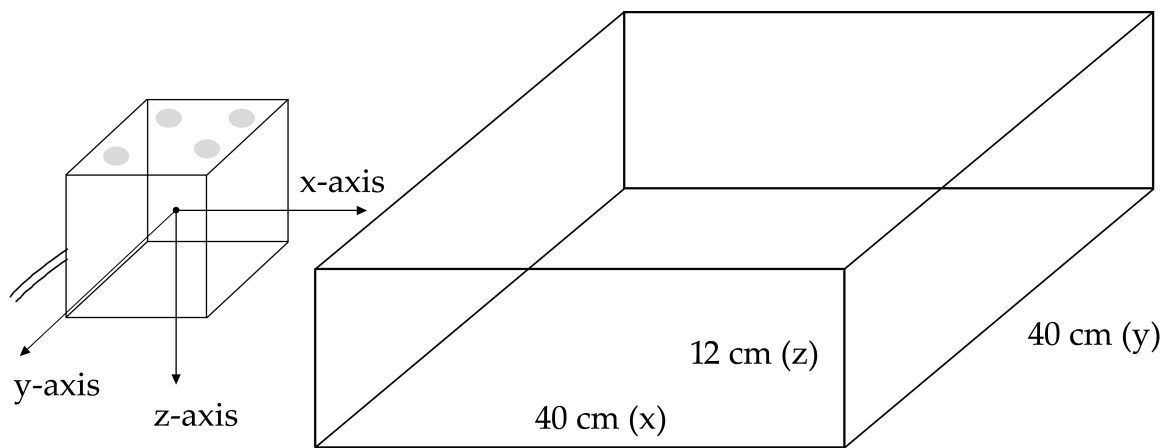


Figure 5.7: This images illustrates the arrangement of the axis in the transmitter of the 3D Guidance / MicroBird tracking system by Ascension and the working volume used during the experiments.

## Experiment 1: Evaluation of the device calibration

The first experiment is designed to evaluate the quality of the device calibration. This is done by executing several device calibrations and comparing the results. During the experiments influences showed up that need to be regarded in order to achieve optimal results.

### 6.1 General course of experiment 1

The device calibration must be done in an undistorted setting. All metals, cables and equipment that generates electromagnetic fields must be removed from the setting. The setting for the device calibration was put up on a wooden table to exclude distortions by metal of the table.

Thirteen poses from the magnetic sensor and the optical markers respectively were recorded at different positions in space and with different orientations using the combined target. The number of thirteen proved to be a good compromise because if more poses were taken, it was difficult to find poses where the threshold for the euler angles between all poses would fit and if less poses were taken, the quality of the device calibration was not good enough. Compare [FWBN05].

More about the course of the experiments can be found in the sections about every experiment as some details changed during time because due to the gained experience.

To evaluate the quality of the gained device calibration transformations  $X$  inside the field-generator and  $Y$  inside the combined target, the poses of 50 points were recorded in the distortion-free setting and saved into a file. The evaluation file contains the ground truth value, the measured uncorrected data of the sensor and the interpolated value for the current pose of the sensor for all 50 points.

As described in chapter 4.1.2, thirteen values for the transformation  $X$  are calculated using the thirteen poses of the combined target and thirteen poses for the field-generator and equation 4.3. The poses for the transmitter were stored additionally with every pose to protect

against movements of the transmitter during collecting the poses. The thirteen computed values for  $X$  are then averaged to one value for  $X$ . For evaluation, the mean error for this thirteen poses was computed and named *meanErrorDC*. The standard deviation was also calculated. MeanErrorDC measures how similar the thirteen calculated values for  $X$  were to the computed  $X$  and therefore tells how good the averaged  $X$  is. The notation *maximumElementDC* describes the element of the thirteen values for  $X$  that has the maximum difference to the averaged  $X$ .

The mean error for the distance between the uncorrected values of the magnetic sensor and the corresponding ground truth values was computed for all 50 points and called *meanErrorEval*. The corresponding standard deviation was also calculated. MeanErrorEval tells how good the device calibration is regarding the 50 recorded points. The point with the maximum value for the distance between ground truth values and the uncorrected value was computed and given as *maximumElementEval*.

## 6.2 Experiments 1.1 to 1.3

	Experiment 1.1 poses were taken everywhere		Experiment 1.2 poses were taken near transmitter	Experiment 1.3 setting distorted consciously
	Trial 1	Trial 2	Trial 1	Trial 1
meanErrorDC	10.60 mm	33.99 mm	2.32 mm	3.25 mm
standard deviation	$\pm 4.17$ mm	$\pm 11.75$ mm	$\pm 1.57$ mm	$\pm 1.76$ mm
meanErrorEval	4.97 mm	21.22 mm	8.18 mm	6.50 mm
standard deviation	$\pm 1.68$ mm	$\pm 8.02$ mm	$\pm 17.27$ mm	$\pm 5.48$ mm
maximumElementDC	18.84 mm	58.68 mm	4.97 mm	6.73 mm
maximumElementEval	8.80 mm	37.19 mm	55.69 mm	21.55 mm

Table 6.1: Overview over the trials of experiment 1.1 to 1.3

In experiment 1.1 the thirteen poses for calculating  $Y$  were taken while the target was put everywhere inside the magnetic tracking volume. It was hold in the hand and moved while a key was pressed to store the current magnetic and optical poses.

The results of the two trials of experiment 1.1 were not as good as expected. The results between trial 1 and trial 2 vary very much. The values for maximumElementDC and maximumElementEval were surprisingly high. I assumed that the reason for this might be outliers that occurred during device calibration as well as during recording the 50 evaluation points. But as the sensor had no malfunction and there was no error in the implemented code, the high amount of supposedly occurred outliers proved that the procedure needed improvement.

To ensure high tracking accuracy, the 50 evaluation points were taken very near to the transmitter instead of being spread all over the volume during experiment 1.2. The distance between the transmitter's origin and the sensor was about 20 cm in the x-coordinate. As you can see in table 6.1, taking poses at the beginning of the tracking volume gave better results

for meanErrorDC than in experiment 1.1. The values for meanErrorEval and its standard deviation are relatively high. MaximumElementEval is also high. Both may be the effect of at least one outliers of the 50 evaluation points.

To examine if the previous settings may have been not distortion-free, I consciously distorted the setting by a light source of an endoscope shown in figure 6.1 during experiment 1.3 The light source measures  $16.5 \times 18 \times 10$  cm and was put diagonally on the left of the transmitter facing the tracking volume and stood outside of the tracking volume.



Figure 6.1: The source of distortion for experiment 1.3 was the light source of an endoscope.

Table 6.1 shows the values for the willingly distorted device calibration. This gives roughly an lower border for the values of a good device calibration. The result of experiment 1.3 showed that experiments 1.1 and 1.2 were not distorted. I suppose that the high value for maximumElementEval may come from a point out of the 50 points that was recorded too near the source of distortion.

The results of experiment 1.1 to 1.3 were not good enough so I continued the experiments.

### 6.3 Suggested changes for the next experiment

Experiments 1.1 to 1.3 showed that a distortion-free setting is important to get a good device calibration. The experiments also arose the suspicion that the synchronization of the electromagnetic and the optical tracking system was not sufficient. I examined this speculation in the next experiment, experiment 1.4.

## 6.4 Experiment 1.4

### 6.4.1 The course of experiment 1.4

To ensure the synchronization of the magnetic and optical tracking system, I thought of a workaround to store the poses statically. The workaround is not thought to be enduring, it only ensures that I can work with the current system and can conduct my experiments.

The problem with synchronization is that the magnetic tracking system by Ascension does not give a timestamp at the moment the data is gained. There is a timestamp available, but from the moment in time after the position of the sensor is computed by the control box. I solved the problem of the uncertain synchronization by instead of holding the target in the hand and taking the poses during the motion of the target, I put the target on the table and on several non-metallic objects and waited for 2 seconds before storing the current pose. This does not really make the two tracking systems synchronized, but as the target does not move for 2 seconds, the stored poses from both tracking systems must belong together although their time stamps may vary.

Additionally, Ascension, the manufacturer of the electromagnetic tracking system, provided me with a new version of the dll that I used during the three trials of this experiment.

### 6.4.2 Results of Experiment 1.4

The values in table 6.2 represent the effect of statically recorded poses for the device calibration. I also used a new .dll for the magnetic tracking system. The meanErrorDCs and its standard deviations as well as meanErrorEval and its standard deviation are both good. They are better than the values for the distorted device calibration in experiment 1.3.

	Trial 1	Trial 2	Trial 3	Trial 4
	poses statically and new .dll			
meanErrorDC	3.26 mm	2.27 mm	2.18 mm	1.96 mm
standard deviation	± 1.30 mm	± 1.18 mm	± 1.48 mm	± 1.15 mm
meanErrorEval	2.13 mm	2.81 mm	2.48 mm	1.98 mm
standard deviation	± 0.86 mm	± 1.32 mm	± 1.17 mm	± 0.88 mm
maximumElementDC	4.76 mm	4.28 mm	4.96 mm	4.45 mm
maximumElementEval	3.70 mm	6.68 mm	6.55 mm	4.85 mm

Table 6.2: Overview over the four trials of experiment 1.4

In this experiment the mean values for all three trials and even the maximum elements are better than in the previous experiments in an undistorted setting. This benefit comes from the static recording of poses as well as the new .dll, but the amount of influence of each factor can not be specified.

## 6.5 General conclusion of experiment 1

The experiments showed two important measurements to improve the device calibration. The first one is to use the new dll and the second one is to ensure the synchronization of the magnetic and the optical tracking system.

As you can see in figure 6.2, the values for meanErrorDC and meanErrorEval as well as maximumElementDC and maximumElementEval could be decreased for experiment 1.4 in comparison to experiment 1.1.

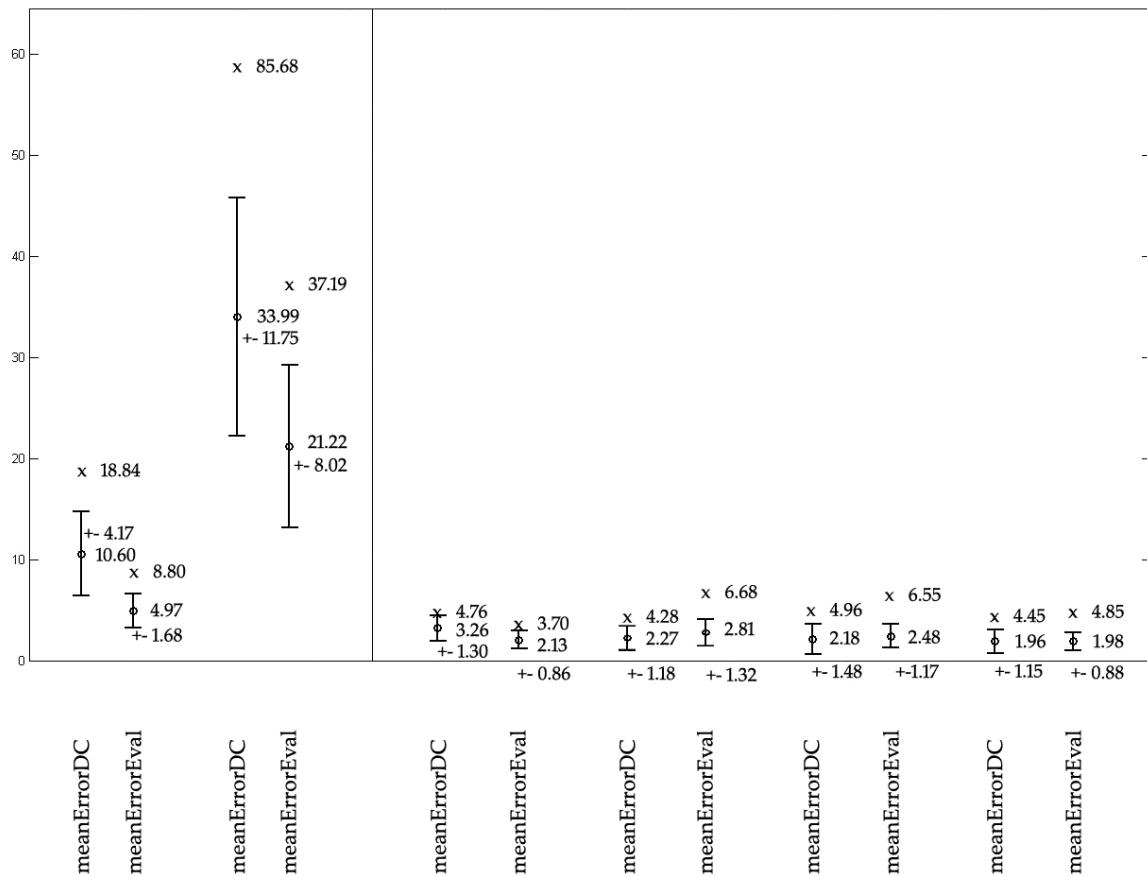


Figure 6.2: The gained improvement between experiment 1.1 (left) and experiment 1.4 (right). The values marked with an x denote maximumElementDC and maximumElementEval.



## Experiment 2: Evaluation of the applied error correction algorithm

The purpose of the second experiment was to analyze the quality of the applied online error correction, namely Hardy's multiquadric method. As during experiment 1, measures are described that can improve the results.

The second experiment must be executed in the distorted setting where the system will be used later to be able to determine the quality of the error correction.

### 7.1 General course of experiment 2

A lookup-table was created containing the ground truth values and the uncorrected measured values of the magnetic sensor. The file was used as input for the interpolation algorithm. To evaluate the quality of Hardy's multiquadric method used for online error correction, a second file was created. The evaluation file contains the ground truth values, the uncorrected measured data from the magnetic sensor and the corresponding corrected data.

Lookup-table and evaluation file were collected in a similar way. To ensure that data from the whole working volume was used, the combined target was moved along a space-filling curve within the volume. To avoid to get identical data for the evaluation file which would result in an pure look-up done by the interpolation algorithm instead of an interpolation, the space-filling curve for the evaluation file was rotated in comparison to the curve of the lookup-table. The space-filling curves for both files can be seen in figure 7.1 on page 80.

More details about the course are given in the sections of each experiment, as it changed during time.

The evaluation file was used to analyze the benefit of the error correction by computing two mean errors. Both were taken only from the evaluation file. The first mean error is called *meanErrorMB* and describes the distance between the ground truth values and the measured values of the magnetic sensor for all entries in the evaluation file. It tells about the amount of distortion in millimeters that occurred during the experiment. The second mean error, *meanErrorHMQ*, denotes the deviation between the ground truth values and interpolated values

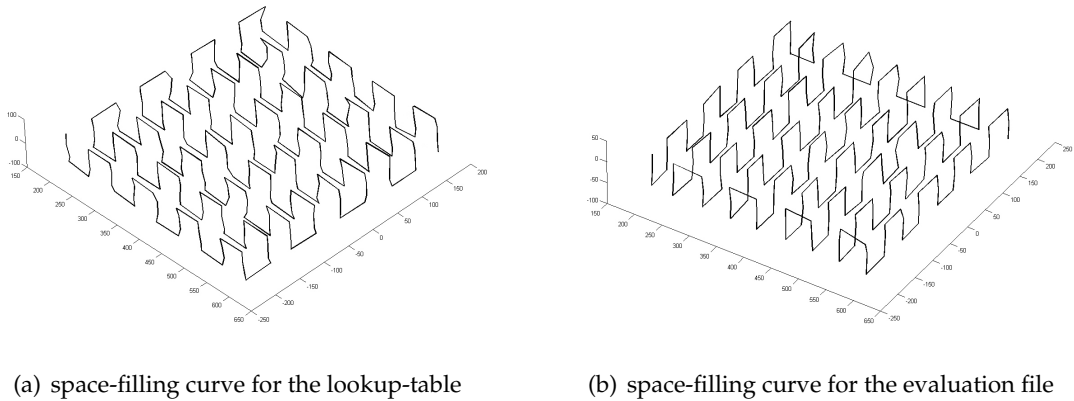


Figure 7.1: The pictures show the space-filling curves along which the lookup-table (left) and the evaluation file (right) were collected during experiment 2.

for all entries in the evaluation file. It shows how big or small the distortion in millimeters is after Hardy's multiquadric interpolation algorithm was applied to the uncorrected data. The standard deviations were calculated for both mean errors. To examine the distortion more detailed, the mean errors and standard deviations were computed for every single axis.

## 7.2 Experiments 2.1 to 2.4

During experiment 2.1 I held the target in my hand and moved it along the space-filling curves shown in figure 7.1 to collect the lookup-table and the evaluation file. Recording one file took about 10 minutes.

The settings for both trials were distorted by the light source of an endoscope than was used during experiment 1.3. It can be seen in figure 6.1 on page 75. The light source was put outside the tracking volume for both trials. In the first trial, the light source was placed left of the transmitter. It was put diagonal with one edge touching the border of the tracking volume. In the second trial, the light source was placed left of the field-generator and stood parallel to the x-axis. The distance between the end of the tracking volume and the light source was 10 cm. The light source was put in a way so that the beginning of the light source was on a line with the beginning of the tracking volume. So in x-direction, it stood 15 cm away from the transmitter's origin and 30 cm in y-direction.

As you can see in table 7.1 on page 81, the online interpolation had better mean errors than the uncorrected data. That means that the distortion could be corrected by the error correction algorithm. But the values for meanErrorHMQ are still about 1 cm for both trials. This is too high for medical applications that need an error of 1 mm to 2 mm or less.

	Experiment 2.1 normal speed		Experiment 2.2 slowly	Experiment 2.3 slow motion
	Trial 1	Trial 2	Trial 1	Trial 1
meanErrorMB	21.72 mm	21.26 mm	20.51 mm	20.12 mm
standard deviation	± 8.36 mm	± 7.93 mm	± 7.02 mm	± 6.50 mm
meanErrorHMQ	11.06 mm	10.32 mm	9.58 mm	7.84 mm
standard deviation	± 7.06 mm	± 6.78 mm	± 6.41 mm	± 5.73 mm
meanErrorMBx	7.11 mm	7.19 mm	6.73 mm	7.38 mm
standard deviation	± 7.81 mm	± 8.14 mm	± 7.42 mm	± 8.22 mm
meanErrorMBy	13.74 mm	13.10 mm	13.66 mm	13.15 mm
standard deviation	± 5.64 mm	± 5.53 mm	± 5.37 mm	± 5.22 mm
meanErrorMBz	12.43 mm	12.42 mm	11.36 mm	10.91 mm
standard deviation	± 14.33 mm	± 13.85 mm	± 12.97 mm	± 11.61 mm
meanErrorHMQx	6.94 mm	6.17 mm	6.37 mm	5.37 mm
standard deviation	± 9.13 mm	± 8.43 mm	± 8.57 mm	± 7.64 mm
meanErrorHMQy	2.12 mm	2.27 mm	1.93 mm	1.35 mm
standard deviation	± 3.39 mm	± 3.76 mm	± 3.16 mm	± 2.09 mm
meanErrorHMQz	5.89 mm	5.59 mm	4.74 mm	3.70 mm
standard deviation	± 8.78 mm	± 8.18 mm	± 7.02 mm	± 5.61 mm

Table 7.1: Overview over the trials of experiment 2.1 to 2.3

	Experiment 2.4		
	old dll Trial 1	Trial 2	new dll Trial 3
meanErrorMB	24.02 mm	19.97 mm	19.86 mm
standard deviation	± 0.82 mm	± 7.29 mm	± 7.44 mm
meanErrorHMQ	12.02 mm	6.66 mm	3.32 mm
standard deviation	± 9.66 mm	± 4.79 mm	± 2.00 mm
meanErrorMBx	14.77 mm	7.41 mm	8.42 mm
standard deviation	± 8.48 mm	± 7.83 mm	± 3.68 mm
meanErrorMBy	9.48 mm	11.41 mm	11.18 mm
standard deviation	± 6.15 mm	± 5.13 mm	± 5.16 mm
meanErrorMBz	12.93 mm	12.18 mm	11.94 mm
standard deviation	± 15.08 mm	± 11.87 mm	± 11.55 mm
meanErrorHMQx	5.60 mm	4.65 mm	0.94 mm
standard deviation	± 7.83 mm	± 6.76 mm	± 1.27 mm
meanErrorHMQy	2.69 mm	1.66 mm	1.46 mm
standard deviation	± 4.37 mm	± 2.49 mm	± 2.02 mm
meanErrorHMQz	8.10 mm	2.83 mm	2.30 mm
standard deviation	± 12.44 mm	± 3.85 mm	± 3.04 mm

Table 7.2: Overview over the three trials of experiment 2.4

In both trials of experiment 2.1, the mean errors for the uncorrected values along the y-axis was highest and the values for the z-axis were also very high. This might be caused by the fact that the light source was put left of the transmitter in both trials, distorting the values towards it. It stands out that in both trials of experiment 2.1 that there was only very little correction of the distortion along the x-axis so that the data recorded far from the transmitter might have had a low accuracy as well as the ground truth values used for error correction.

Before performing experiment 2.2 I checked the code for programming errors and the sensor for malfunctions, but found no errors.

To examine if the bad result may come from a poor synchronization of the optical and the magnetic tracking system, I moved the target slowly along the space-filling curves during experiment 2.2. The recording of one file lasted at about 15 minutes. The light source was put right of the field-generator. It was put diagonally outside the tracking volume next to the field-generator.

The values for experiment 2.2 are shown in table 7.1. The interpolation could correct the distortion of the uncorrected data. The slow movement of the target along the space-filling curve for both the lookup-table and the evaluation file resulted in a slightly better mean value for corrected values, but also the distortion in the setting was slightly better than in the previous experiment. This does not clearly tell if the slow movement of the target had an effect so I decided to take the files even slower next time.

I moved the target even slower during experiment 2.3. I moved it in slow motion as slowly as I could. Collecting one file lasted at about 20 minutes. The setting was distorted by the light source. It placed outside the tracking volume parallel to the x-axis in a distance of 30 cm along the y-axis and 15 cm along the x-axis from the transmitter's origin.

The results for experiment 2.3 taken in slow motion showed that the interpolation could correct the uncorrected data a little bit more than in experiment 2.2 where both files were only taken slower than normal. This shows that the synchronization is not sufficient enough and needs to be improved.

I wanted to record the files statically next, but meanwhile I got a new .dll for the electromagnetic tracking system by Ascension and examined its impact first. That is why I moved the target in slow motion again for experiment 2.4 and used first the old .dll and then the new one. During the radiation the gantry will distort the setting from behind the transmitter, so I changed my setting for experiment 2.4 to make it more similar to this condition. The setting was the same for all three trials. The light source was put behind the field-generator in a distance of 7 cm.

Table 7.2 shows that effect of the new dll on the quality of the interpolation in comparison to the old dll. The distortion in trial 2 with the old dll and trial 3 with the new dll was very similar. With the old dll, the interpolation could correct that distortion to 6.66 mm while with the new dll, the interpolation corrected the distorted data to 3.32 mm. This proves that the new dll has a positive impact on the interpolation of the distorted values. You can also see that trial 3 has no reduced correction along the x-axis as it occurred in experiment 2.1, but trial 1 and 2 have. This improvement might also be caused by the new dll.

## 7.3 Suggested changes for the next experiment

The new version of the dll for the electromagnetic tracking system should be used as the new dll showed its benefit during experiment 2.4. The synchronization of both tracking systems must be ensured to gain good results.

## 7.4 Experiment 2.5

### 7.4.1 The changed course for experiment 2.5

To ensure the synchronisation of the tracking systems, I did no longer collect the lookup-table and the evaluation file in motion while holding the target in my hand but did it completely statically instead. That means I always put the target on the table or on a non-metallic object, waited for 2 seconds and then recorded the pose of the target. The lookup-table was taken in four planes along its space-filling curve, the evaluation file was collected in three planes along its space-filling curve. Both planes are illustrated in figure 7.2. The planes of the evaluation file were in between the planes of the lookup-table to ensure that there were interpolation values available for every point of the evaluation file. This procedure took very long in comparison to the previous experiments. It took about 1 hour to collect one file, that means two hours for one trial.

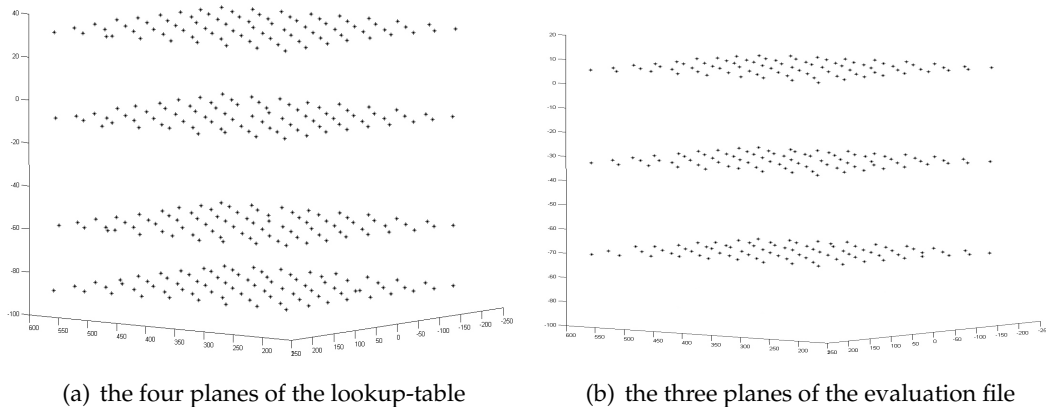


Figure 7.2: During experiment 2.5, the lookup-table and the evaluation file were collected in planes along their space-filling curves as illustrated in this picture.

Three trials were done statically and with the new dll for experiment 2.5. They differ in the used source of distortion and the height in which the planes for the evaluation file were recorded. It has to be noted that the magnetic sensor inside the target is not located quite at the bottom of the hole inside the target, but some millimeters higher. Therefore the measured position of the sensor is a little bit higher than the denoted height of the planes.

For the lookup-table, the target was put sequentially on the wooden table with 0 cm height, the second plane with 4 cm height, the third plane with 9 cm height and the fourth plane with

12 cm height. The height for the evaluation files differed during the trials and is reported there. Both files were recorded along their space-filling curves that were illustrated in figure 7.1 on page 80.

The source of distortion for trial 1 was a gamma probe made from tungsten that was put on two lead blocks and a pencilbox made from sheet. The probe is 16 cm long, 5 cm wide and 3.5 cm high. The lead blocks measure  $4 \times 4 \times 3$  cm and  $4 \times 4.5 \times 4$  cm. The box measures  $19 \times 8 \times 2$  cm. The buildup can be seen on figure 7.3. The planes for the evaluation file were taken in a distance of 0 cm, 7 cm and 10 cm over the table.



Figure 7.3: The source of distortion for trial 1 of experiment 2.5. It is composed of two lead blocks, a pencilbox and a gamma probe.

For trial 2 a computer tower distorted the setting. It stood parallel to the small side of the table with the front facing the south. The distance between the long side of the tower and the transmitter was 5 cm. The tower is 19 cm broad, 43 cm deep and 45 cm high. The evaluation file was recorded in heights of 2.5 cm, 6.5 cm and 10 cm.

In trial 3, the setting was distorted by the computer tower from trial 2 that was layed down on the side. There were 5 cm between the transmitter and the tower. The target was put on planes 2.5 cm, 6.5 cm and 10 cm high for the evaluation file.

#### 7.4.2 Results of Experiment 2.5

The results of this experiment with the new dll and statically recorded files in planes are summarized in table 7.3 on page 85. In all three cases, the interpolation gave very good results. The mean error meanErrorHMQ for the interpolated values was smaller than 1 mm in all three trials. The results are finally in the range where they can be used for medical applications.

The impact of the new dll was reported in experiment 2.4. The additional improvement in comparison to experiment 2.4 hence comes from the statically recording of lookup-table and evaluation file in planes.

	Trial 1	Trial 2	Trial 3
meanErrorMB	7.03 mm	33.08 mm	40.55 mm
standard deviation	$\pm 2.81$ mm	$\pm 13.82$ mm	$\pm 16.93$ mm
meanErrorHMQ	0.63 mm	0.47 mm	0.60 mm
standard deviation	$\pm 0.41$ mm	$\pm 0.33$ mm	$\pm 0.50$ mm
meanErrorMBx	6.16 mm	26.85 mm	33.59 mm
standard deviation	$\pm 2.08$ mm	$\pm 9.98$ mm	$\pm 12.80$ mm
meanErrorMBy	2.83 mm	11.80 mm	14.48 mm
standard deviation	$\pm 2.39$ mm	$\pm 8.13$ mm	$\pm 9.99$ mm
meanErrorMBz	0.83 mm	13.92 mm	15.81 mm
standard deviation	$\pm 1.05$ mm	$\pm 8.15$ mm	$\pm 8.90$ mm
meanErrorHMQx	0.25 mm	0.20 mm	0.25 mm
standard deviation	$\pm 0.38$ mm	$\pm 0.31$ mm	$\pm 0.43$ mm
meanErrorHMQy	0.35 mm	0.24 mm	0.33 mm
standard deviation	$\pm 0.39$ mm	$\pm 0.33$ mm	$\pm 0.44$ mm
meanErrorHMQz	0.35 mm	0.25 mm	0.29 mm
standard deviation	$\pm 0.28$ mm	$\pm 0.34$ mm	$\pm 0.41$ mm

Table 7.3: Overview over the three trials of experiment 2.5

The results also prove that the synchronization of the optical and the magnetic tracking system without using the workaround is not sufficient enough to use both tracking systems together.

The source of distortion for trial 1 was not solely composed of ferromagnetic objects. As you can see in table 7.3, the measured distortion is lower than during trial 2 and 3, but the error correction was as well able to reduce the distortion. This shows that Hardy's multiquadric method also works correctly in a nearly distortion-free setting.

The only disadvantage of the workaround to ensure synchronization is that it makes the recording of the lookup-table and the evaluation file too slowly to accept it in the medical workflow.

## 7.5 General discussion of experiment 2

The previous experiments showed that much can be done to achieve good results for the error correction of the uncorrected values of the magnetic sensor. First, the newest version of the .dll should be used and second, the synchronization of the optical and the magnetic tracking system should be ensured.

Figure 7.4 illustrates the benefit of a good dll and a given synchronization. Although the distortion was higher during experiment 2.5, the improvement by the error correction increased in comparison to experiment 2.1.

Both tracking systems provide a time stamp, but it is taken at different moments in time. The time stamp of the dtrack system by Advanced Realtime Tracking comes from the moment in time when the data is recorded while the time stamp of the magnetic tracking system 3D Guidance / MicroBird by Ascension Technologies is taken at the moment after the position of the sensor is computed. This time shift between both time stamps causes the implemented synchronization to fail.

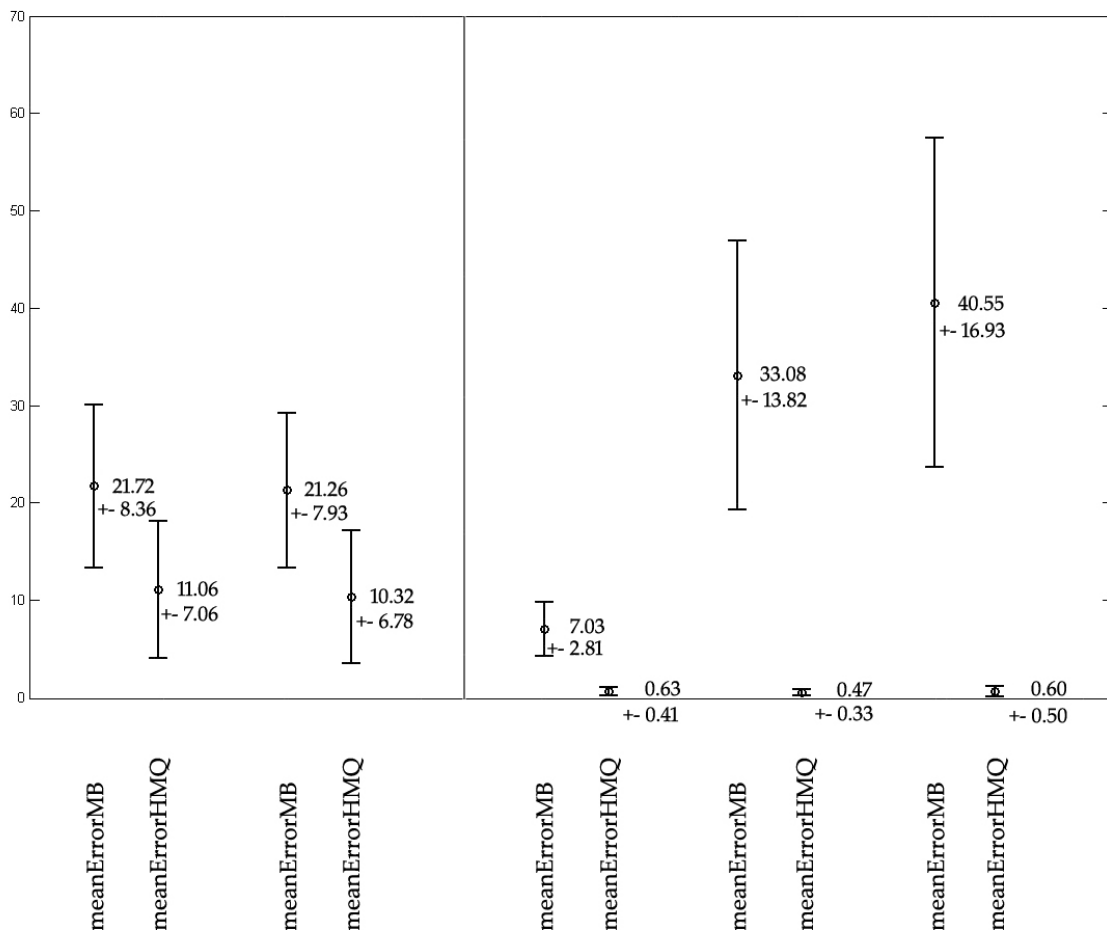


Figure 7.4: The gained improvement between experiment 2.1 (left) and experiment 2.5 (right)

## **Part IV**

# **Conclusion and Future Work**



## Conclusion

In this diploma thesis an application was implemented to correct the readings of a sensor of an electromagnetic tracking system that are distorted by ferromagnetic metal in its range. An optical tracking system was used to obtain the undistorted position of the sensor of the magnetic tracking system. The distortion field in the distorted setting was saved in the form of a lookup-table. The implementation of the lookup-table contains distorted poses of the sensor and the corresponding undistorted poses. Hardy's multiquadric method was applied to the current distorted pose of the sensor to interpolate the correct pose of the sensor using entries from the lookup-table.

In the beginning, the error correction algorithm could correct the uncorrected values, but not to a satisfactory level. I spent much time to explore the reason. It turned out that the synchronization between the optical and the electromagnetic tracking system was not sufficient. The time stamps are generated at different moments in time and prevent a correct synchronization of both tracking systems. The time stamp of the magnetic tracking system is taken at the moment in time after the pose of the magnetic sensor is computed by the control unit while the time stamp of the optical tracking system is taken when the cameras shoot a picture.

A temporary workaround was considered to avoid the lack of synchronization. The workaround was to collect the lookup-table statically on planes instead of moving around the sensor while holding it in the hand. I also waited for two seconds before storing poses. A similar workaround was used for the device calibration. There, the poses were stored after the target did not move for two seconds.

I got the opportunity to test the impact of a new dll for the electromagnetic tracking system from the manufacturer Ascension Technologies. It proved to improve the results.

With the workaround and the new dll the interpolation achieved optimal results for the error correction of the distorted values of the magnetic sensor. The deviation between the true position of the sensor and the corrected position was less than 1 mm in the end.



## Future Work

### 9.1 Ensure the synchronization of the magnetic and the optical tracking system

It turned out during this diploma thesis that the current synchronisation of the electromagnetic tracking system and the optical tracking system is not sufficient. This led to a workaround that is very time-consuming and cannot be accepted for the clinical workflow.

The inadequate synchronization is due to the fact that the electromagnetic tracking system does not provide a proper time stamp. The time stamp that can be queried from the magnetic tracking system is from the moment in time after the position of the sensor is computed. There is no time stamp available for the moment when the tracking data is collected. The best moment for a time stamp would be after the data was collected and before it is manipulated.

The manufacturer, Ascension, told that they sold mainly systems that are used as the only tracking system in the medical workflow. Therefore they see no or only less need for a change in the time stamp. Most of their customers even do not use the offered time stamp. A solution has to be worked out to get a time stamp after the data was formulated.

To continue the work of this diploma thesis, the other magnetic tracking systems of the market should get examined if there is any other system available that comes with a proper time stamp. The implemented application can easily be adjusted to a different magnetic tracking system and does not depend on the use of a 3D Guidance / MicroBird system.

### 9.2 Expand the implemented application with a radiation therapy application

Another important future work is to expand the application with methods so that it can be used in the radiation room. Therefore registration between the electromagnetic tracking system, the patient and the preoperatively gained image data of the patient is needed.

The aim of this radiation therapy application is to know the position of the cancer in the coordinate system of the magnetic sensor and to transform this into the coordinate system

of the radiation table where the patient is laying. Then the table is moved so that the prostate cancer is located in the isocenter of the gantry of the linear accelerator.

Two registrations are needed: one between the electromagnetic tracking system and the patient's table and a second one between the electromagnetic tracking system and the CT images. The patient does not need to be registered with the magnetic tracking system as it is possible to site him in the same way every day using a laser system that is installed in the radiation room and labels on his skin. The coordinate system of the magnetic tracking system could be used as reference coordinate system.

The involved coordinate transformations in the radiation room can be seen on figure 9.1.

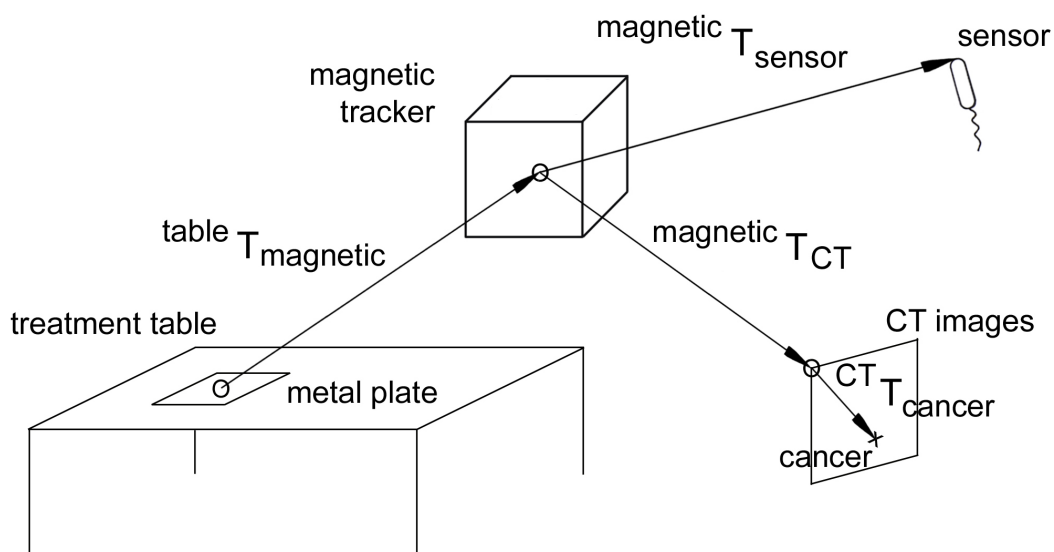


Figure 9.1: Overview over the involved coordinate systems and coordinate transformations in the radiation room

The registration between the magnetic tracking system and the patient's table could be done using point-based registration and a metal plate. There is a metal plate that can be screwed to the patient's table. Its origin is also the origin of the treatment table. By touching some points on the plate with a magnetic sensor and storing its values, an algorithm for point-based registration could compute the transformation between the coordinate systems. The four edges and the center of the plate could be used as registration points and their fix coordinates in the table's coordinate system could be stored permanently in the application.

The registration between the magnetic tracking system and the patient's CT images could be done using skin markers. These skin markers would be rigidly attached to the patient's skin on non-moving structures like the hip-bones. The patient would be scanned with the skin markers attached so that the markers as well as the prostate cancer can be seen on the computer tomography images. The skin markers enable an assignment between patient and computer tomography coordinates.

## **9.3 New medical approaches**

### **9.3.1 Attaching the sensor to the balloon catheter**

Another topic for future work could be to find a good way to attach the magnetic sensor to the balloon catheter. A rigid attachment might be useful, but this would mean to have one magnetic sensor for every radiation patient.

### **9.3.2 Permanently inserted intraprostatic markers**

The disadvantage of the balloon catheter in the current medical workflow is that it should be inserted into the rectum in exact the same way every day. This is because the position of the balloon shall agree with the position of the balloon on the “old” CT images as the patient is scanned regularly, but not every day. This identic alignment can not be fully ensured at the moment.

An approach with wireless magnetic sensors permanently implanted to the prostate should be considered. This method could make the registration process between the involved coordinate systems in the radiation room more convenient and might also substitute the balloon catheter.

New results from the research may also come up with promising new approaches that might be useful for the further course of this work.



**Part V**

**Appendix**



# List of Figures

2.1	The picture shows the position of the prostate in the abdomen. Picture taken from <a href="http://en.wikipedia.org/Prostate">http://en.wikipedia.org/Prostate</a> . . . . .	7
2.2	The picture shows a linear accelerator that is used during external beam radiation. Picture taken from <a href="http://de.wikipedia.org/wiki/Strahlentherapie">http://de.wikipedia.org/wiki/Strahlentherapie</a> . . . . .	10
2.3	These seeds are implanted into the prostate during low-dose brachytherapy. Picture taken from <a href="http://en.wikipedia.org/wiki/Prostate_cancer">http://en.wikipedia.org/wiki/Prostate_cancer</a> . . . . .	10
2.4	A multi-leaf collimator by Varian that is attached to the linear accelerator to shape the radiation beam during radiation. Picture taken from <a href="http://welchcancercenter.org/Radiation%20Therapy%20Equip/multileaf%20collimator.htm">http://welchcancercenter.org/Radiation%20Therapy%20Equip/multileaf%20collimator.htm</a> . . . . .	16
2.5	The left picture shows a collimator by Brainlab. In the right picture you can see the same collimator attached to a linear accelerator. Pictures taken from <a href="http://www.brainlab.com/scripts/website_english.asp?categoryID=19&amp;pageTypeID=11&amp;article_short_headline=Oncology%20Products">http://www.brainlab.com/scripts/website_english.asp?categoryID=19&amp;pageTypeID=11&amp;article_short_headline=Oncology%20Products</a> . . . . .	16
2.6	The picture shows the screen of the Varian Medical Systems Newsroom displaying an IMRT treatment plan for prostate cancer. The area of high dose is shown in red, low dose is shown in blue. Picture taken from <a href="http://varian.mediaroom.com/index.php?s=media_library&amp;cat=8">http://varian.mediaroom.com/index.php?s=media_library&amp;cat=8</a> . . . . .	18
2.7	A rectal balloon catheter. Picture taken from [vLFH <sup>+</sup> 06] . . . . .	19
2.8	This images shows a frame-based stereotactic frame that is attached to the patient’s head to establish a coordinate system. Picture taken from [Neu]. . . . .	21
2.9	This image shows the prostate with permanently implanted wireless sensors, called “beacons” by the manufacturer Calypso Medical Solutions. Picture taken from [Cal]. . . . .	22
2.10	Ultrasound probes for different purposes. Picture taken from [GE]. . . . .	23

2.11	This pictures shows gold markers that are used to establish a permanent internal patient reference system. The special surface of the rods shall avoid movements after implantation. Picture taken from [MED] . . . . .	23
3.1	This image illustrates the original setting of hand-eye calibration. . . . .	31
3.2	This images illustrates the situation according to equation 3.1 where one motion is given as input to the hand-eye calibration algorithm. . . . .	32
3.3	The polymer block used by Kaur for one approach of distortion correction for electromagnetic tracking. Picture taken by Kaur. . . . .	39
3.4	The optical setting with the involved transformations. Picture taken from [Kau06] . . . . .	40
3.5	This picture illustrates the formula for the bilinear interpolation. Picture taken from [Kau06] . . . . .	42
3.6	This pictures illustrates the formula for the trilinear interpolation. Picture taken from [Kau06] . . . . .	43
3.7	The distorted setting for the bilinear interpolation. Picture taken by Kaur. . .	45
3.8	The points used for the lookup-table are marked with a red asterisk, blue asterisks mark the points used for validation. Picture taken from [Kau06] . . . .	46
3.9	Position error as function of the distance from the sensor to the transmitter. Picture taken from [Kau06] . . . . .	48
3.10	These grids visualize the $y$ - $z$ -plane in the coordinate system of the magnetic tracking system. All graphs are in the same orientation as the polymer block was during data collection. The horizontal axis is the $y$ -axis. It ranges from -60 mm to 40 mm. The vertical axis is the $z$ -axis, ranging from -80 mm to 20 mm. The original grid in subfigure (a) is based on the ground truth data. Grids taken from [Kau06] . . . . .	49
4.1	The involved transformations for the device calibration. $S1$ denotes the magnetic sensor inside the combined target, while $S2$ stands for the optical markers attached on top of the combined target. $S3$ describes the optical markers on the transmitter of the electromagnetic tracking system that are used to track the field-generator by the optical tracking system. . . . .	55
4.2	Average reconstruction error for retroreflective markers depending on the hand-eye calibration method and number of poses. Picture taken from [FWBN05]. . . . .	57
4.3	An exemplary distortion field stored in a lookup-table, illustrated by 20 displacement vectors . . . . .	58
4.4	This is the ToUCam Pro Camera, a webcam manufactured by Philips that is used during the pacman game. . . . .	59
4.5	The pacman character, used to visualize the pose of the combined target during the creation of the lookup-table . . . . .	60

4.6	This screenshot of the pacman game reflects the view of the webcam. The yellow frame does not quite match the field-generator due to insufficient optical tracking data for the webcam that was hold outside the tracking volume to take the picture. . . . .	60
5.1	The 3D Guidance system by Ascension Technologies. The control box is shown in the center, the transmitter on the left side and the sensor is inside the combined target in the right. The target does not belong to the tracking system. . . . .	66
5.2	One Model 130 sensor of the 3D Guidance tracking system . . . . .	67
5.3	MicroBird manufactured by Ascension Technologies. Picture taken from [Ascb]	68
5.4	The picture shows one camera, model ARTtrack2, manufactured by Advanced Realtime Tracking GmbH. . . . .	69
5.5	The combined target with four optical markers attached on top. The electromagnetic sensor is located in a hole inside the target. . . . .	70
5.6	The transmitter of the 3D Guidance system with attached optical markers on top. . . . .	71
5.7	This images illustrates the arrangement of the axis in the transmitter of the 3D Guidance / MicroBird tracking system by Ascension and the working volume used during the experiments. . . . .	72
6.1	The source of distorton for experiment 1.3 was the light source of an endoscope.	75
6.2	The gained improvement between experiment 1.1 (left) and experiment 1.4 (right). The values marked with an x denote maximumElementDC and maximumElementEval. . . . .	77
7.1	The pictures show the space-filling curves along which the lookup-table (left) and the evaluation file (right) were collected during experiment 2. . . . .	80
7.2	During experiment 2.5, the lookup-table and the evaluation file were collected in planes along their space-filling curves as illustrated in this picture. . . . .	83
7.3	The source of distortion for trial 1 of experiment 2.5. It is composed of two lead blocks, a pencilbox and a gamma probe. . . . .	84
7.4	The gained improvement between experiment 2.1 (left) and experiment 2.5 (right) . . . . .	86
9.1	Overview over the involved coordinate systems and coordinate transformations in the radiation room . . . . .	92



# List of Tables

6.1	Overview over the trials of experiment 1.1 to 1.3 . . . . .	74
6.2	Overview over the four trials of experiment 1.4 . . . . .	76
7.1	Overview over the trials of experiment 2.1 to 2.3 . . . . .	81
7.2	Overview over the three trials of experiment 2.4 . . . . .	81
7.3	Overview over the three trials of experiment 2.5 . . . . .	85



# Bibliography

- [ABW01] B. ALLEN, G. BISHOP, and G. WELCH, *Tracking: Beyond 15 minutes of thought: Siggraph 2001 course 11*, Course Notes, Annual Conference of Computer Graphics and Interactive Techniques, (2001). <http://www.cs.unc.edu/~tracker/media/pdf/SIGGRAPH2001.CoursePack.11.pdf>.
- [Adv] ADVANCED REALTIME TRACKING GMBH (A.R.T), *ARTtrack & DTrack Manual, version 1.20*. <http://www.ar-tracking.com/>.
- [AP99] T. AUER and A. PINZ, *The integration of optical and magnetic tracking for multi-user augmented reality*, *Computers & Graphics*, 23 (1999), pp. 805–808. <http://www.emt.tu-graz.ac.at/~pinz/onlinepapers/CAG99.pdf>.
- [Asca] ASCENSION TECHNOLOGY CORPORATION, *3D Guidance - Installation and Operation Guide*. <http://www.ascension-tech.com>.
- [Ascb] ASCENSION TECHNOLOGY CORPORATION, *MicroBird product description page*. <http://www.ascension-tech.com/products/microbird.php>.
- [Bir00] W. BIRKFELLNER, *Tracking Systems in Surgical Navigation*, Doktorarbeit, Universitat Wien, (2000). <http://www.meduniwien.ac.at/zbmtp/people/birkwol/wbdiss.pdf>.
- [Cal] CALYPSO MEDICAL TECHNOLOGIES, INC., *Product page of Calypso Medical Technologies, Inc.* <http://www.calypsomedical.com/products/>.
- [CF91] R. CARLSON and T. FOLEY, *The parameter  $R^2$  in multiquadric interpolation*, *Computer & Mathematics with Applications*, 21 (1991), pp. 29–42.
- [Dan99] K. DANILIDIS, *Hand-Eye Calibration Using Dual Quaternions*, *The International Journal of Robotics Research*, 18 (1999), pp. 286–298. .
- [FN80] R. FRANKE and G. M. NIELSON, *Smooth interpolation of large sets of scattered data*, *International Journal for Numerical Methods in Engineering*, 15 (1980), pp. 1691–1704.
- [Fra79] R. FRANKE, *A Critical Comparison of Some Methods for Interpolation of Scattered Data*, Naval Postgraduate School, 1979. Technical Report NPS-53-79-003.

- [Fra82] R. FRANKE, *Scattered data interpolation: test of some methods.*, Mathematics of Computation, 38 (1982), pp. 181–200.
- [FSC<sup>+</sup>04] M. FUSS, B. SALTER, S. CAVANAUGH, C. FUSS, A. SADEGHI, C. FULLER, A. AMEDURI, J. HEVEZI, T. HERMAN, and C. THOMAS JR, *Daily ultrasound-based image-guided targeting for radiotherapy of upper abdominal malignancies*, International journal of radiation oncology, biology, physics, 59 (2004), pp. 1245–1256.
- [FWBN05] M. FEUERSTEIN, S. M. WILDHIRT, R. BAUERNSCHMITT, and N. NAVAB, *Automatic Patient Registration for Port Placement in Minimally Invasive Endoscopic Surgery*, in Medical Image Computing and Computer-Assisted Intervention - MICCAI 2005, 8th International Conference, J. S. Duncan and G. Gerig, eds., vol. 3750 of Lecture Notes in Computer Science, Palm Springs, CA, USA, September 2005, Springer Verlag", pp. 287–294.  
<http://campar.in.tum.de/Main/MarcoFeuerstein>.
- [GE ] GE HEALTHCARE, *Ultrasound Transducers*. [http://www.gehealthcare.com/usen/ultrasound/products/probe\\_care.html](http://www.gehealthcare.com/usen/ultrasound/products/probe_care.html).
- [Har71] R. L. HARDY, *Multiquadric equations of topography and other irregular surfaces*, Journal of Geophysical Research, 76 (1971), pp. 1905–1915.
- [HD95] R. HORAUD and F. DORNAIKA, *Hand-eye calibration*, International Journal of Robotics Research, 14 (1995), pp. 195–210.  
<http://perception.inrialpes.fr/Publications/1995/HD95/HoraudDornaika-IJRR95.pdf>.
- [HL93] J. HOSCHEK and D. LASSER, *Fundamentals of computer aided geometric design*, ISBN 1-56881-007-5, AK Peters, Ltd. Natick, MA, USA, 1993.
- [IBHH01] M. IKITS, J. BREDESON, C. HANSEN, and J. HOLLERBACH, *An improved calibration framework for electromagnetic tracking devices*, Proc. IEEE Virtual Reality, (2001), pp. 63–70.  
[http://www.cs.utah.edu/~ikits/publications/Ikits\\_VR\\_01.pdf](http://www.cs.utah.edu/~ikits/publications/Ikits_VR_01.pdf).
- [Kau06] S. KAUR, *Error Correction for ElectroMagnetic Tracking*, Master's thesis, Technische Universität München, 2006.
- [Kin99] V. KINDRATENKO, *Calibration of electromagnetic tracking devices*, Virtual Reality, 4 (1999), pp. 139–150. <https://netfiles.uiuc.edu/kindrtnk/www/papers/article11.pdf>.
- [Kin00] V. KINDRATENKO, *A survey of electromagnetic position tracker calibration techniques*, Virtual Reality, 5 (2000), pp. 169–182.  
<http://www.cours.polymtl.ca/inf6802/notes/calibration.pdf>.
- [KT07] P. KNESCHAUREK and J. TRAUB, *Dose Escalation with Photons. Emerging Technologies: a Physicist's Point of View*, in 8th International Meeting on Progress in Radio-Oncology, May 16-19 2007. <http://www.icrooegro.org/>.

- [KWM<sup>+</sup>05] P. KUPELIAN, T. WILLOUGHBY, S. MEEKS, A. FORBES, T. WAGNER, M. MAACH, and K. A. O. LANGEN, *Intraprostatic fiducials for localization of the prostate gland: Monitoring intermarker distances during radiation therapy to test for marker stability*, *International journal of radiation oncology, biology, physics*, 62 (2005), pp. 1291–1296.
- [MED] MED-TEC, *ACCULOC gold markers and ISOLOC software*. <http://www.additec.de/medtec/PRODUCTS/PATPOS/ACCULOC/ISOLOC.HTM>.
- [MHP<sup>+</sup>05] S. MANGAR, R. HUDDART, C. PARKER, D. DEARNALEY, V. KHOO, and A. HORWICH, *Technological advances in radiotherapy for the treatment of localised prostate cancer*, *European journal of cancer*, 41 (2005), pp. 908–921.
- [Mic86] C. MICCHELLI, *Interpolation of scattered data: Distance matrices and conditionally positive definite functions*, *Constructive Approximation*, 2 (1986), pp. 11–22.
- [Neu] NEUROSURGICAL MEDICAL CLINIC, INC., *Stereotactic surgery*. <http://www.sd-neurosurgeon.com/practice/stereotactic.html>.
- [Pow92] M. D. J. POWELL, *The theory of radial Basis Function approximation in 1990*, in *Advances in Numerical Analysis*, vol. II, Clarendon Press, Oxford, 1992, pp. 105–210.
- [RBSJ79] F. H. RAAB, E. B. BLOOD, T. O. STEINER, and H. R. JONES, *Magnetic position and orientation tracking system*, *IEEE Transactions on Aerospace and Electronic Systems*, 15 (1979), pp. 709–718.
- [SA89] Y. SHIU and S. AHMAD, *Calibration of wrist-mounted robotic sensors by solving homogeneous transform equations of the form AX=XB*, *Robotics and Automation*, *IEEE Transactions on*, 5 (1989), pp. 16–29.
- [SBI<sup>+</sup>06] C. F. SERAGO, S. J. BUSKIRK, T. C. IGEL, A. A. GALE, N. E. SERAGO, and J. D. EARLE, *Comparison of daily megavoltage electronic portal imaging or kilovoltage imaging with marker seeds to ultrasound imaging or skin marks for prostate localization and treatment positioning in patients with prostate cancer*, *International journal of radiation oncology, biology, physics*, 65 (2006), pp. 1585–1592.
- [SFT<sup>+</sup>06] T. SIELHORST, M. FEUERSTEIN, J. TRAUB, O. KUTTER, and N. NAVAB, *CAMPAR: A software framework guaranteeing quality for medical augmented reality*, *International Journal of Computer Assisted Radiology and Surgery*, 1 (2006), pp. 29–30.
- [SVN03] J. SCHMIDT, F. VOGT, and H. NIEMANN, *Robust Hand-Eye Calibration*, in 25. Symposium für Mustererkennung, DAGM 2003, Magdeburg, B. Michaelis and G. Krell, eds., vol. 2781 of LNCS, Springer-Verlag, Berlin, 2003. <http://citeseer.ist.psu.edu/schmidt03robust.html>.
- [TL88] R. Y. TSAI and R. K. LENZ, *Real time versatile robotics hand/eye calibration using 3D machine vision*, *IEEE International Conference on Robotics and Automation. Proceedings*, (1988), pp. 554–561.

- [Ume91] S. UMEYAMA, *Least-Squares Estimation of Transformation Parameters Between Two Point Patterns*, IEEE Transactions on Pattern Analysis and Machine Intelligence, 13 (1991), pp. 376–380.
- [vLFH<sup>+</sup>06] E. VAN LIN, J. FUTTERER, S. HEIJMINK, L. VAN DER VIGHT, A. HOFFMANN, P. VAN KOLLENBURG, H. HUISMAN, T. SCHEENEN, J. WITJES, J. LEER, et al., *IMRT boost dose planning on dominant intraprostatic lesions: Gold marker-based three-dimensional fusion of CT with dynamic contrast-enhanced and <sup>1</sup>H-spectroscopic MRI.*, International journal of radiation oncology, biology, physics, 65 (2006), pp. 291–303.
- [WKP<sup>+</sup>06] T. WILLOUGHBY, P. KUPELIAN, J. POULIOT, K. SHINOHARA, M. AUBIN, M. ROACH 3RD, L. SKRUMEDA, J. BALTER, D. LITZENBERG, S. HADLEY, et al., *Target localization and real-time tracking using the Calypso 4D localization system in patients with localized prostate cancer.*, International journal of radiation oncology, biology, physics, 65 (2006), pp. 528–34.
- [WSV91] M. WALKER, L. SHAO, and R. VOLZ, *Estimating 3-D location parameters using dual number quaternions*, CVGIP: Image Understanding, 54 (1991), pp. 358–367.
- [Zac97] G. ZACHMANN, *Distortion Correction of Magnetic Fields for Position Tracking*, in Computer Graphics International (CGI 1997), Belgium, June 23-27 1997. <http://zach.in.tu-clausthal.de/papers/cgi97.pdf>.